NRC·CNRC Flight Research - Aerospace Research Centre

4STAR hyperspectral sunphotometry measurements during the Oil Sands 2018 campaign near Fort McMurray, Alberta

by Konstantin Baibakov[1], Samuel LeBlanc[2,3], Kian Molani[4], Mengistu Wolde[1], Kristina Pistone[2,3], Connor Flynn[5], Jens Redemann[5] and Roy Johnson[3]

1 *Flight Research Lab, National Research Council, Ottawa, Canada*
2 *Bay Area Environmental Research Institute, Moffett Field, CA, USA*
3 *NASA Ames Research Center, Moffett Field, CA, USA*
4 *NRC Co-op program, Ottawa, Canada*
5 *Oklahoma University, Norman, OK, USA*

Ottawa, July 2019

National Research Council Canada | Conseil national de recherches Canada

Canada

FLIGHT RESEARCH LABORATORY

4STAR hyperspectral sunphotometry measurements during the Oil Sands 2018 campaign near Fort McMurray, Alberta

Report No.: LTR-FRL-2018-0116

Date: 18 July 2019

Authors/Auteurs: Konstantin Baibakov – NRC, Samuel LeBlanc – BAER/NASA, Kian Molani – NRC Co-op, Mengistu Wolde – NRC, Kristina Pistone – BAER/NASA, Connor Flynn – U of Oklahoma, Jens Redemann – U of Oklahoma and Roy Johnson - NASA

Classification:	Unclassified	**Distribution:**	Unlimited
For:			
Reference:			
Submitted by:	Konstantin Baibakov		
Approved by:	Kirk Shaw, FRL director		

Pages: 108	**Copy No:** 1
Fig. : 73	**Diagrams:** 0

Abstract

In 2018, the Environment and Climate Change Canada (ECCC) in close collaboration with the National Research Council (NRC) planned and conducted an intensive airborne oil sands measurement campaign (OSMC) based out of Fort McMurray, Alberta. The campaign was conducted in two phases: Phase I (April 3-15) and Phase II (May 28-July 5). In preparation for the OSMC the NRC, together with NASA, have integrated a novel 4STAR sunphotometer on board the Convair-580 for the measurements of aerosols and trace gases. The 4STAR primary capability is to supply hyperspectral measurements of the aerosol optical depth (AOD) - the most important aerosol radiative parameter indicative of the total column vertical extinction due to aerosols. The main purposes of this report are to describe the performance of the 4STAR during the OSMC, discuss data availability statistics and provide a first look at some of the initial results.

In summary, the 4STAR was run on each of the 24 science flights of Phase II acquiring close to 100 hours of data. It was operated in tandem with a comprehensive suite of in-situ instruments, including DMT UHSAS (particle sizer and counter), DMT SP2 (black carbon mass and particle sizer) and TSI 3775 CPC (total particle counter). During the representative flights of June 9 and 18, the 4STAR was able to detect aerosol plumes emanating from industrial sources and characterize the aerosol loading in terms of fine (sub-micron) and coarse-mode (super-micron) contributions. Narrow duration fine-mode AOD peaks of up to 0.45 associated with the plumes were detected. In general, these peaks were correlated in time and amplitude with the in-situ measurements (such as UHSAS total particle concentration) giving more credence to the observed 4STAR dynamics. In addition to the June 9 and 18 cases, a series of quick look plots are also presented for June 20, 24, 25 and July 5 flights that are likely to have the most potential for scientific investigation.

The analysis presented in this document constitutes a first step in the processing of the 4STAR data with future work including the analysis of the sky radiance measurements, evaluation of the trace gas retrievals, development of cloud screening routines and comparisons between 4STAR and in-situ optical measurements.

Résumé

En 2018, Environnement et Changement climatique Canada (ECCC), en étroite collaboration avec le Conseil national de recherches du Canada (CNRC), a planifié et conduit une campagne intensive de mesures aériennes des sables bitumineux, à partir de Fort McMurray, en Alberta. La campagne a été menée en deux phases : la première phase (du 3 au 15 avril) et la seconde (du 28 mai au 5 juillet). Pour préparer cette campagne, le CNRC, en collaboration avec la NASA, a installé un nouvel photomètre solaire 4STAR à bord du Convair-580 pour la mesure des aérosols et des gaz à l'état de traces. Le 4STAR sert principalement à obtenir une mesure hyperspectrale de l'épaisseur optique des aérosols, la propriété radiative des aérosols la plus importante qui indique l'extinction totale due à ces particules sur une colonne verticale. L'objectif du présent rapport est de décrire les performances du 4STAR durant la campagne, de discuter la statistique de la disponibilité des données et de fournir un premier aperçu des résultats initiaux.

En résumé, le 4STAR a été utilisé durant chacun des 24 vols scientifiques de la seconde phase et a permis d'acquérir près de 100 heures de données. Le 4STAR était intégré à un ensemble complet d'instruments de mesure in situ comprenant un compteur et calibreur de particules UHSAS (DMT), un SP2 (DMT) pour mesurer la masse et la taille des particules de carbone noir et un compteur de particules TSI 3775. Durant les vols représentatifs effectués entre le 9 et le 18 juin, le 4STAR a été capable de détecter plusieurs panaches d'aérosols émanant de sources industriels et de caractériser la charge d'aérosols en fonction des contributions de la fraction fine (submicronique) et de la fraction grossière (supermicronique). Des pics d'épaisseur optique allant jusqu'à 0,45, de durée courte, ont été détectés dans les panaches pour la fraction fine. En général, ces pics étaient corrélés temporellement et en amplitude avec les mesures in situ (telles que la concentration totale des particules fournie par l'UHSAS), ce qui a rendu plus crédibles les variations mises en évidence par le 4STAR. En plus des cas observés les 9 et 18 juin, une série de graphes récapitulatifs sont aussi présentés pour les vols des 20, 24 et 25 juin et du 5 juillet qui offrent le plus de possibilités d'analyse scientifique.

L'analyse exposée dans le présent document est la première étape du traitement des données fournies par le 4STAR. Les étapes ultérieures consisteront à analyser les mesures de luminance du ciel, à évaluer indirectement la concentration des gaz à l'état de traces, à développer des algorithmes de filtrage des nuages et à comparer les données du 4STAR aux mesures optiques in situ.

Contents

List of figures

Appendix A

Appendix B

List of tables

Appendix A

List of abbreviations

4STAR	Spectrometer for Sky-scanning, Sun-Tracking Atmospheric Research
AGL	Above ground level
ASL	Above sea level
AOSR	Alberta Oil Sands Region
AOD	Aerosol Optical Depth
BC	Black carbon
CLAP	Continuous Light Absorption Photometer
CPC	Condensation particle counter
DMT	Droplet Measurement Technologies
ECCC	Environment and Climate Change Canada
FWHM	Full Width at Half Maximum
NIR	Near infrared
NRC	National Research Council Canada
OSMC	Oil Sands Measurement Campaign
PSD	Particle size distribution
SDA	Spectral Deconvolution Algorithm
SSA	Single Scattering Albedo
SWIR	Short-wave infrared
UHSAS	Ultra-high sensitivity aerosol spectrometer

Introduction

The Alberta Oil Sands Region (AOSR) is home to some of the largest oil sands deposits in the world. The oil sands operations associated with oil extraction and upgrading, however, can have a significant impact on the environment and human health. In particular, it has been shown that the AOSR industrial emissions are a large source of secondary produced aerosols – small particles suspended in the air that are formed via the gas-to-particle conversion (Liggio et al, 2016). Aerosols can have a significant impact on the Earth radiative balance and, consequently, on the global climate, but contrary to the well-understood effect of the greenhouse gases such as CO_2, aerosol effects are still associated with some of the largest uncertainties in climate models. Understanding and quantifying the aerosol properties in the AOSR is thus essential to evaluating the AOSR environmental impact.

In 2018, as a follow-up to the successful 2013 measurement campaign, the Environment and Climate Change Canada (ECCC), in close collaboration with the National Research Council (NRC), planned and conducted an intensive airborne oil sands measurement campaign (OSMC) based out of Fort McMurray, Alberta. The campaign was conducted in two phases: Phase I (April 3-15) and Phase II (May 28-July 5). For the purposes of OSMC, the NRC Convair-580 aircraft was jointly equipped with a state-of-the-art suite of in-situ and remote sensing instruments in order to develop a comprehensive view of aerosols and trace gases. In particular, in preparation for the OSMC the NRC, together with NASA, have integrated a novel 4STAR sunphotometer on board the Convair-580 to measure total column atmospheric extinction, from which the aerosol and trace gas properties can be derived. The 4STAR primary capability is to supply hyperspectral measurements of the aerosol optical depth (AOD) - the most important aerosol radiative parameter indicative of the total column vertical extinction due to aerosols. The 4STAR has been flown on every flight during the Phase II of the campaign and whenever possible acquired information on aerosols and trace gases. The main purposes of this report are to describe the performance of the 4STAR during the OSMC, discuss data availability statistics and provide a preliminary look at some of the initial results. The comprehensive scientific analysis of the 4STAR dataset is thus beyond the scope of this report and will be presented elsewhere.

The remainder of this document is structured as following. We first describe the instrumentation used during the OSMC with an emphasis on 4STAR, followed by a presentation of the flight-by-flight 4STAR data acquisition statistics during Phase II. We then provide a description of the 4STAR data processing and discuss two representative flights from the campaign: an emissions flight on June 18 and a transformation flight on June 9. We conclude the document with a brief summary and an outlook for further data analysis.

Instrumentation

While the primary focus of this document is the 4STAR instrument, many of its underlying fundamental principles are based on the ground-based sunphotometry – now a mature technique used extensively throughout the world. We judge it, therefore, to be more instructive to discuss the ground-based aspects of sunphotometry first and then extend the discussion to the airborne sunphotometry and the 4STAR.

Additionally during the OSMC, the Convair-580 was equipped with a comprehensive ensemble of instruments for aerosol and trace gas measurements. Detailed descriptions of these instruments[1] lie out of scope of the present work and can be found elsewhere (eg. Liggio et al, 2016, Li et al, 2017). In this report we only provide brief descriptions of those instruments that support the discussion of the 4STAR results.

Ground-based sunphotometry

Aerosol optical depth

Ground-based sunphotometry is a means of measuring the extinction of solar radiation through the atmosphere (Figure 1). While sunphotometry can be employed to study certain trace gases, such as ozone and water vapor, its principal use is the measurement of aerosols (Shaw, 1983). In particular, sunphotometry provides robust measurements of the spectral aerosol optical depth (AOD, τ_a) - the most important aerosol (extensive) radiative parameter indicative of the total column vertical extinction due to aerosols (Kaufman et al, 2002).

The fundamental transmission equation of sunphotometry is described by the Beer-Lambert law:

$$I = I_0 e^{-m\tau_t} \quad (1)$$

By measuring solar intensity on the ground (spectral irradiance I, W/m^2/nm) and comparing it to the value at the top of the atmosphere (spectral irradiance I_0, W/m^2/nm), a value of the total optical depth (τ_t, dimensionless) is calculated. The sun's angular displacement from the zenith position is accounted for in terms of the air mass factor, m, which for solar zenith angles $\theta < 60°$ is simply $\frac{1}{cos\theta}$.

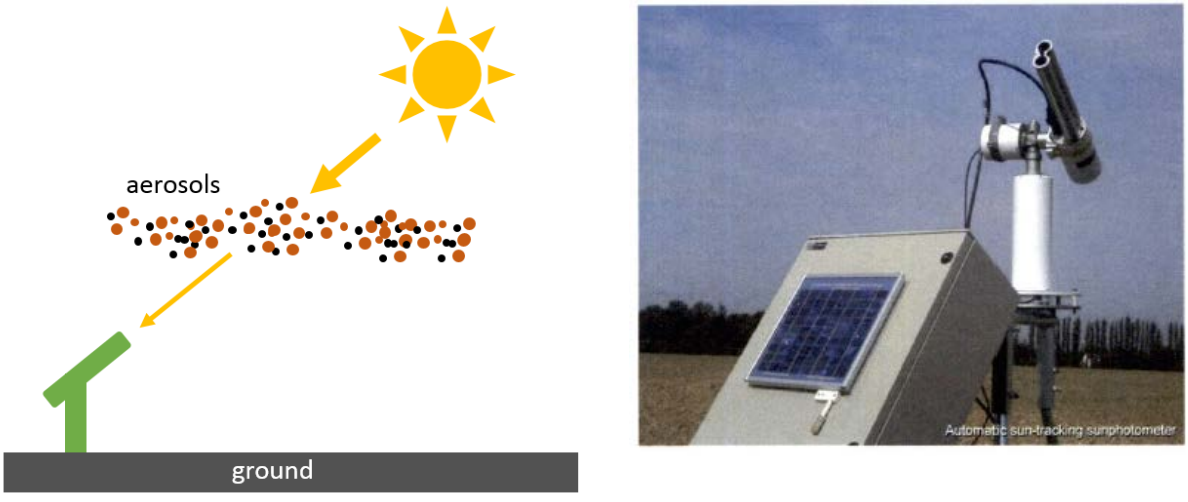

Figure 1. Left: conceptual representation of the sunphotometry principle. Right: CIMEL-CE-318 sunphotometer (source: CIMEL)

[1] such as Aerodyne Aerosol Mass Spectrometer, Thermo Environmental/Thermo Fisher Scientific TECO Gas Analyzers (NO, NO_2, SO_2, O_3), Picarro Cavity Ring-Down Spectroscopy Analyzers (CO, CO_2, CH_4) and others

Total optical depth evaluated between the ground level (z=0) and the top of the atmosphere (z=TOA) is given by:

$$\tau_t = \int_0^{TOA} \alpha(z)dz \quad (2)$$

where $\alpha(z)$ (units of inverse length) is the extinction coefficient representing the fraction of light which will be attenuated per unit distance in any direction.

The value of τ_t can be decomposed as (Shaw et al., 1973):

$$\tau_t = \tau_{Ray} + \tau_a + \tau_{O_3} + \tau_{H_2O} + \tau_{NO_2} \quad (3)$$

where τ_{Ray} is the optical depth of molecular scattering (Rayleigh scattering) and τ_a is the optical depth due to aerosols. The remaining three terms, τ_{O_3}, τ_{H_2O}, and τ_{NO_2} are the optical depths due to absorption by ozone, water vapor, and nitrogen dioxide respectively. These three molecular components dominate the molecular absorption in the visible and near infrared (NIR) regions of the electromagnetic spectrum (Seinfeld and Pandis, 2006). The estimation of AOD involves the estimation of all non-aerosol components (NAC) in order to back out τ_a from equation (3). The NAC can be estimated from the remote sensing or balloon measurements, as well as from satellites and models.

CIMEL CE-318 sunphotometer

There is a variety of modern sunphotometers that differ in specifications such as a number, positioning and width of the spectral bands, detector type, field of view (FOV) and tracking style (handheld or automatic). The most common, however, is the CIMEL CE-318 sunphotometer (Figure 1) with hundreds of systems deployed around the world as a part of the AERONET network (Holben et al, 1998). A standard CE-318 takes measurements of the direct solar radiance in eight spectral bands (340, 380, 440, 500, 675, 870, 1020 and 1670 nm) from which spectral AODs can be estimated. The instrument has a 940 nm channel dedicated to water vapor measurements (which are employed to correct for water absorption effects in the other "aerosol" bands).

In addition to being a sunphotometer, CE-318 is a sky radiometer which acquires sky radiance measurements regularly throughout the day. Within certain limitations, sky radiance measurements can be inverted to yield additional information about aerosols, including particle size distribution, refractive index and single scattering albedo (Dubovik and King, 2000). CE-318 has two distinct data acquisition modes for sky radiances: almucantar and principal plane. The almucantar mode consists of the sky radiance measurements with a zenithal angle held constant and equal to the zenith solar angle with varying azimuthal angle. The principal plane mode on the other hand consists of sky radiance measurements at a constant azimuthal angle and varying zenithal angle. Both concepts are depicted schematically in Figure 2 with additional details provided in Appendix B.

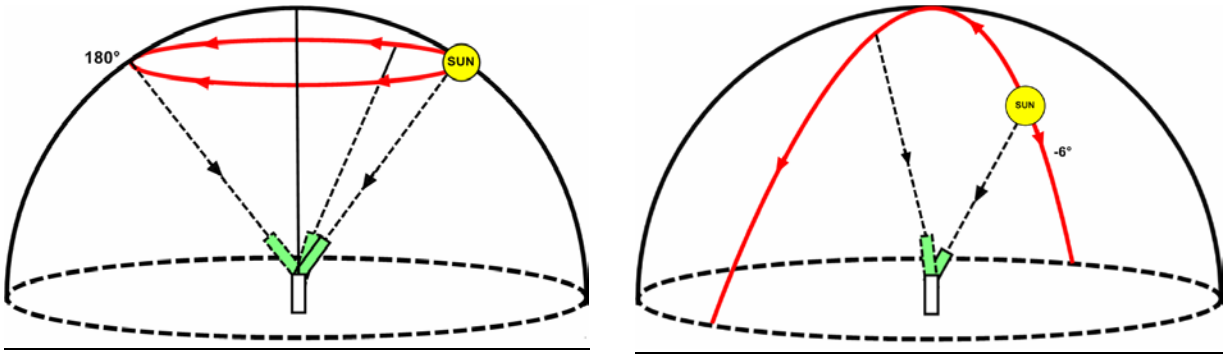

Figure 2. Conceptual depiction of the CE-318 almucantar (left) and principal plane (right) sky measurement modes. Source: Cimel, 2015.

Calibration

As can be seen from equation (1) sunphotometers need to be calibrated in order to estimate the value of the extra-terrestrial irradiance I_0. In many cases, these calibrations are performed using a Langley method at high-altitude sites (i.e. Mauna Loa, Hawaii) known for low aerosol concentration levels. During a Langley calibration, sun radiances are acquired at different air masses in the presence of a stable (fixed AOD) atmosphere, allowing the resulting signal levels to be extrapolated to an air mass of zero – the signal level that the instrument would measure if it were located above the atmosphere.

Cloud screening

Sunphotometry data needs to be routinely screened for cloud-contaminated data. Given the fact that clouds exhibit much higher temporal-spatial variability than aerosols, AERONET uses a series of checks that eliminate high-frequency temporal variations based on the maximum permissible AOD variation in a certain time interval, eg. 1 min (Smirnov et al, 2000). Another method is to exploit the fact that cloud particles are significantly larger than most aerosols resulting in different spectral signatures. A combination of temporal and spectral techniques (eg. O'Neill et al, 2016) is likely to produce the best cloud screening results, especially for an airborne sunphotometer for which relying only on the temporal criteria might be inefficient due to faster changing observational conditions.

NASA 4STAR sunphotometer

4STAR (Spectrometer for Sky-scanning, Sun-Tracking Atmospheric Research) is a hyperspectral sunphotometer developed by the NASA Ames Research Center and designed for airborne measurements of aerosols and trace gases (Figure 3).

Figure 3. a. 4STAR at Fort McMurray installed on the Convair-580 aircraft; b. 4STAR head and its optical cables sitting inside the aircraft

The 4STAR is comprised of a movable optical head that protrudes through the top of the aircraft fuselage, an accompanying instrument rack inside the aircraft and the optical cables that connect the two. The 4STAR optical head contains two sets of optics: a sunlight collector (FOV: 1.25 deg.) for sun-tracking measurements and a skylight collector (FOV: 2 deg.) for sky radiance measurements. The hyperspectral measurements are obtained with two Tec5 spectrometers located in the instrument rack: UV-VIS-NIR (210-995 nm, full width at half maximum (FWHM): 2-7 nm) and SWIR (950-1703 nm, FWHM: 5 nm) resulting in a total of 1536 spectral channels. A more detailed technical description of the 4STAR can be found in Dunagan et al, 2013 and Shinozuka et al, 2013.

While significantly different in terms of technical implementation, the 4STAR principles of operations and data processing are very similar to those of CE-318. The most notable distinction between the instruments is the 4STAR hyperspectral capability resulting in AODs acquired in hundreds of spectral bands as opposed to only 8 channels for CE-318.

Similarly to CE-318, 4STAR can operate in the sun-tracking or the sky-scanning mode either supplying the AODs or the sky radiance measurements for subsequent inversions. 4STAR can also operate in the zenith-pointing mode designed for the retrievals of cloud properties. Given that the focus of the OSMC was primarily on aerosols and trace gases, this mode was rarely used during the campaign and the associated results are not discussed in this document.

Because of the 4STAR fine spectral resolution, its measured solar radiances can be used to derive trace-gas concentrations, including columnar water vapor, nitrogen dioxide, ozone and potentially other trace gases, such as formaldehyde (Segal-Rosenheimer et al, 2014).

In the sun-tracking mode, the 4STAR continuously obtains optical depth values using the Beer-Lambert law. Assuming that the detector output is linearly proportional to the measured irradiance and expressing Eq. (1) in terms of measured and reference spectrometric counts, $C(\lambda)$ and $C_0(\lambda)$, respectively, yields:

$$C = C_0 e^{-m\tau_t} \quad (4)$$

Solving for τ_t gives:

$$\tau_t = \frac{1}{m}\ln\left(\frac{C_0}{C}\right) \quad (5)$$

from which τ_a can be estimated using equation (3):

$$\tau_a = \tau_t - (\tau_{Ray} + \tau_{O_3} + \tau_{NO_2}) \quad (6)$$

It should be noted that equation (5) assumes the same air mass for all atmospheric components which is true only for solar zenith angles less than about 60° (eg. Russell et al, 1993). For angles larger than 60°, equation (5) becomes:

$$\tau_t = \frac{1}{m_a}\left[\ln\left(\frac{C_0}{C}\right) - m_{Ray}\tau_{Ray} - m_{O_3}\tau_{O_3} - m_{NO_2}\tau_{NO_2}\right] \quad (7)$$

where m_i are individual air masses for aerosols, Rayleigh particles, ozone and nitrogen dioxide. The details of estimation of τ_{Ray}, τ_{O_3}, and τ_{NO_2} and the corresponding air masses in 4STAR calculations can be found in Shinozuka et al, 2013.

Ultra-High Sensitivity Aerosol Spectrometer – (UHSAS)

Ultra-High-Sensitivity Aerosol Spectrometer (UHSAS) manufactured by Droplet Measurement Technologies (DMT) uses light scattering techniques to derive concentrations and size distributions of particles with diameters ranging from 65 to 1000 nm. UHSAS counts and sizes aerosols by measuring the amount of light scattered by particles as they traverse a focused laser beam (operated at 797 nm). Two pairs of Mangin optics are used to collect scattered light. The first pair images onto an avalanche photodiode (APD) for detecting the smallest particles, while the other pair, images onto a low-gain PIN photodiode for detecting larger particles. Particle size is determined by comparing the amplitude of the measured voltage pulses to the reference signal from the calibration particles of known size and composition. For more information on UHSAS, see for example Cai et al, 2008, Kupc et al, 2018.

ECCC instrumentation

Single Particle Soot Photometer (SP2)

A DMT Single Particle Soot Photometer (SP2) estimates black carbon (soot) mass by measuring laser-induced incandescence. Light-absorbing aerosols (predominantly Black Carbon, BC) are heated to vaporization by a Nd:YAG laser beam operated at 1064 nm. As they vaporize, refractory materials emit significant visible thermal radiation that is characteristic of the composition and mass of the particle refractory component. Assuming a BC density of 1.8 g/cm^3, the instrument can measure particle masses ranging from 70 to 500 nm mass-equivalent diameters. SP2 can also measure particles that do not absorb enough energy to heat significantly. This is done on the basis of the amount of light that they scatter out of the laser beam. The measured particle size range for the scattering signal is between 200

and 430 nm. For a more detailed description of SP2, see for example Schwartz et al, 2006, Liu et al, 2010.

TSI 3775 Condensation Particle Counter (CPC)

The TSI 3775 Condensation Particle Counter (CPC) is a general-purpose counter used to derive concentrations of aerosol particle samples with diameters ranging from 4 nm to 3000 nm. CPC is an alcohol-based instrument that condenses butanol supersaturated vapor on individual particles of the aerosol sample in order to grow the resulting droplets large enough to be optically detected. For lower particle concentrations (0 to 50,000 particles/cm^3), individual light pulses scattered by each particle are counted ("single count mode"). For higher concentrations (50,000 to 10,000,000 particles/cm^3), measurements are made by comparing the total amount of scattered light with a reference calibration value ("photometric mode"). Particle concentration accuracies are ±10% in single count mode and ±20% in photometric mode.

4STAR dataset

General comments and statistics

The OSMC2018 (or simply OSMC) is a follow-up to the OSMC2013 when the Convair-580 was deployed to the Oil Sands region for the first time (see e.g. Liggio et al, 2016, Li et al, 2017). During Phase II of the OSMC relevant to the 4STAR operations, a total of 24 science flights were conducted for a total of approximately 100 flying hours. The 4STAR was installed on every flight with data acquired whenever possible. Little to no 4STAR data was acquired whenever the sun was obstructed by optically thick clouds or whenever the instrument was having technical problems. The 4STAR was predominantly run in the sun-tracking mode with occasional sky radiance measurements. As each sky radiance measurement takes up to 90 s to complete, the AOD time series have corresponding gaps whenever the almucantar or principal plane measurement mode was engaged. Table 1 presents a summary of all the OSMC flights and shows, for each flight, 4STAR data acquisition statistics. Based on data availability and the observed features, we identified six flights ("primary flights", highlighted in green in Table 1) believed to have the most potential for scientific analysis.

Two types of flights were performed during the OSMC: emissions and transformation flights, resulting in "box" and "screen" flight patterns, respectively. As the names imply, the former was directed at characterizing pollution emissions from individual facilities, while the latter aimed at studying the fate of the pollutants as they got transported away from the source. For each flight, the flight plan usually started at 500 ft above ground level (AGL) and progressively increased altitude in discreet intervals of 250, 500 or more feet, until either reaching the top of the boundary layer or moving on to the next box/screen, typically resulting in 4-6 altitude levels. The transformation flights were conducted in Lagrangian patterns designed to intercept the same plume perpendicular to the wind direction. As can be seen from Table 1, the 4STAR has acquired measurements from 16 emissions flights and 8 transformation flights. In some cases (eg. June 19), whenever the conditions allowed, the emission boxes were followed by one or several transformation screens. In many cases, during the execution of a particular box or screen, a spiral profile was also performed in order to estimate the height of the boundary layer and acquire vertically resolved aerosol and trace gas measurements.

Flights table

Green: Flights with significant amount of acquired 4STAR data and distinct aerosol features ("primary flights")
White: Flights with some 4STAR data suitable for scientific analysis
Orange: Flights for which there is little or no 4STAR data available due to clouds or instrument problems

Cloud screened points were excluded from the direct-sun statistics, except for June 25 (marked with *) when no cloud screening was applied.

All durations are rounded to the nearest minute.

Table 1. Summary of the acquired 4STAR data during Phase II of the OSMC

Date (2018)	Flight # (NRC)	Flight # (ECCC)	Transf. / Emissions	Facilities / Flight details	Direct (scrn., min)	% points screened	Almucantar (min)	Princip. Plane (min)	Total 4STAR (min)	Total flight time (min)	**Data avail. (%)**	Comments
May 30	21	7	E	CNRL	7	85 %	1	0	8	154	**5 %**	
May 31	22	8	E	CNRL, Suncor Fort Hills, Syncrude Aurora	178	25 %	0	0	178	300	**59 %**	
June 1	23	9	E	Suncor Firebag, Suncor Millenium	0	100 %	0	0	0	226	**0 %**	No 4STAR data acquired
June 6	24	10	E	Syncrude Mildred Lake	4	88 %	0	0	4	162	**2 %**	
June 6	25	11	E	Suncor Millenium	89	11 %	7	6	102	164	**62 %**	
June 7	26	12	E	Devon Jackfish, MEG Christina Lake, Cenovus Christina Lake	90	30 %	1	1	92	255	**36 %**	
June 7	27	13	E	CNRL Muskeg River and Jackpine	0	91 %	1	0	1	160	**1 %**	
June 9	28	14	T	Transformation flight to the West of the facilities.	175	23 %	0	2	177	294	**60 %**	Visually opaque plume. 4STAR measurements are mostly available during

				Following the plume of Syncrude Mildred Lake and CNRL Horizon								the first and seconds screens, but then become heavily influenced by clouds.
June 13	29	15	E	CHOPS facilities near Lloydminster	0	100 %	0	0	0	289	**0 %**	Honeywell problems; purge issues
June 13	30	16	E	CHOPS facilities near Lloydminster	39	45 %	0	0	39	150	**26 %**	
June 15	31	17	E	CNRL Horizon, Suncor MacKay River	168	24 %	0	1	169	279	**61 %**	Deposition box around YAJP tethered balloon site
June 16	32	18	E	Facilities near Cold Lake	96	43 %	0	11	107	289	**37 %**	
June 18	33	19	E	Syncrude Mildred Lake, Suncor MacKay River	138	14 %	13	16	167	228	**73 %**	Strong and visually impressive plume clearly measureable on the eastern side of the Syncrude box. Sky radiance measurements are available including inside the plume. Huge SO_2 concentrations up to 2 ppm. RH was too high in the spectrometer – the data might need corrections.
June 19	34	20	E / T	Brion Energy MacKay River, Syncrude Mildred Lake. Two transformation screens eastward of Syncrude.	128	35 %	1	10	139	267	**52 %**	
June 20	35	21	E	Imperial Kearl Oil Sands, Suncor Millenium	187	2 %	0	8	195	227	**86 %**	The Suncor Mil. Box was followed by a screen on the northern side of the box in order to characterize a potential effect from flares. There is a consistent AOD increase of 0.03-0.04 over the southern side of the Suncor Mil. box.
June 21	36	22	T	3 transformation screens to the West of the facilities.	49	50 %	0	0	49	264	**19 %**	Cloudy throughout: some cloud contaminated 4STAR data during the first 1.5 screens and then complete overcast.
June 22	37	23	E	Imperial Kearl Oil Sands, Suncor Firebag and Brion Energy Mackay River South.	6	61 %	0	0	6	172	**3 %**	

				Failed transformation screens NW								
June 24	38	24	T	Transformation flight with three screens set up to the north-east of the facilities	172	4 %	16	14	202	266	**76 %**	Sunny almost the entire flight. No sharp AOD peaks - low (~0.15) slowly evolving values. Several sky scan measurements. High AODs (~0.7) on landing and on the ground - possibly forest fires
June 25*	39	25	T	Forest fire transformation flight with three screens set up from the Alberta-Saskatchewan border towards Fort McMurray	198	0 %	7	19	224	271	**82 %**	Sunny for the majority of the flight with some occasional cirrus contamination. Multiple sky scans. No cloud screening.
June 25	40	26	T	An additional forest fires transformation screen set up north-west of the facilities	70	35 %	0	1	71	181	**39 %**	This last screen was mostly cloudy with only few 4STAR data points.
June 26	41	27	T	Two transformation screens east of Suncor	42	21 %	0	0	42	205	**21 %**	
June 29	42	-	-	Wind calibration flight	-		-	-	-	-	**-**	
June 30	43	28	E	Facilities near Cold Lake and Lloydminster	187	17 %	0	3	190	281	**68 %**	
June 30	44	-	-	Facilities near Cold Lake and Lloydminster	35	29 %	0	0	35	57	**61 %**	Transit flight back to Fort McMurray
July 4	45	29	T	Four screens set up east-west perpendicularly to winds south of the facilities	110	45 %	0	0	110	287	**38 %**	4STAR was mostly impacted by clouds. AOD values were low and typically below 0.1. There was more structure later in the flight
July 5	46	30	T	Three screens set up to the north east of the facilities similarly to June 24.	242	5 %	0	8	250	300	**83 %**	AODs seem to be getting slightly higher with each consecutive screen

Data processing

As the sky scan products and the trace gas retrievals were still being evaluated at the time of writing, in this section we only discuss the primary 4STAR output - the AOD measurements obtained in the sun-tracking mode.

Sun-tracking measurements

The detailed description of the 4STAR data processing can be found elsewhere (e.g. Shinozuka et al, 2013). Here we only provide a brief summary of estimating the instrument transmittance with 4STAR. The 4STAR count rate, C, is calculated by subtracting the dark counts (measured once every 20 min) from the raw spectrometric counts (1 Hz sampling rate), and dividing the result by the integration time. The integration time was set to 50 ms for the UV-VIS-NIR spectrometer (six spectra averaged per one sampling period) and 400 ms for the SWIR (1 spectrum per one sampling period). The instrument transmittance is derived by dividing the measured count rate C by the instrument reference spectrum, C_0 (derived from Langley calibrations, see section on calibration) and by the corresponding Earth-Sun distance correction. The total (τ_T) and aerosol (τ_a) optical depths are then derived from the Beer-Lambert's law using equations (1) and (6).

Once the spectral AODs are derived, we apply the Spectral Deconvolution Algorithm (O'Neill et al, 2003) in order to separate the total measured AOD into its fine (submicron) and coarse (supermicron) mode components. Similarly to AERONET data processing, we use 380, 440, 500, 675 and 860 nm channels as inputs to SDA. We expect that in most cases the anthropogenically produced aerosols observed in the AOSR are fine mode in nature, since coarse-mode aerosols are usually associated with natural sources (eg. winds lifting up dust particles or ocean waves generating sea-salt aerosols). Consequently, with the exception of dust aerosols potentially resulting from surface mining, the coarse-mode dominant AODs in the AOSR will usually be associated with cloud contamination.

Several techniques have already been developed in order to screen the 4STAR data from the interference by clouds. They usually pertain to screening the data based on significant count rate variations within a certain time interval or the relatively flat spectral shape characteristic of clouds. While no cloud-screening method is perfect, the above mentioned techniques can often reduce the cloud contamination to 10-20% of AOD (Shinozuka et al, 2013). At this stage of data analysis, however, we chose to apply only a very basic cloud screening test by classifying points as clouds when either the fine-mode AOD exceeded 0.5 or the total AOD exceeded 0.8, i.e. in several cases we eliminated points with $\tau_f > 0.5$ or $\tau_t > 0.8$ (referred to as "default cloud screening"). This choice was dictated by the fact that the existing cloud screening methods were eliminating some of the valid fine-mode peaks supported by the in-situ measurements. The thresholds were chosen in such a way that the test could be applied to the entire dataset with the exception of June 25, when the AODs were uncharacteristically high. We anticipate to apply more sophisticated algorithms for cloud screening in the future as we gain more insight into the measured AOD dynamics during the OSMC.

Flight examples

Appendix A provides a series of comprehensive quicklooks for each of the 4 transformation and 2 emissions primary flights. It should be emphasized that at the time of writing the data has not undergone extensive quality assurance review and thus can contain errors and/or artifacts. In this

section we discuss two representative flights from the campaign: an emissions flight on June 18 and a transformation flight on June 9. During both of these flights, the Convair-580 studied the aerosol plumes mainly emanating from the Syncrude Mildred Lake facility. On June 9, however, the aircraft was likely to have intercepted the emissions from the CNRL (Canadian Natural Resources Limited) Horizon facility as well.

Syncrude Mildred Lake emissions flight – June 18, 2018

During the NRC flight 33 (ECCC flight 19), the Convair-580 flew in a "box" flight pattern around the Syncrude Mildred Lake (SML) site in order to characterize the emissions from the facility. There was a significant and clearly visible industrial plume emanating from the SML chimneys (Figure 4).

Figure 4. A photo of the Syncrude plume, taken during the eastern side of the box facing approximately south west.

The boxes were set up at 7 nominal altitudes of 500, 750, 1000, 1250, 1500, 1750 and 2000 ft above ground. Additionally, the aircraft flew at 2250, 2500 and 2750 ft over the eastern side of the box. With stable winds blowing from the south-west, the plume was repeatedly intercepted on the eastern side of the box (Figure 5).

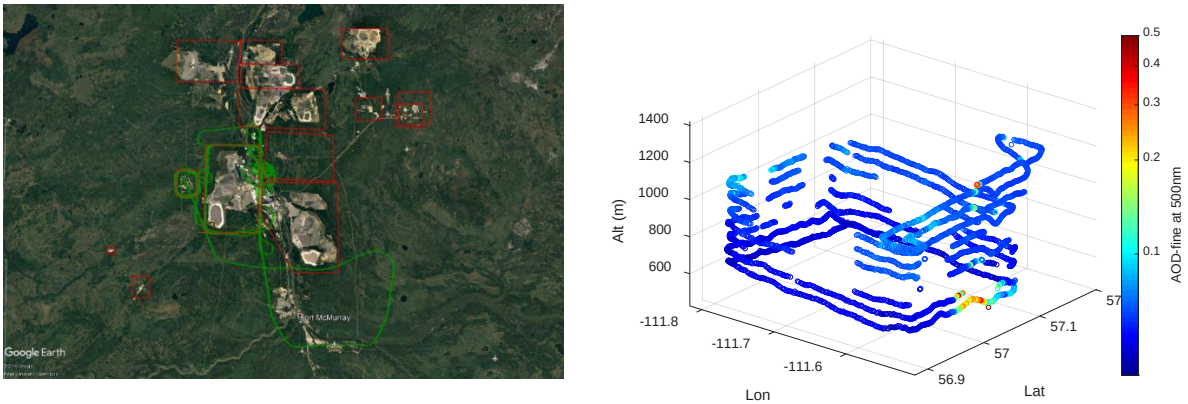

Figure 5. Left: the NRC Convair-580 flight track (green) during the NRC flight 33 superimposed on the Google Earth satellite image of the area. Red boxes signifiy the approximate boundaries of individual facilities. Right: fine-mode aerosol optical depth measured with 4STAR. The plume was repeatedly intercepted on the eastern side of the box.

Figure 6 shows a number of time series plots during the Syncrude box (for the detailed timing of the altitude legs see Appendix A). The fine-mode AOD is reproduced on several plots to facilitate the comparisons. From top to bottom are: a) total, fine and coarse mode AODs at 500 nm derived from the SDA of the 4Star data; b) UHSAS total particle concentration (all sizes), particles/cm^3, c) size-resolved UHSAS-NRC particle concentrations, particles/cm^3; d) black carbon concentrations from SP2, counts; e) total particle count from CPC, counts.

The 4STAR measurements show that for the duration of the Syncrude box the total AOD was relatively low and stable around 0.05-0.07, except for the narrow duration AOD peaks of up to 0.45 associated with the plume on the eastern side of the box. All 7 transects of the plume can be readily detected in the in-situ data with the associated peaks in BC, UHSAS and CPC signals. The AOD peaks, on the other hand, can be clearly identified only at 500, 750, 1250 and 1500 ft. The peak at 1000 ft was likely missed because of the 4STAR performing a sky scan, while for the 1750 and 2000 ft the 4STAR signal was likely too weak to be distinguished from the background level. It should be noted that the BC peaks while corresponding approximately in time with the peaks in other instruments are delayed on average by as much as 2-3 minutes relative to the latter. This phenomenon is being investigated.

The SDA results show that with the exception of several coarse-mode peaks the detected plume is essentially fine mode (submicron) in nature. The UHSAS data corroborates this finding: while in the plume, the UHSAS particle concentrations were mostly enhanced in the lowest part of the size spectra from 60 to ~150 nm (Figure 7). It can be seen that the particle concentrations inside the plume could be more than 3 times higher than the level-averaged values.

In order to study the vertical distribution of the plume, the Convair-580 performed a spiral up maneuver from 17:23 to 17:35 increasing in altitude from 500 to 1900 m ASL. The aircraft was going in and out of the plume as can be seen in Figure 8 but the AOD peaks could still be detected as high as 1600 m. Figure 9 presents a more detailed look at the spiral data. The fine-mode AOD peaks centered around 17:23:30, 17:25:00 and 17:27:00 (altitude range between 500 and 1000 m) all show relatively high maximum AOD values between ~0.5 and 0.7. The signal expectedly decreases with altitude with the last detectable fine-mode AOD peak of ~0.09 occurring at 1800 m. Several regularly appearing coarse-mode peaks could also be identified, primarily at 17:24, 17:26 and 17:28. While the coarse-mode peaks are often associated with clouds, other sources are required (such as in-situ information on super micron particle size distribution) to label these peaks as such. It can be seen (Figure 9, pane 3) that the UHSAS PSD spectra is different during the spiral maneuver than during the box patterns inasmuch as UHSAS PSD during the spiral is essentially bimodal with significant contributions from particles in the 150 to 500 nm size range (bottom of Figure 7).

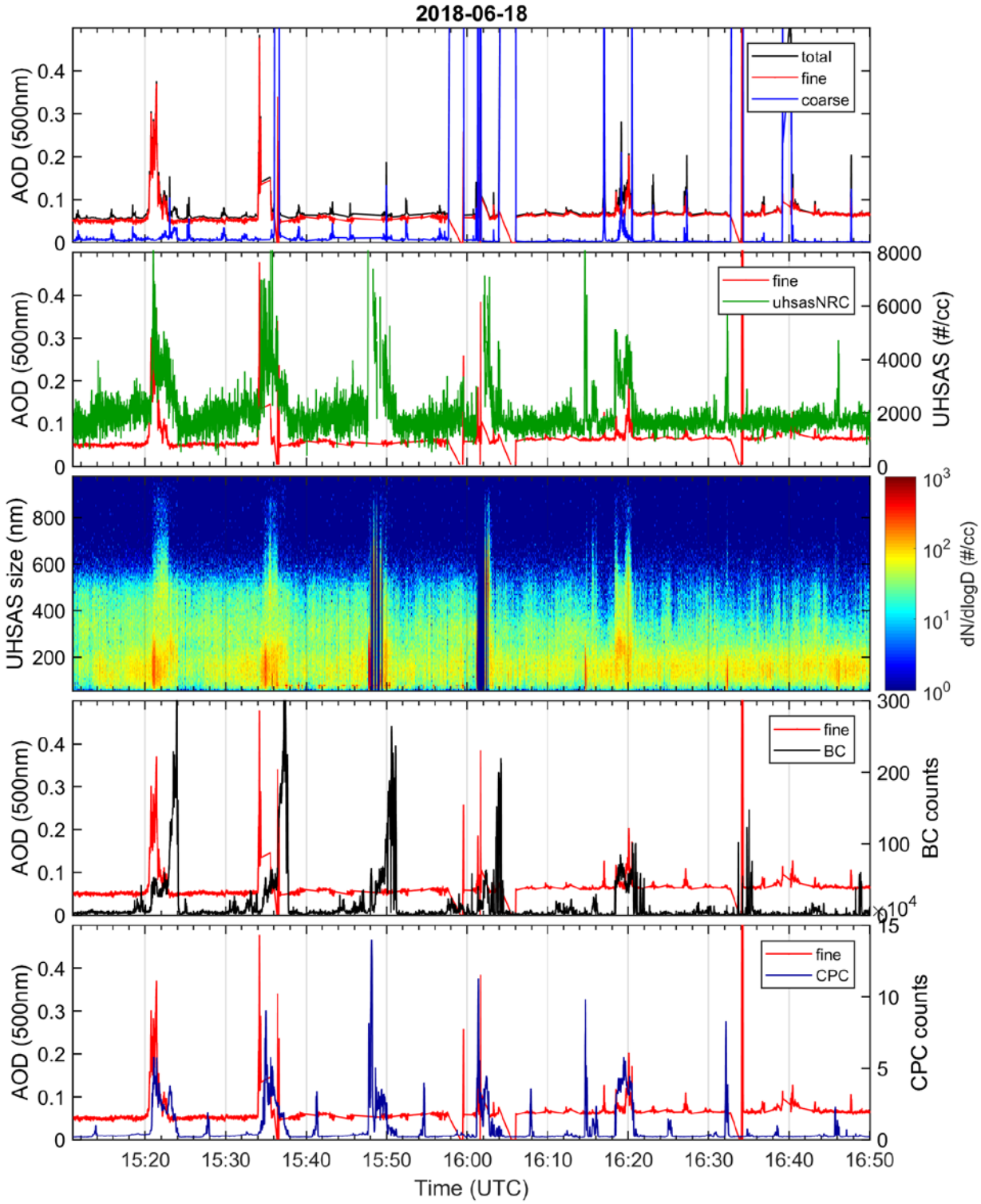

Figure 6. From top to bottom: SDA dynamics; fine-mode AOD and UHSAS-NRC total particle count; size-resolved UHSAS-NRC particle concentrations; fine-mode AOD and black carbon; fine-mode and CPC counts. See text for more details.

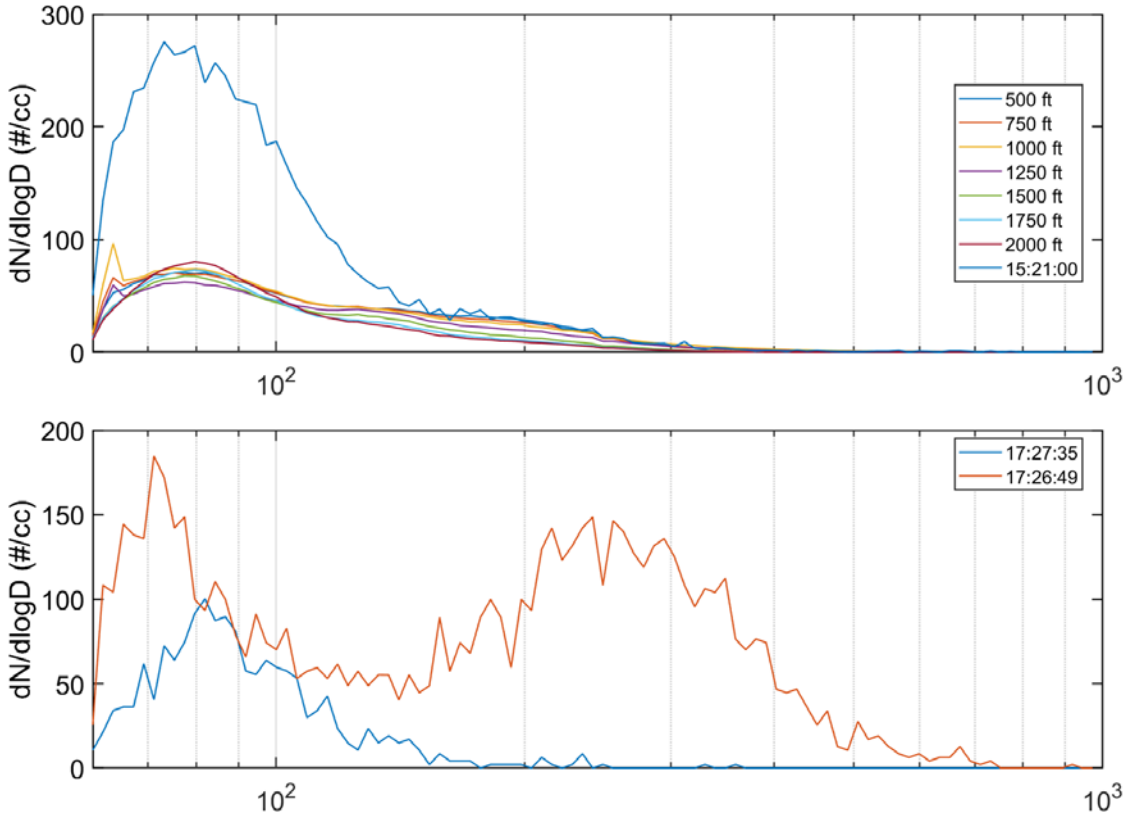

Figure 7. UHSAS size spectra. Top: averaged particle size distributions for each of the 7 nominal altitudes. A 7-second averaged size spectrum centered around 15:21:00 is also shown corresponding to the time when the plume was intercepted at 500 ft. Bottom: averaged size spectra corresponding to inside (17:26:49) and outside (17:27:35) of the main plume when performing a spiral up maneuver. A shorter integration time of 3 seconds was used as the aircraft was coming in and out of the plume.

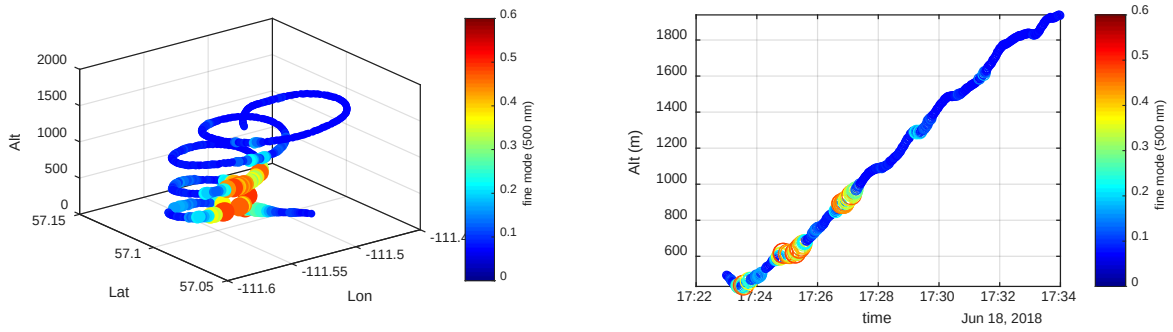

Figure 8. Fine-mode dynamics during a spiral maneuver on the eastern side of the Syncrude Mildred Lake box. Default cloud screening.

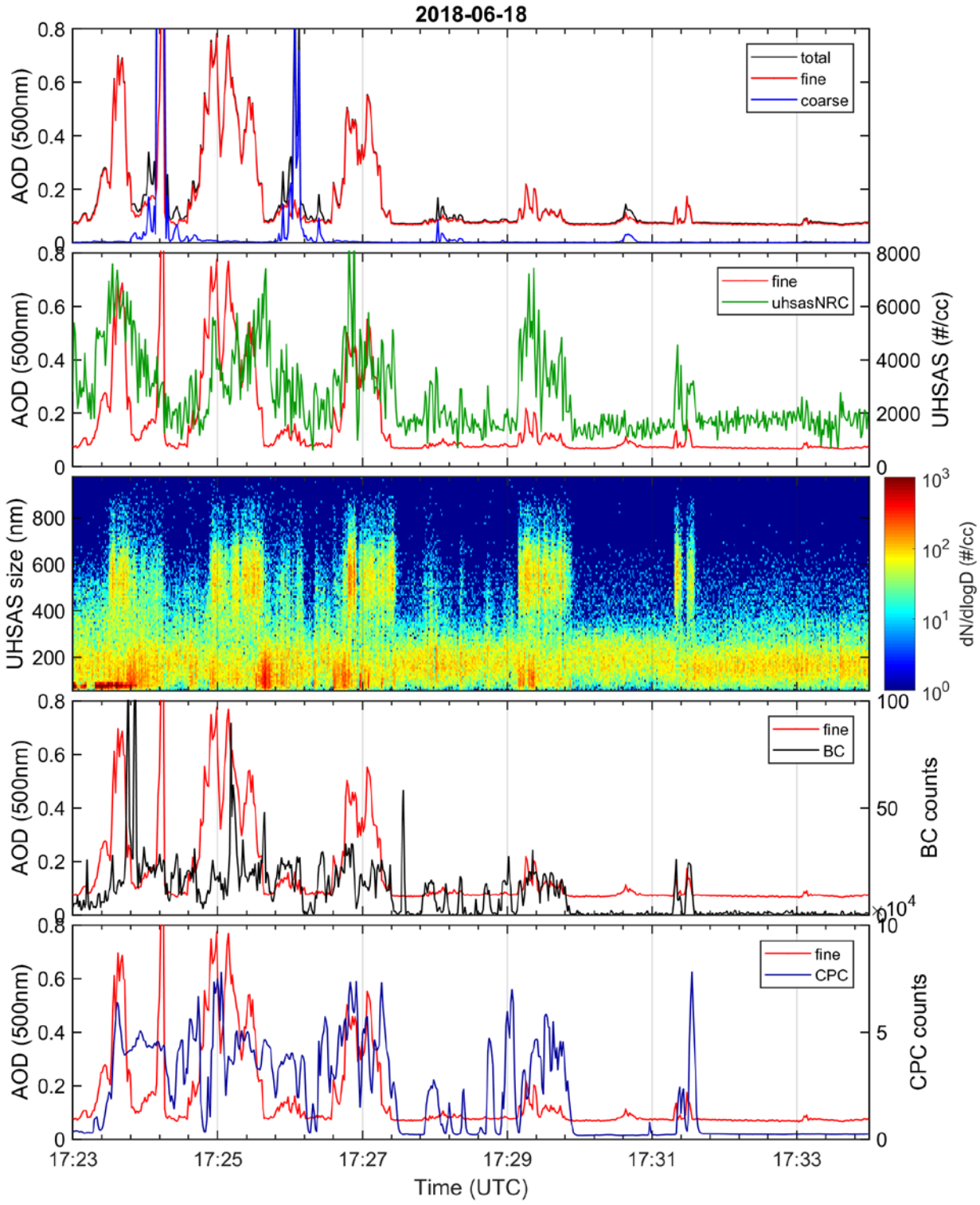

Figure 9. Description as in Figure 6 but for the spiral up maneurve on the eastern side of the emissions box between 17:23 and 17:35.

Syncrude Mildred Lake transformation flight – June 9, 2018

On June 9 (NRC flight 28/ECCC flight 14) the Convair-580 conducted a transformation flight to the west of the Oil Sands facilities. With the winds blowing from the south west, the aircraft flew 4 screens set up perpendicular to the wind direction intercepting the emission plumes from Syncrude Mildred Lake and the CNRL Horizon. At the start of the first screen closest to the facilities, the SML plume was perceived as visually opaque with the spatial boundaries clearly identifiable by the pilots (Figure 10). The source of the plume could also be traced back to the distinct chimney stacks of SML.

Figure 10. Photographic imagery from the flight. The right-hand side photo taken at the end of the flight shows the plume source originating at the Suncrude Mildred Lake facility.

For each screen the aircraft flew at multiple nominal altitudes with 4 common ones being 500, 750, 1000 and 1250 ft above ground (see Appendix A for details). Several spirals were also performed where the plume was considered to be the strongest based on the instrumentation readings. Figure 11 shows the flight track for June 9 as well as all fine-mode AODs measured in-flight.

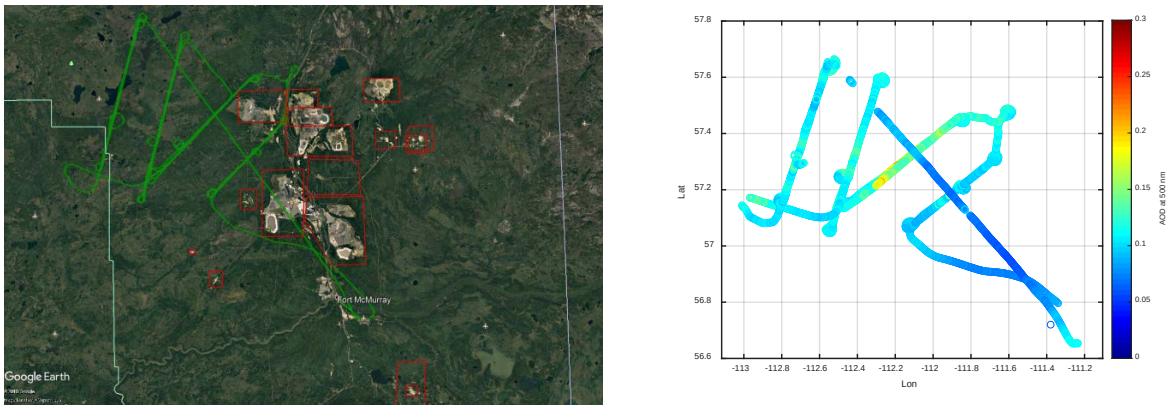

Figure 11. Same description as in Figure 5 but for June 9 (NRC flight 28/ECCC flight 14).

While the first screen was relatively cloudless, the cloud cover increased as the flight progressed reaching almost a complete overcast by the end of the flight. Consequently, the 4STAR data for screens 3 and 4 is heavily contaminated by clouds and is of limited value. Figure 12 shows vertically-resolved fine-mode AOD values for each screen while Figure 13 and Figure 14 show time series plots for screens one and two, respectively (similar plots for screens 3 and 4, heavily

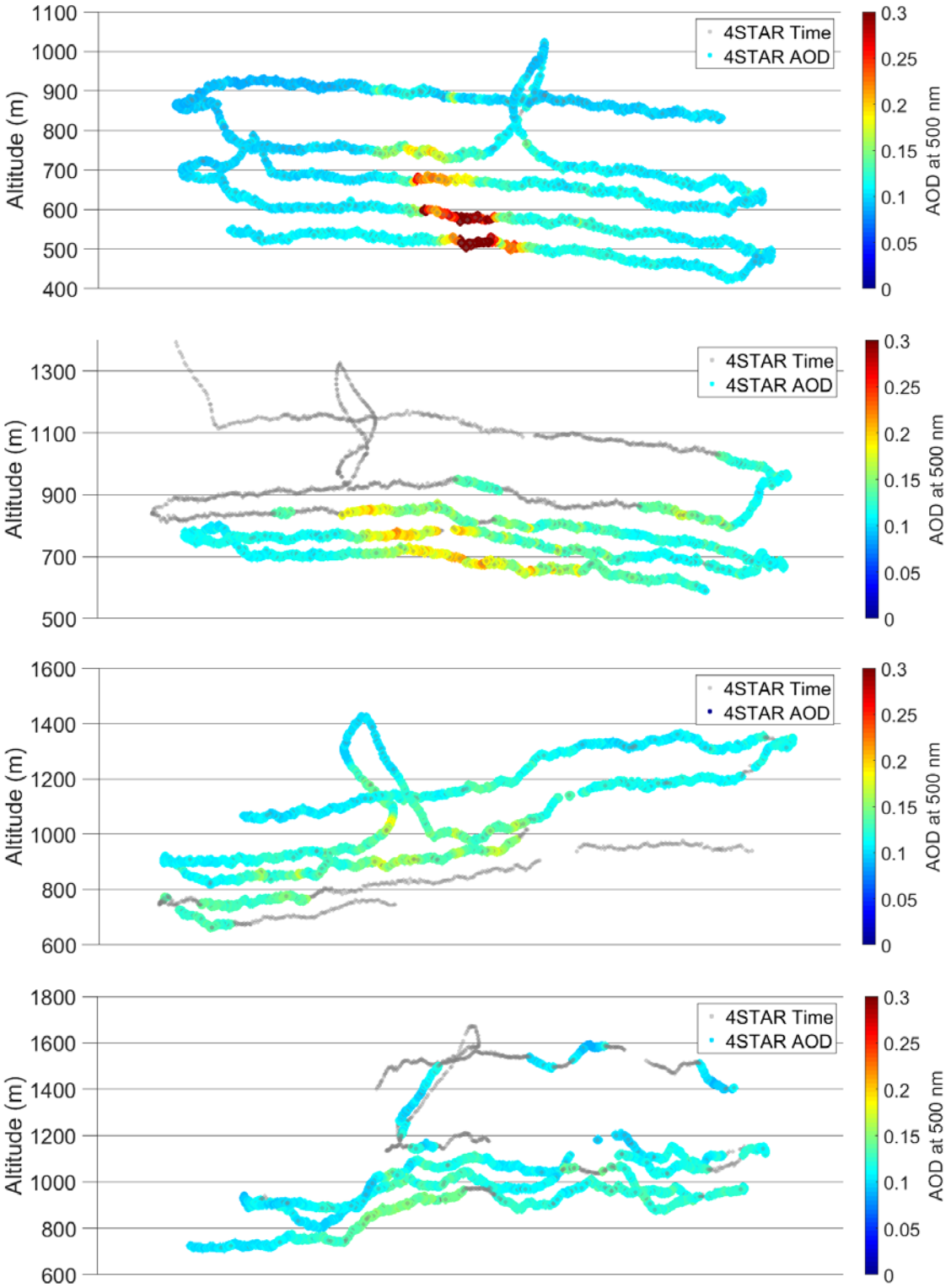

Figure 12. Fine mode AOD dynamics for transformation screens 1 to 4 (top to bottom). The X-axis is parallel to the flight track.

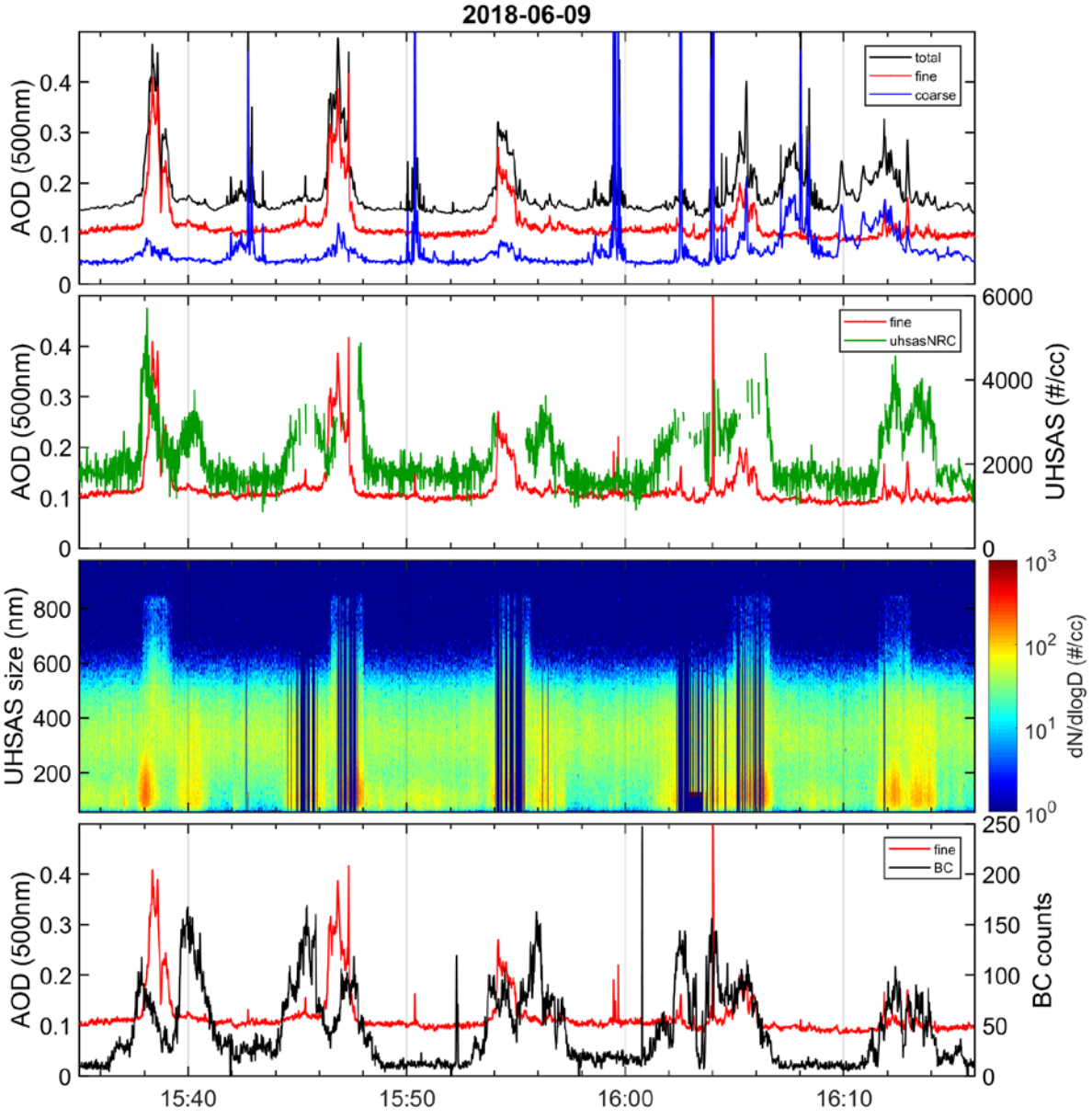

Figure 13. Screen 1 time series on June 9. Description as in Figure 6 for the first 4 panes.

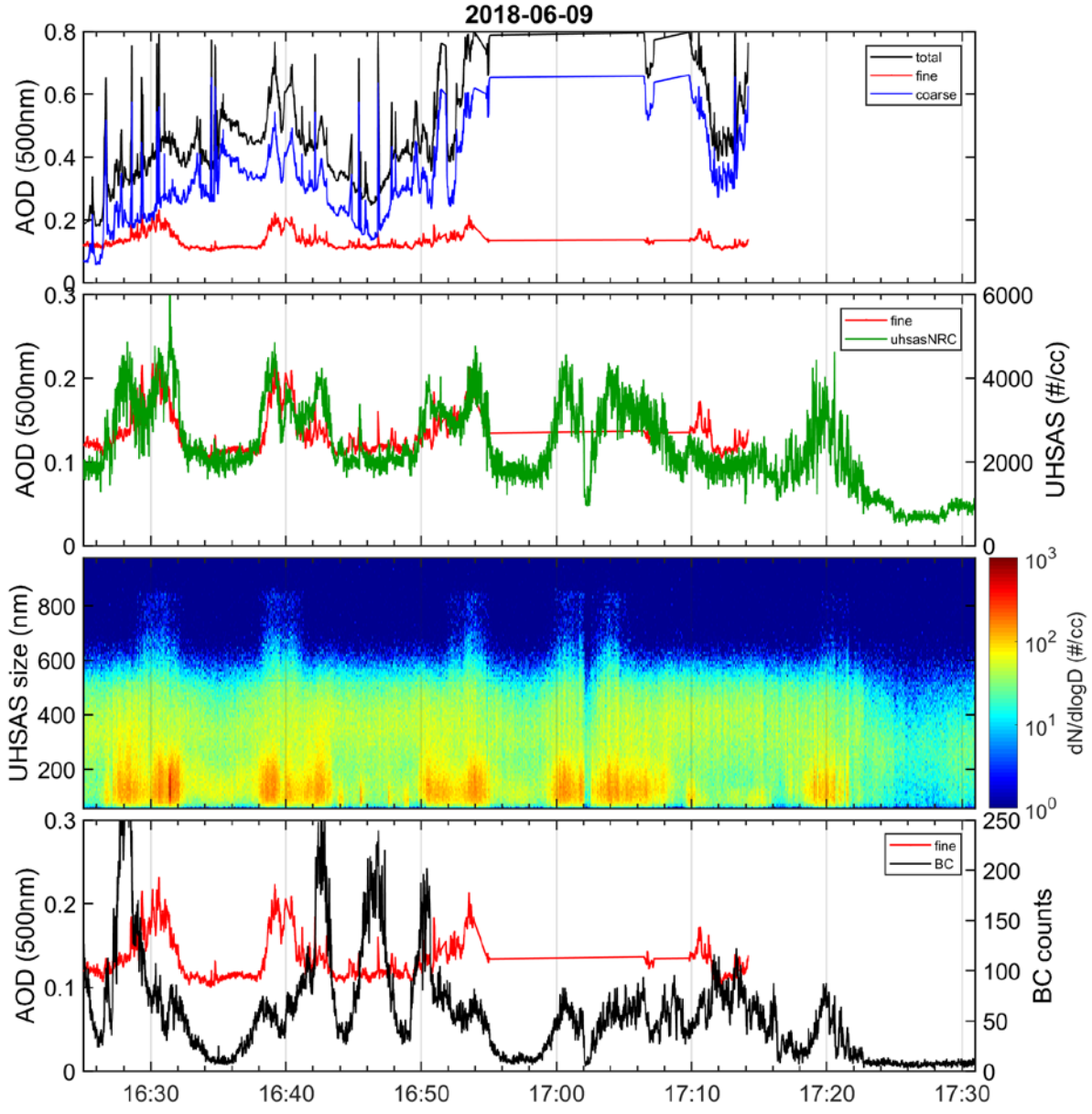

Figure 14. Screen 2 time series on June 9. Description as in Figure 13. Default cloud screening applied.

influenced by clouds, are presented in Appendix A). The top panel of Figure 13 shows that the Syncrude plume could be clearly identified in the 4STAR data near the middle of the track at each of the altitude levels during screen 1. With the average fine-mode AODs of ~0.10 outside of the plume, the values reached as high as 0.4 within the plume. During screen 2 (Figure 14), established ~20 km to the west of screen 1, the signal is dominated by the coarse-mode AOD (likely clouds). However, the fine mode dynamics appear to be real and coherent with UHSAS total particle concentration (and to a lesser extent BC concentrations) at least for the first 2-3 altitudes. The highest fine-mode AODs are ~0.2 for screen 2 suggesting that the plume has been diluted as it moved away from the source. On the other hand, the average τ_f values remained around ~0.11 whenever outside of the main plume.

Turning to the analysis of the UHSAS PSD data (Figure 15), certain differences between screens 1 and 2 can be observed. For screen 1, the averaged PSDs match very closesly for all alitude levels and show comparable particles concentrations of 40-60 cm^{-3} for sizes between 60 and 150 nm, tailing off gradually with insignificant concentrations after 350 nm. As in the June 18 case, whenever inside the plume, the data shows a significant increase (for certain sizes a factor of 3) in smaller size aerosols between 60 and 150 nm. Comparing data between screens 1 and 2 shows that the maximum particle concentrations in the plume are higher for screen 1, but the averaged PSDs for screen 2 have greater values in the 60-150 nm range at all altitudes with the exception of the 2000 ft results.

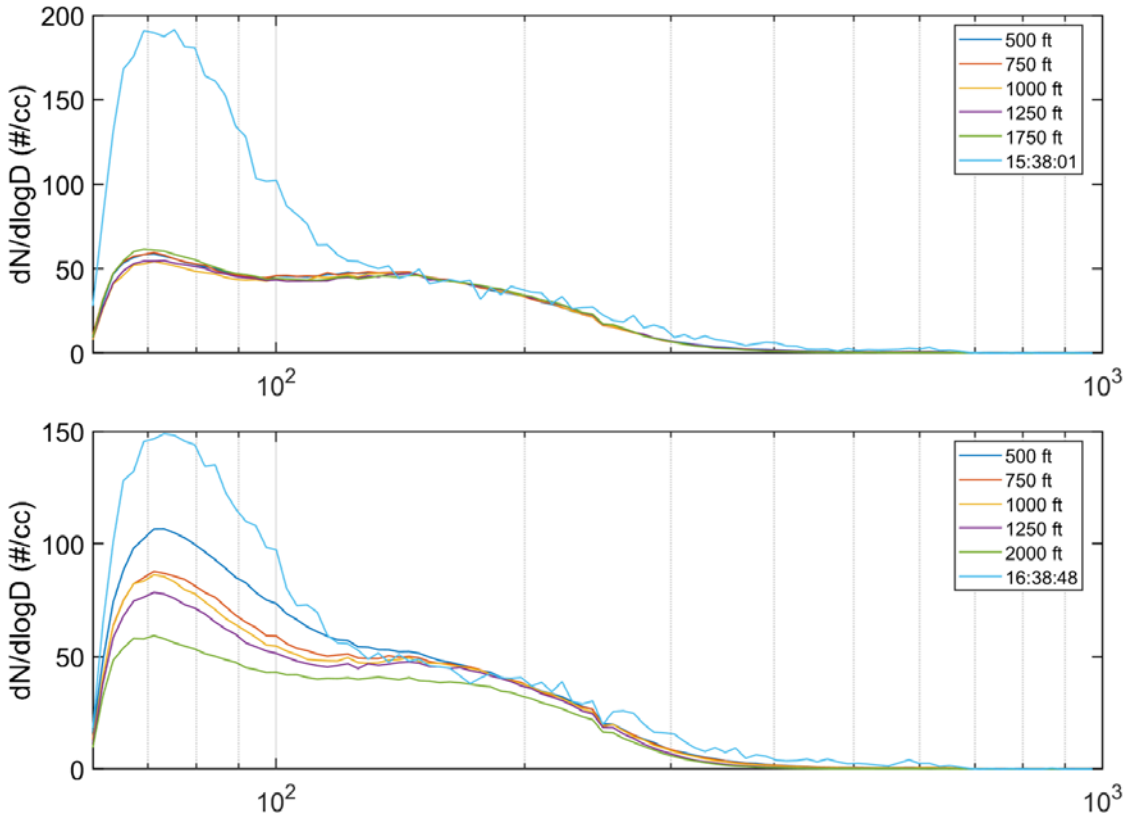

Figure 15. Averaged UHSAS particle size distributions for each of the 5 nominal altitudes during screen 1 (top) and screen 2 (bottom). Also shown are 7-second averaged spectra while inside the plume at 500 ft during screen 1 (15:38:01) and screen 2 (16:38:48).

In addition, during screen 2 there is a significantly greater spread between the altitude-averaged PSDs, with the highest concentrations at 500 ft and decreasing with each consecutive leg. This is indicative of a larger vertical variability as the plume spatially disperses and thins out. The AOD dynamics are less clear for the remaining screens because of the more significant cloud cover.

Summary, conclusions and outlook

During Phase II of the OSMC 2018, the NASA 4STAR hyperspectral sunphotometer was flown on each of the 24 science flights, acquiring close to 100 hours of aerosols and trace gas data. The 4STAR was predominantly run in the sun-tracking mode with occasional sky radiance measurements. It was operated in tandem with a comprehensive suite of in-situ instruments, including DMT UHSAS (particle sizer and counter), DMT SP2 (black carbon mass and particle sizer) and TSI CPC (total particle counter). Two types of flights were performed during the OSMC: emissions and transformation flights, resulting in "box" and "screen" flight patterns, respectively. The former were directed at characterizing pollution emissions from individual facilities, while the latter aimed at studying the fate of the pollutants as they got transported away from the source. Based on data availability and the observed features we identified 4 transformation (June 9, June 24, June 25 and July 5) and 2 emissions (June 18 and June 20) flights that were likely to have the most potential for scientific analysis.

Based on the analysis of two representative flights from the campaign (June 18 emission flight and June 9 transformation flight) several observations about 4STAR performance could be made. For the June 18 emissions flight around the Syncrude Mildred Lake facility, the 4STAR measurements show that the total AOD was relatively low and stable around 0.05-0.07, except for the short duration AOD peaks of up to 0.45 associated with the clearly visible plume intercepted on the eastern side of the box. The AOD peaks were generally correlated in time with in-situ peaks, except for BC, where the latter were on average delayed by 2-3 minutes. The results from Spectral Deconvolution Algorithm applied to the 4STAR data show that the plume is essentially fine mode (submicron) in nature. The UHSAS data corroborates this finding: while in the plume, the UHSAS particle counts were mostly enhanced (by as much as 3 times) in the lowest part of the size spectra from 60 to ~150 nm. During the spiral maneuver performed on the eastern side of the box, the 4STAR fine-mode peaks of up to 0.7 continued to be correlated in time and amplitude with the UHSAS total particle concentrations, but the UHSAS size distribution showed a significant contribution from particles in the 150 to 500 nm size range – something not seen while flying in a box pattern.

For the June 9 flight, the Convair-580 flew 4 screens set up perpendicular to the wind direction intercepting the emission plumes from Syncrude Mildred Lake and the CNRL Horizon. While the first screen was relatively cloudless, the cloud cover increased as the flight progressed reaching almost a complete overcast by the end of the flight. The data shows that the Syncrude plume could be clearly identified in the 4STAR data near the middle of the track at each altitude level during screen 1. With the average fine-mode AODs of ~0.10 outside of the plume, the values reached as high as 0.40 within the plume. For the same screen, the averaged UHSAS PSDs matched very closely between alitude levels and showed that most particles were in the 60 to 200 nm size range. For screen 2, established ~20 km to the west of screen 1, the highest fine-mode AODs were ~0.20 indicating that the plume has been diluted as it moved away from the source. Compared to screen 1, averaged PSDs for screen 2 had greater particle concentrations in the 60-150 nm range at all altitudes except the 2000 ft. Additionally, there was a significantly greater spread between the altitude-averaged PSDs, with the highest counts at 500 ft and decreasing with each consecutive leg.

In these and other cases, 4STAR was able to detect aerosol plumes emanating from industrial sources or resulting from forest fires and characterize the aerosol loading in terms of fine and coarse-mode contributions. In general, 4STAR derived AOD peaks associated with a plume were temporally correlated with in-situ measurements giving more credence to the observed 4STAR dynamics. The analysis presented in this document constitutes a first step in the processing of the 4STAR data. Future work will include:

- Application of the final calibration values
- Quality control and enhanced cloud screening
- Analysis of the 4STAR sky radiance measurements and their quality
- Analysis of the 4STAR trace gas retrievals and their quality
- Comparisons between 4STAR and in-situ optical measurements obtained with a nephelometer and Continuous Light Absorption Photometer (CLAP).

Acknowledgements

Funding for the NRC Convair-580 participation in the Oil Sands 2018 field project was provided by ECCC and NRC. We would like to acknowledge the NRC and ECCC project crew that supported the field project. We also acknowledge Warren Gore from NASA for his efforts in bringing the 4STAR to Canada for the duration of the project.

References:

Cai, Y., D. Montague, W. Mooiweer-Bryan, and T. Deshler, "Performance characteristics of the ultra high sensitivity aerosol spectrometer for particles between 55 and 800 nm: Laboratory and field studies," Journal of Aerosol Science 39 (2008) 759-769.

Cimel, 2015, Multiband photometer CE318-N, User's manual, Revision 5.0, April 2015, 70 p.

Dubovik, O. and M. D. King, 2000: A flexible inversion algorithm for retrieval of aerosol optical properties from Sun and sky radiance measurements, J. Geophys. Res., 105, 20 673-20 696

Dunagan, S.E.; Johnson, R.; Zavaleta, J.; Russell, P.B.; Schmid, B.; Flynn, C.; Redemann, J.; Shinozuka, Y.; Livingston, J.; Segal-Rosenhaimer, M. Spectrometer for Sky-Scanning Sun-Tracking Atmospheric Research (4STAR): Instrument Technology. *Remote Sens.* 2013, *5*, 3872-3895.

Holben, B. N., T. F. Eck, I. Slutsker, D. Tanré, J. P. Buis, A. Setzer, E. Vermote, J. A. Reagan, Y. J. Kaufman, T. Nakajima, F. Lavenu, I. Jankowiak, and A. Smirnov (1998), AERONET—a federated instrument network and data archive for aerosol characterization, Remote Sensing of Environment, 66 (1), 1–16.

Kaufman, Y. J., D. Tanré, and O. Boucher (2002), A satellite view of aerosols in the climate system., Nature, 419 (6903), 215–23, doi:10.1038/nature01091.

Kupc, A., Williamson, C., Wagner, N. L., Richardson, M., and Brock, C. A.: Modification, calibration, and performance of the Ultra-High Sensitivity Aerosol Spectrometer for particle size distribution and volatility measurements during the Atmospheric Tomography Mission (ATom) airborne campaign, Atmos. Meas. Tech., 11, 369-383, https://doi.org/10.5194/amt-11-369-2018, 2018.

Li et al, 2017, Differences between measured and reported volatile organic compound emissions from oil sands facilities in Alberta, Canada, Proceedings of the National Academy of Sciences May 2017, 114 (19) E3756-E3765; DOI: 10.1073/pnas.1617862114

Liu, D., Flynn, M., Gysel, M., Targino, A., Crawford, I., Bower, K., Choularton, T., Jurányi, Z., Steinbacher, M., Hüglin, C., Curtius, J., Kampus, M., Petzold, A., Weingartner, E., Baltensperger, U., and Coe, H.: Single particle characterization of black carbon aerosols at a tropospheric alpine site in Switzerland, Atmos. Chem. Phys., 10, 7389-7407, https://doi.org/10.5194/acp-10-7389-2010, 2010.

Liggio J, et al. (2016) Oil sands operations as a large source of secondary organic aerosols. Nature 534:91–94.

O'Neill, N. T., T. F. Eck, A. Smirnov, B. N. Holben, and S. Thulasiraman (2003), Spectral discrimination of coarse and fine mode optical depth, *J. Geophys. Res.*, 108, 4559, doi: 10.1029/2002JD002975, D17.

O'Neill, N. T., Baibakov, K., Hesaraki, S., Ivanescu, L., Martin, R. V., Perro, C., Chaubey, J. P., Herber, A., and Duck, T. J.: Temporal and spectral cloud screening of polar winter aerosol optical depth (AOD): impact of homogeneous and inhomogeneous clouds and crystal layers on climatological-scale AODs, Atmos. Chem. Phys., 16, 12753-12765, https://doi.org/10.5194/acp-16-12753-2016, 2016.

Russell, P. B., et al. (1993), Pinatubo and pre-Pinatubo optical-depth spectra: Mauna Loa measurements, comparisons, inferred particle size distributions, radiative effects, and relationship to lidar data, *J. Geophys. Res.*, 98(D12), 22969–22985, doi:10.1029/93JD02308.

Schwarz, J. P., et al. (2006), Single-particle measurements of midlatitude black carbon and light-scattering aerosols from the boundary layer to the lower stratosphere, J. Geophys. Res., 111, D16207, doi:10.1029/2006JD007076.

Segal-Rosenheimer, M., et al. (2014), Tracking elevated pollution layers with a newly developed hyperspectral Sun/Sky spectrometer (4STAR): Results from the TCAP 2012 and 2013 campaigns, *J. Geophys. Res. Atmos.*, 119, 2611–2628, doi: 10.1002/2013JD020884.

Seinfeld, J. H., and S. N. Pandis (2006), Atmospheric Chemistry and Physics. From Air Pollution to Climate Change, 2 ed., 1232 pp., John Wiley & Sons, Hoboken, NJ.

Shaw, G. E., J. A. Reagan, and B. M. Herman (1973), Investigations of atmospheric extinction using direct solar radiation measurements made with a multiple wavelength radiometer, Journal of Applied Meteorology, 12 (2), 374–380.

Shaw, G. E. (1983), Sun photometry, Bulletin of the American Meteorological Society, 64 (1), 4–10.

Shinozuka, Y., et al. (2013), Hyperspectral aerosol optical depths from TCAP flights, J. Geophys. Res. Atmos., 118, 12,180–12,194, doi:10.1002/2013JD020596.

Smirnov, A., B.N.Holben, T.F.Eck, O.Dubovik, and I.Slutsker (2000), Cloud screening and quality control algorithms for the AERONET database, Rem.Sens.Env., 73, 337–349

Appendix A – Primary 4STAR flights

June 09, 2018 – Syncrude Mildred Lake Transformation flight

Observations

- The plume can be readily identified at all of the 5 heights during screen 1 with AODs as high as 0.4. The total AOD is dominated by the fine-mode
- During screen 2 the signal is dominated by the coarse-mode AOD (likely clouds). However, the fine mode dynamics seems to be real and coherent with UHSAS total count variations at least for the first 2-3 heights.
- Beyond screens 2 and 3, that data is heavily influenced by clouds
- No CPC data available during this flight

Flight maneuvers table

Table A1. Flight plan for June 9, 2018.

Date	NRC flight #	ECCC flight #	Flight pattern	Alt (ft)	From Time	To Time
2018/06/09	28	14	Take off		15:19:44	
Screen 1						
2018/06/09	28	14	transformation	500	15:35:00	15:41:36
2018/06/09	28	14	transformation	750	15:43:36	15:49:41
2018/06/09	28	14	transformation	1000	15:52:00	15:58:17
2018/06/09	28	14	transformation	1250	16:00:08	16:07:39
2018/06/09	28	14	spiral up		16:02:06	16:03:37
2018/06/09	28	14	spiral down		16:03:38	16:04:36
2018/06/09	28	14	transformation	1750	16:10:08	16:16:44
Screen 2						
2018/06/09	28	14	transformation	500	16:26:28	16:33:52
2018/06/09	28	14	transformation	750	16:35:54	16:45:21
2018/06/09	28	14	transformation	1000	16:47:34	16:56:26
2018/06/09	28	14	transformation	1250	16:58:12	17:11:22
2018/06/09	28	14	spiral up		17:00:39	17:02:24
2018/06/09	28	14	spiral down		17:02:25	17:04:32
2018/06/09	28	14	transformation	2000	17:13:53	17:22:13
2018/06/09	28	14	transformation	4500	17:25:30	17:31:01
Screen 3						
2018/06/09	28	14	transformation	500	17:35:47	17:46:30
2018/06/09	28	14	transformation	750	17:47:38	17:59:23

2018/06/09	28	14	transformation	1000	18:00:32	18:12:32
2018/06/09	28	14	transformation	1250	18:13:26	18:26:51
2018/06/09	28	14	spiral up		18:17:19	18:19:37
2018/06/09	28	14	spiral down		18:19:38	18:20:48
2018/06/09	28	14	transformation	1750	18:28:22	18:39:10
Screen 4						
2018/06/09	28	14	transformation	500	18:47:58	18:59:07
2018/06/09	28	14	transformation	750	19:01:02	19:11:44
2018/06/09	28	14	transformation	1000	19:12:17	19:23:08
2018/06/09	28	14	transformation	1250	19:24:19	19:37:50
2018/06/09	28	14	spiral up		19:32:24	19:34:19
2018/06/09	28	14	spiral down		19:34:20	19:35:25
2018/06/09	28	14	transformation	1750	19:38:48	19:48:16
2018/06/09	28	14	Landing			20:13:00

Flight imagery

Figure A1. Photographic imagery from the flight. The bottom photo taken at the end of the flight shows the plume source originating at the Suncrude Mildred Lake facility.

Comparisons with AERONET before/after flight

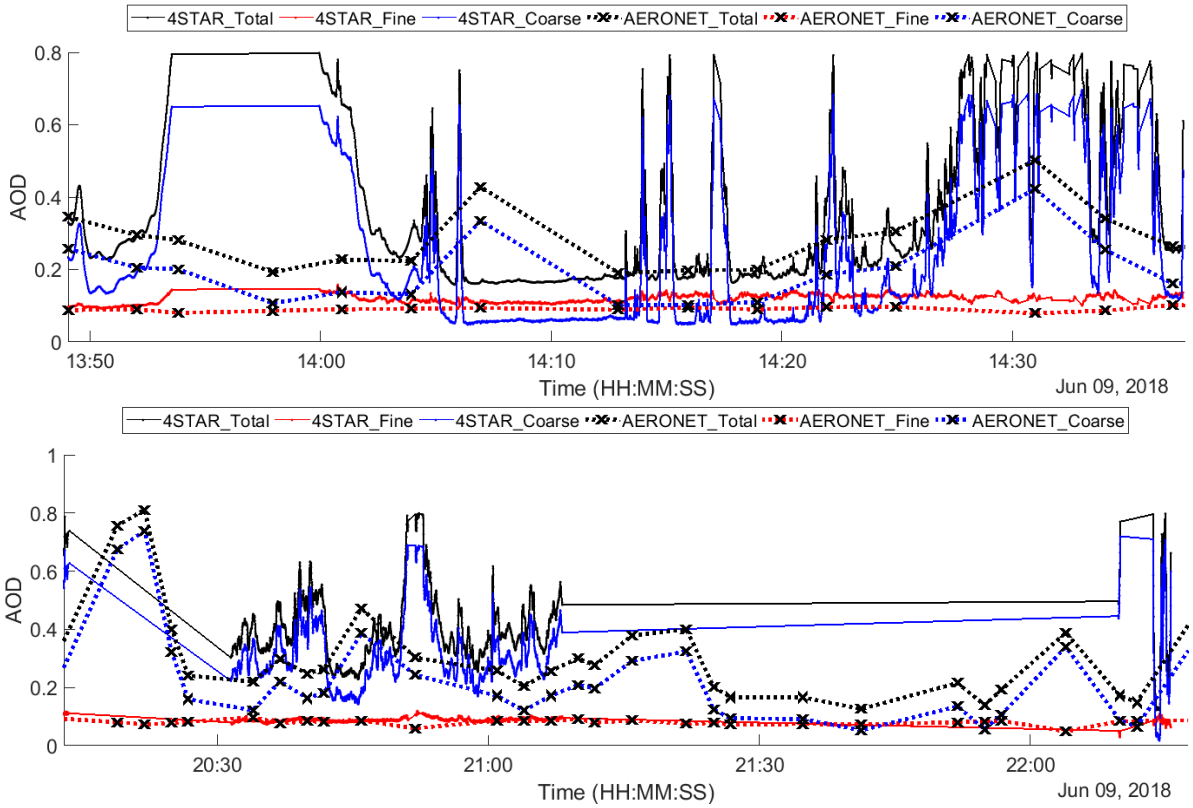

Figure A2. Comparisons with AERONET. Top: before the flight, bottom: after the flight. After the flight, the data was acquired on the ground with uncleaned optics until 21:30 and then with the cleaned optics starting at 22:10. Default 4STAR cloud screening.

Flight track

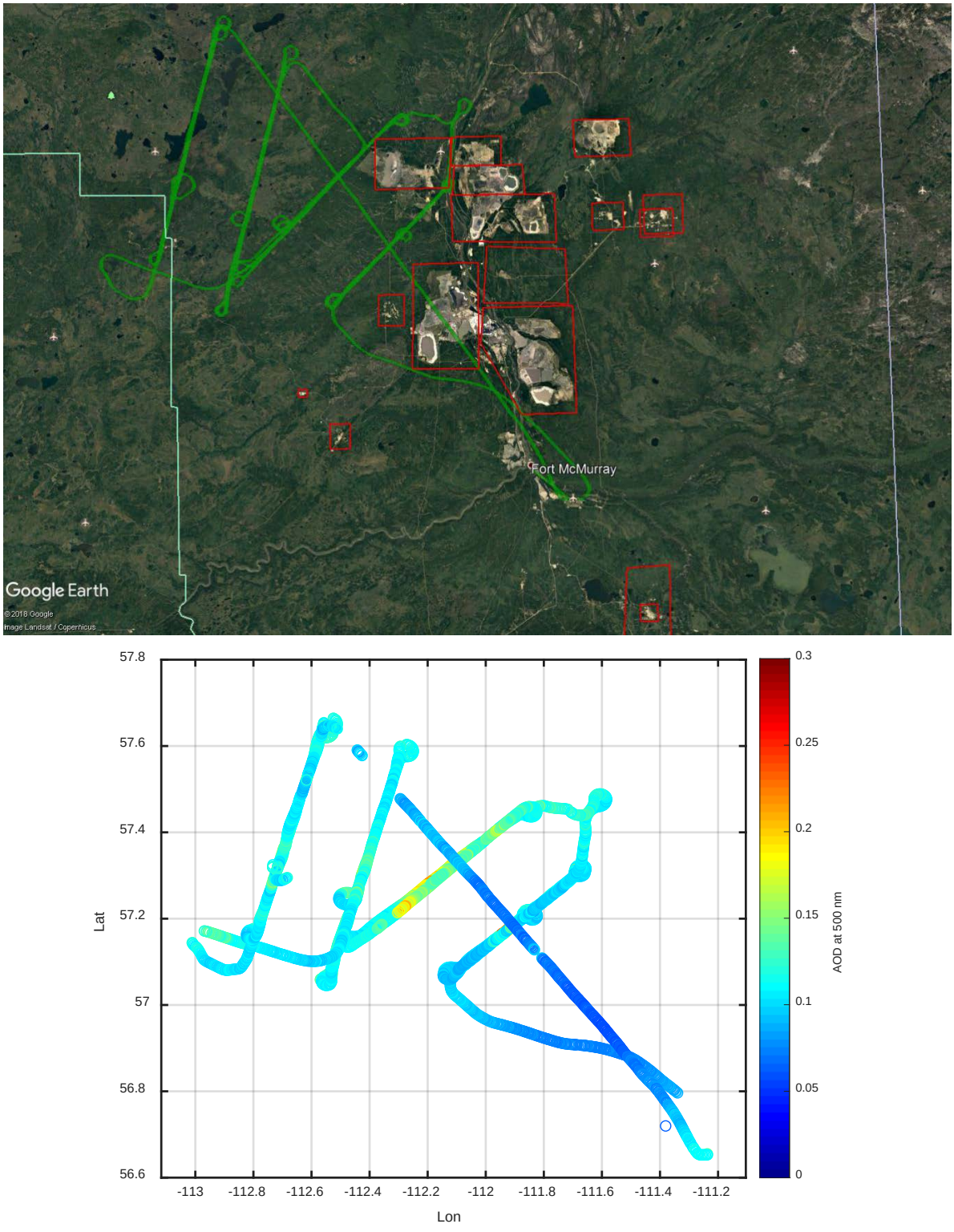

Figure A3. Top: Convair-580 flight path superimposed on the facilities map near Fort McMurray. Bottom: in-flight 4STAR AOD (fine mode).

AOD dynamics for each screen

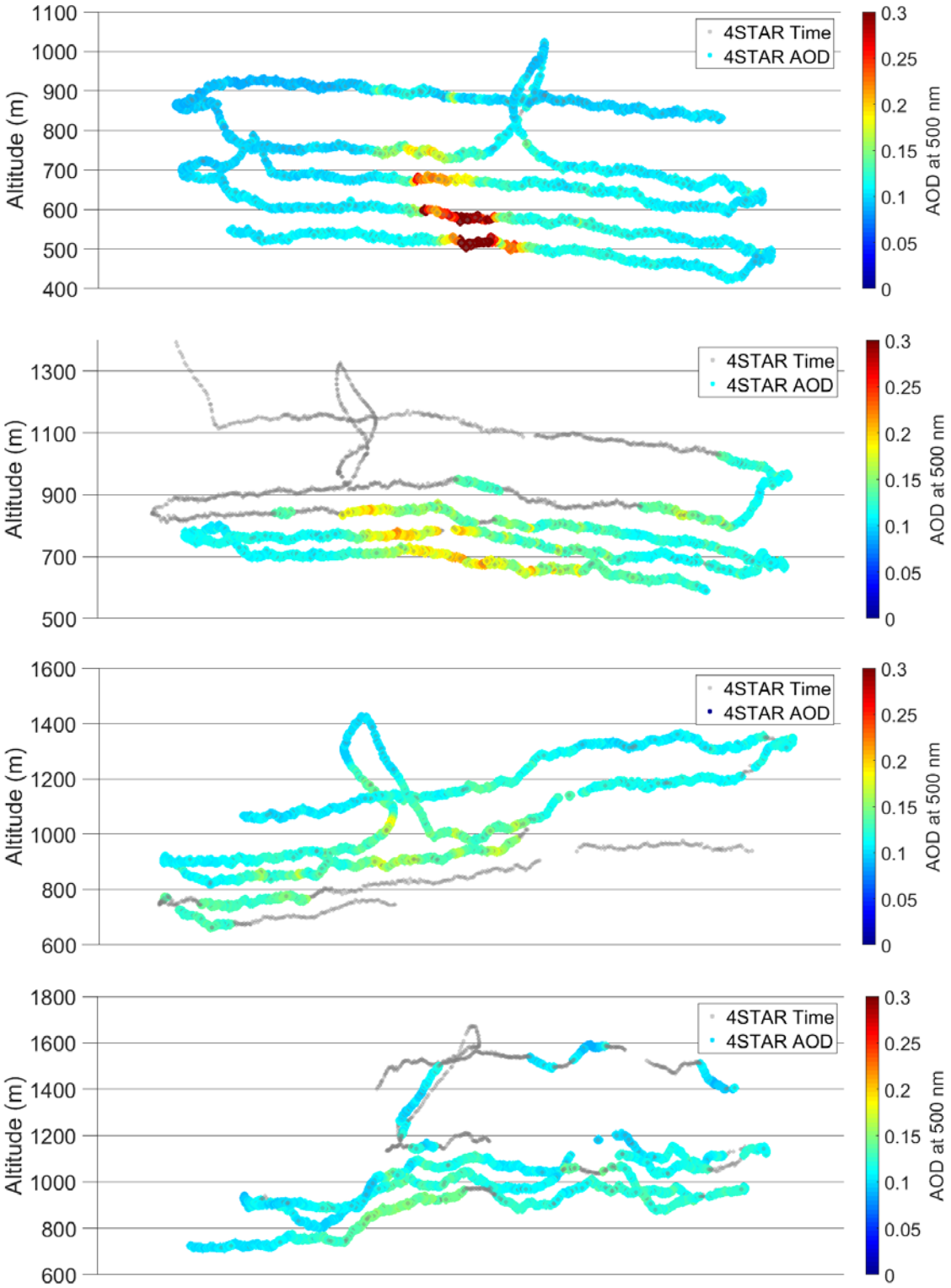

Figure A4. Fine mode AOD dynamics for transformation screens 1 to 4 (top to bottom). The X-axis is parallel to the flight track.

SDA dynamics and intercomparisons

Screen 1

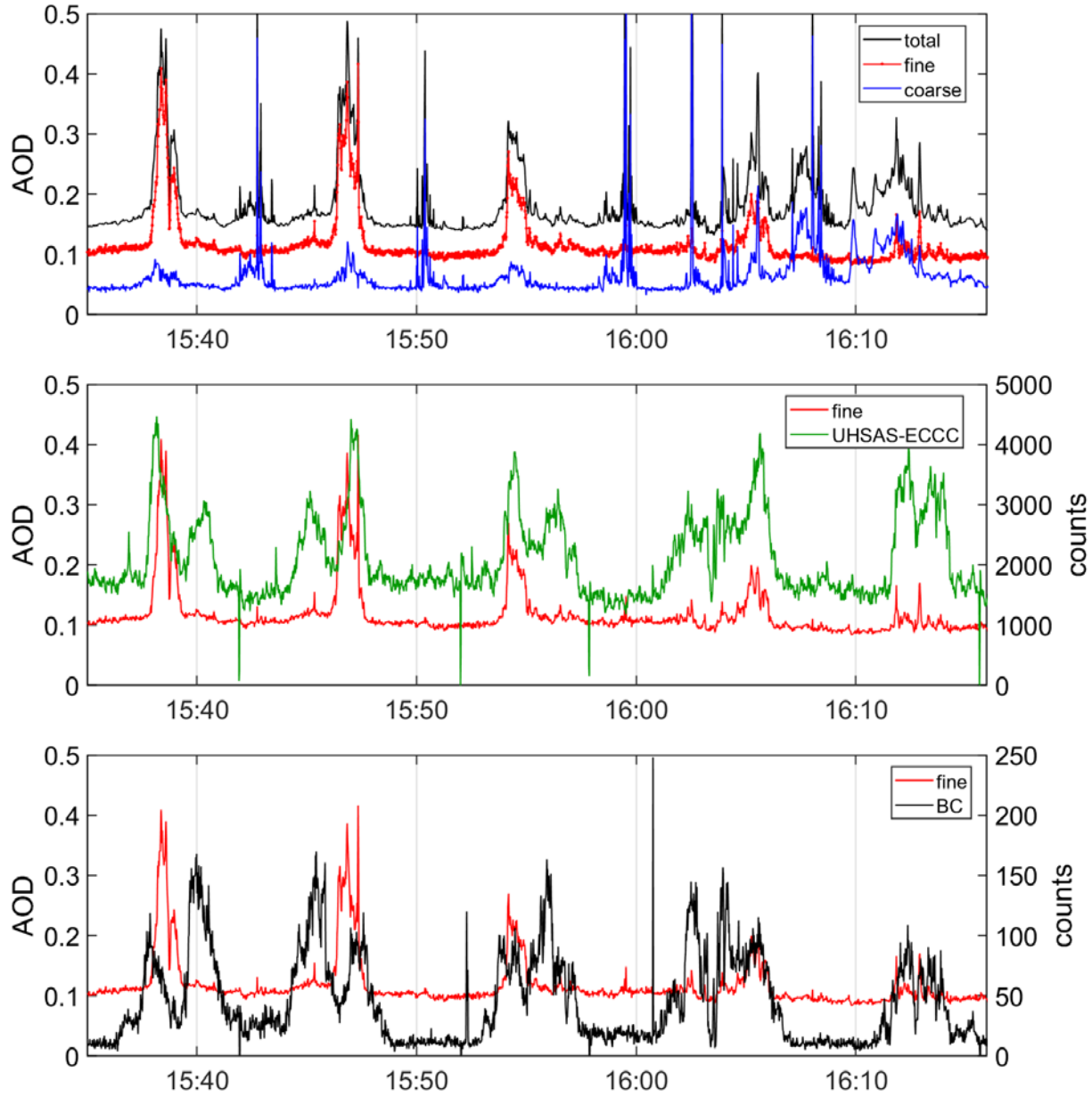

Figure A5. Screen 1 on June 9, 2018. From top to bottom: SDA dynamics; fine-mode AOD and UHSAS-ECCC; fine-mode AOD and black carbon

Screen 2

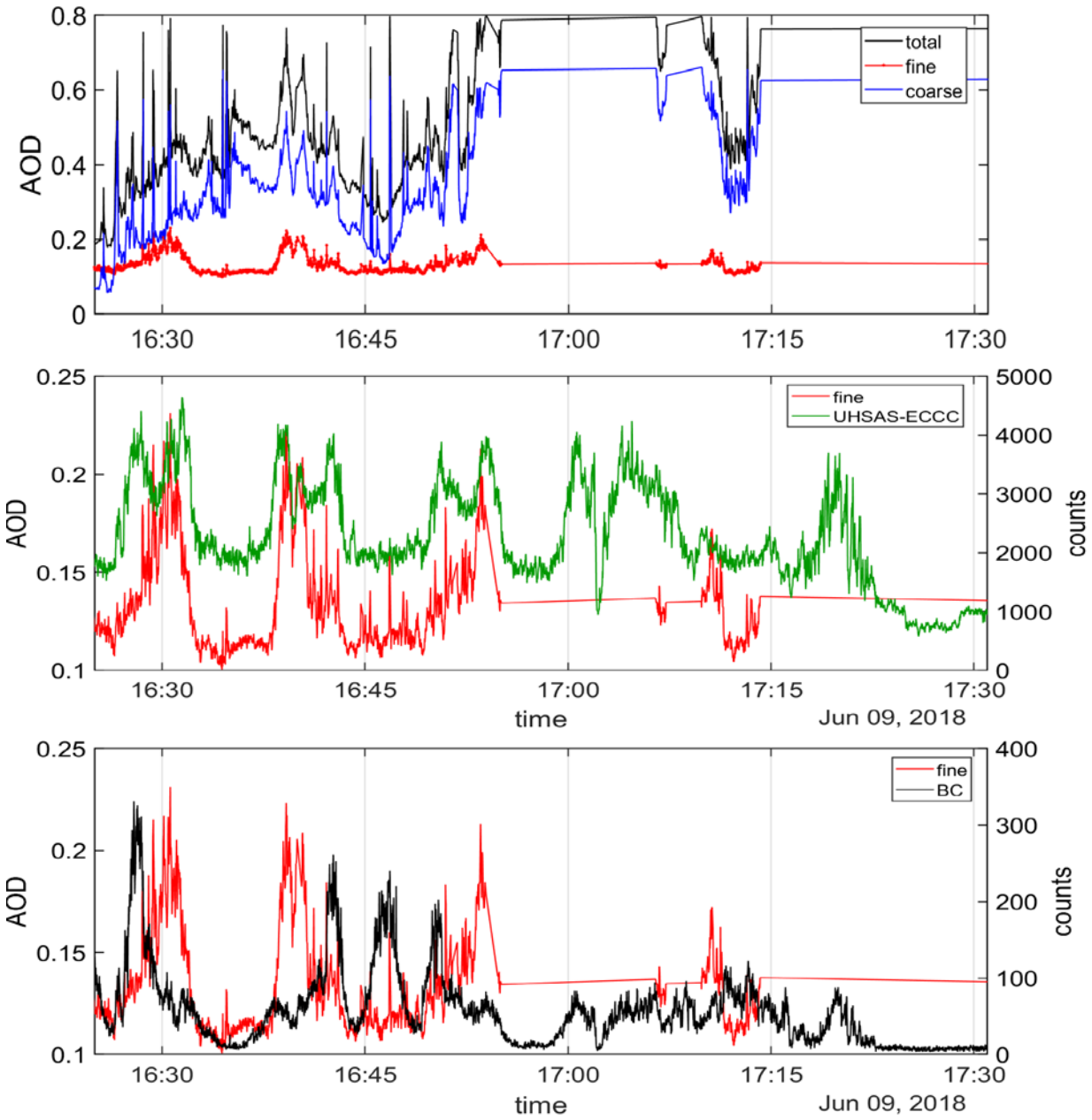

Figure A6. Screen 2 on June 9, 2018. Description as in Figure A5

Screen 3

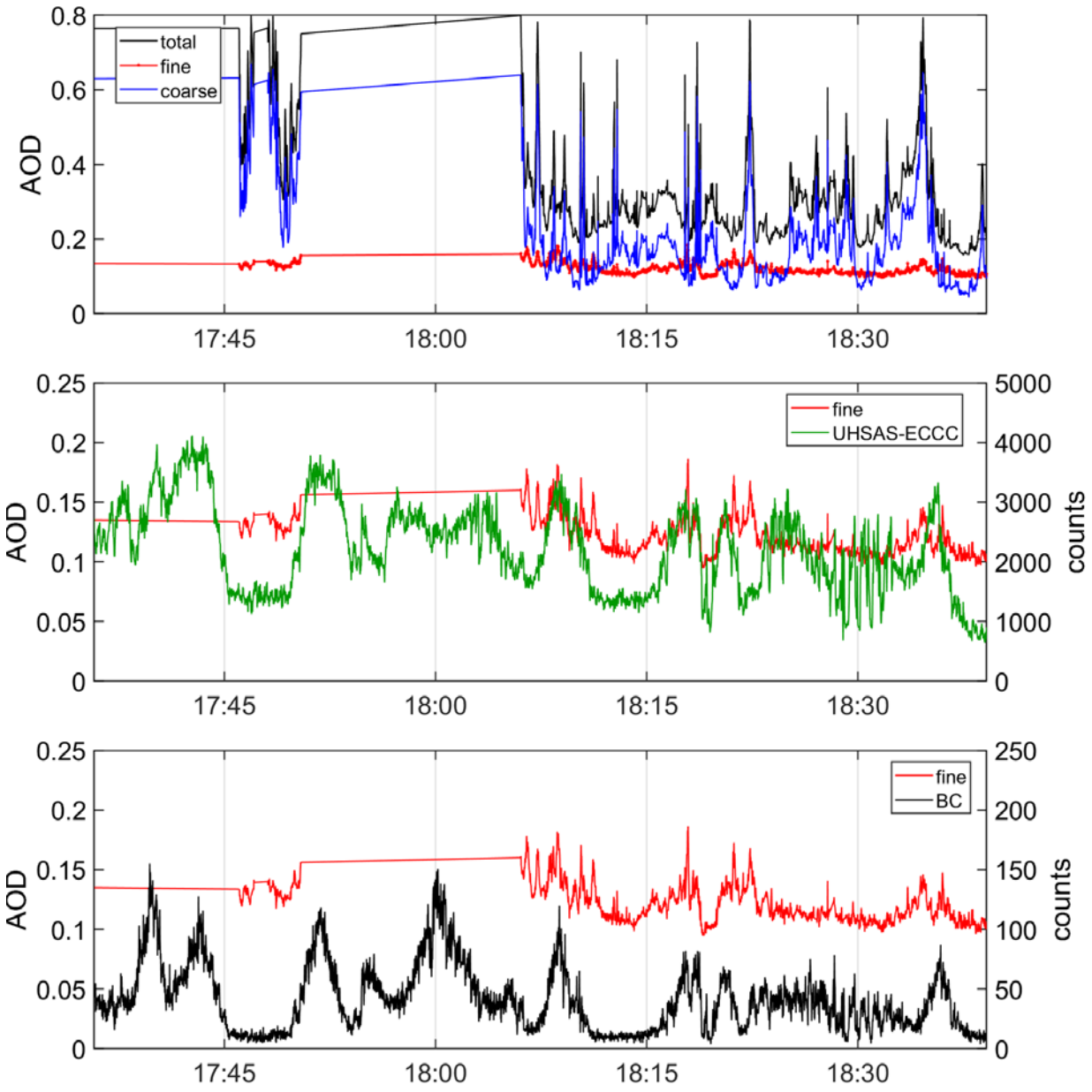

Figure A7. Screen 3 on June 9, 2018. Description as in Figure A5

Screen 4

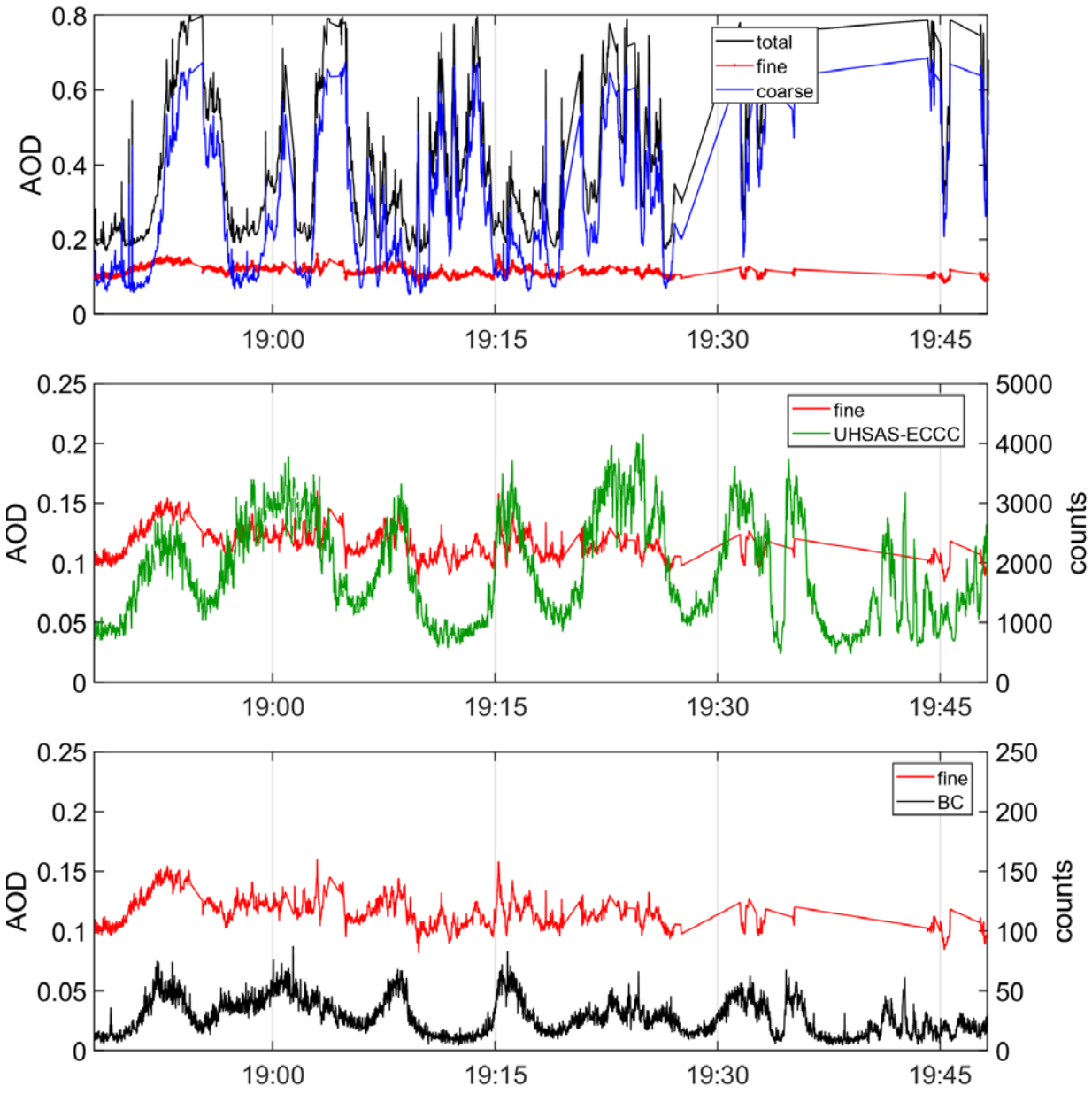

Figure A8. Screen 4 on June 9, 2018. Description as in Figure A5

Spiral data

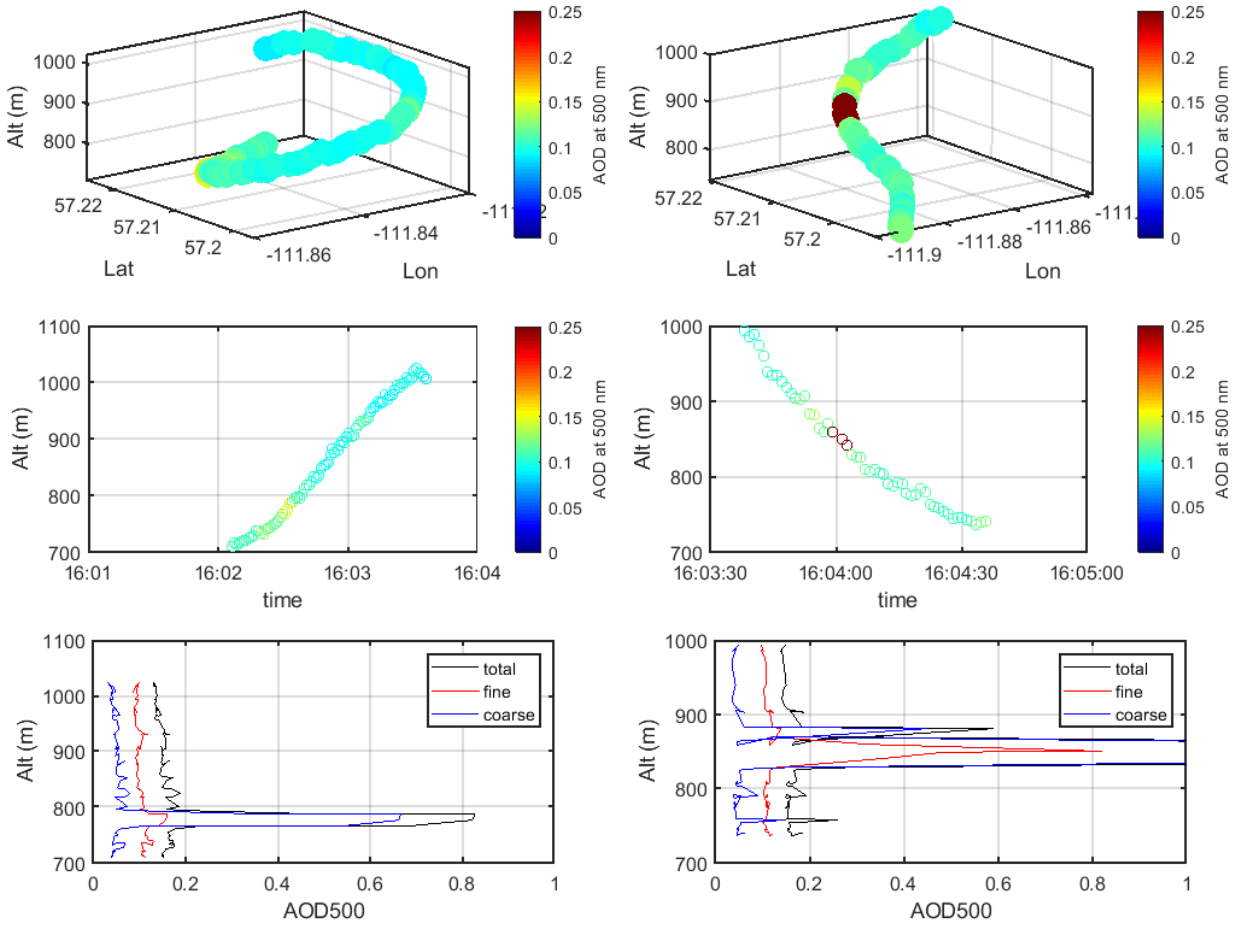

Figure A9. Ascending (left) and descending (right) spirals performed during screen 1. Top and middle panes: fine-mode AOD with default cloud screening applied. Bottom: SDA results.

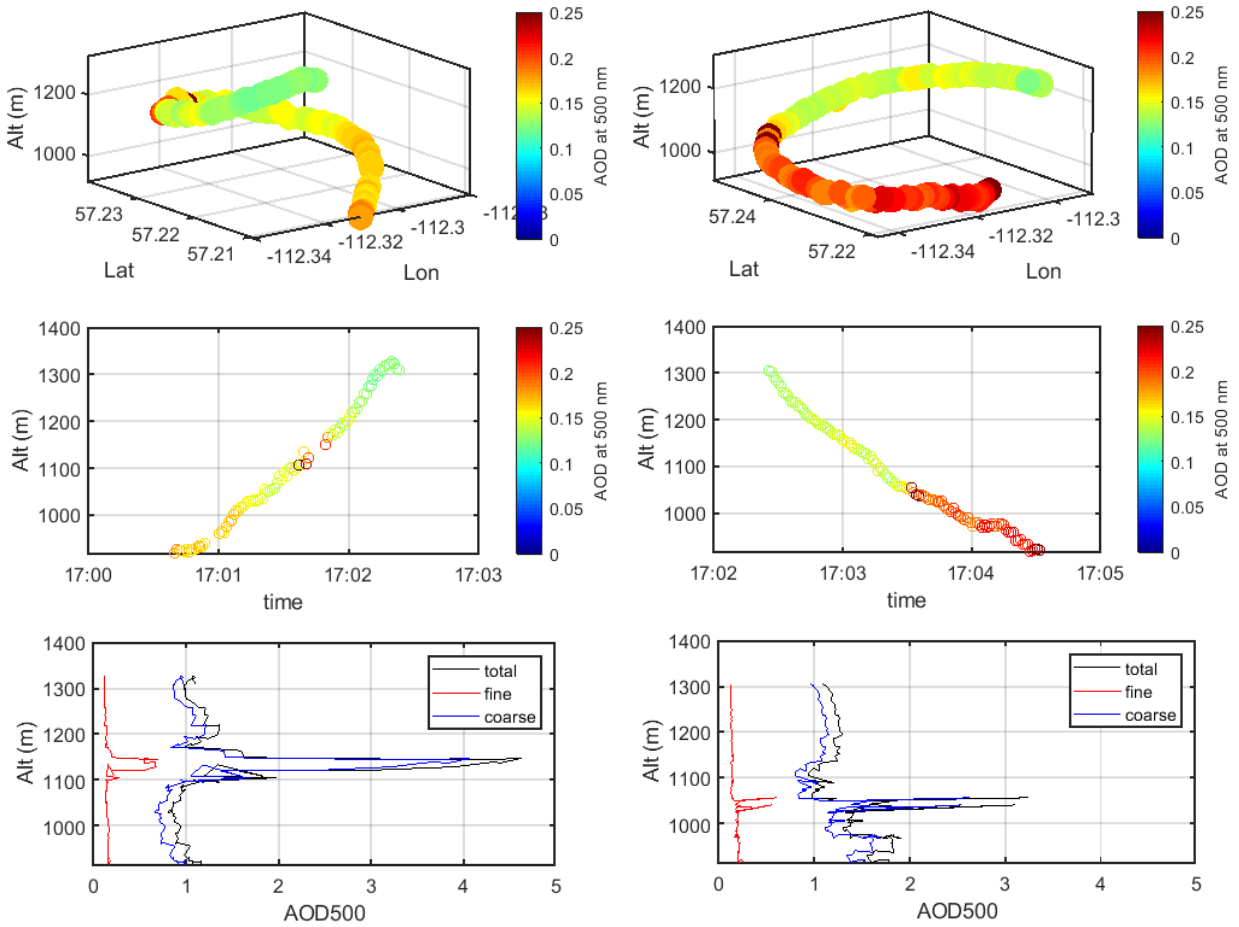

Figure A10. Spirals during screen 2. June 9, 2018. Description as in Figure A9

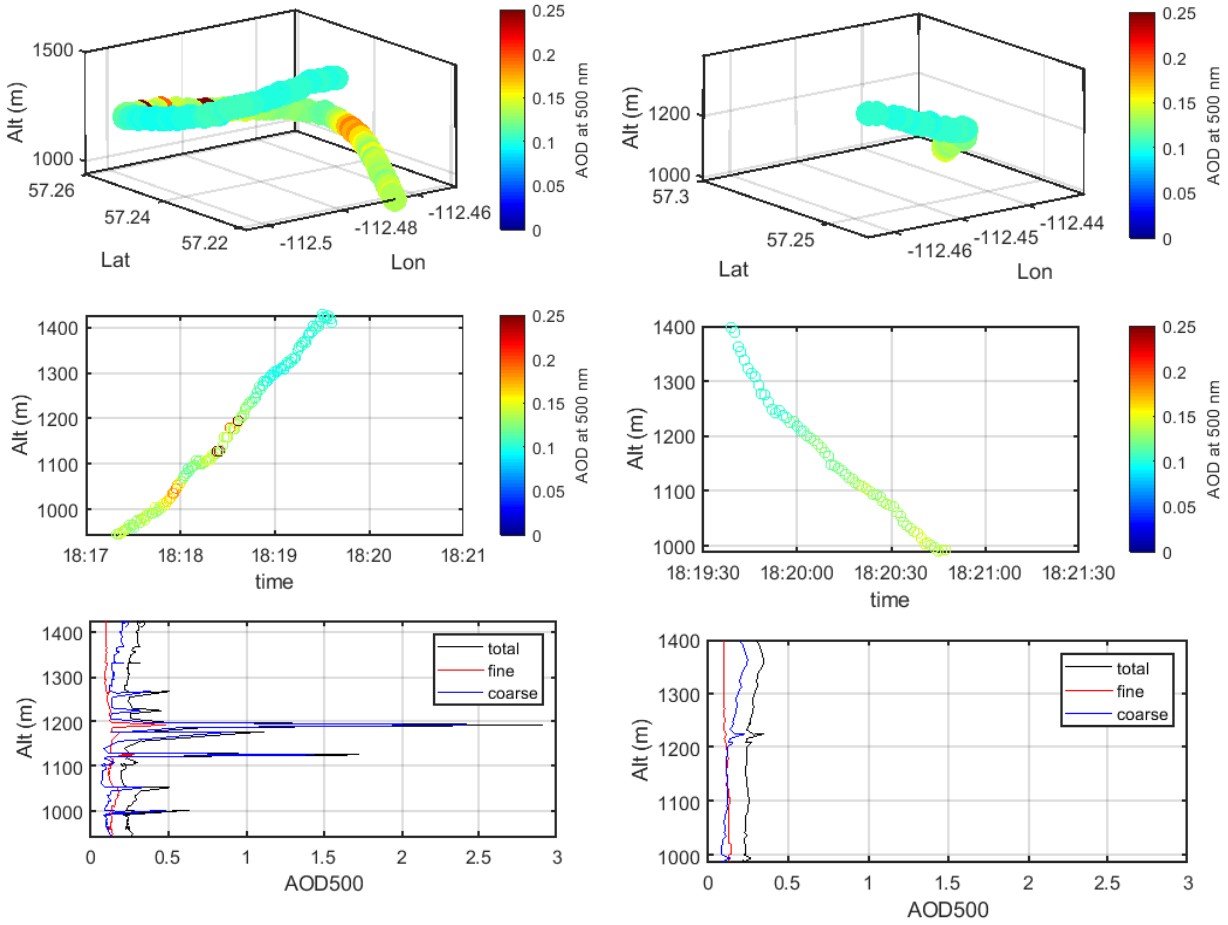

Figure A11. *S*pirals during screen 3. June 9, 2018. Description as in Figure A9

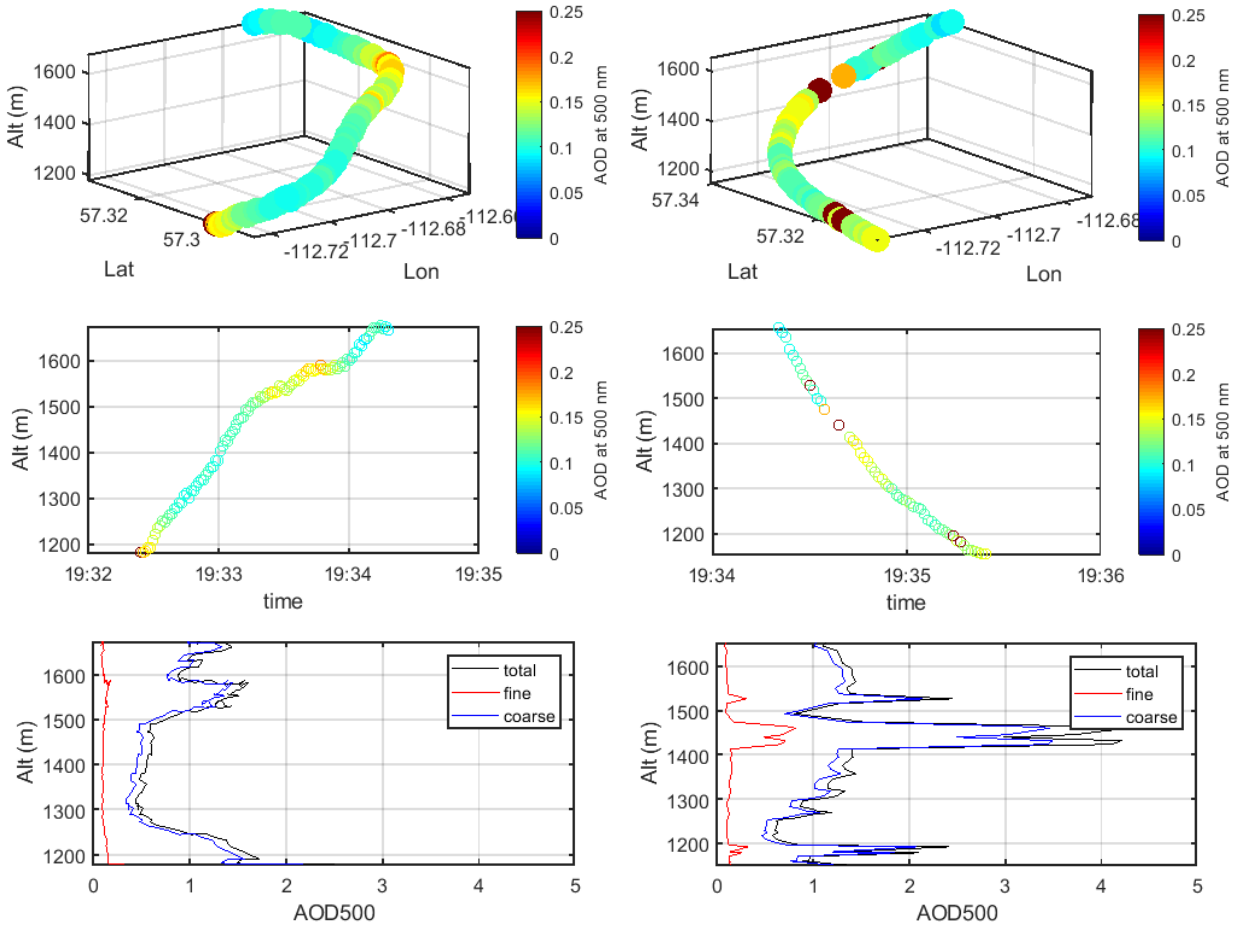

Figure A12. *S*pirals during screen 4. June 9, 2018. Description as in Figure A9

June 18, 2018 – Emissions over Syncrude Mildred Lake and Suncor MacKay River

Observations

Syncrude

- The Syncrude plume can be readily detected in the 4STAR data with AODs reaching as high as 0.35 with the background AODs around 0.05 slowly increasing with altitude.
- The AOD fine-mode peaks associated with the plume clearly correspond to the peaks in the UHSAS and BC data. Some additional peaks might have been missed while the 4STAR was in the sky scanning mode
- A long upward spiral was performed around 17:23 from ~500 to 2000 m clearly showing the fine-mode nature of the plume. During the preceding spiral down maneuver the bank angle was too large for the 4STAR to be able to track the sun.
- The aircraft have overflown the Fort McKay AERONET station, so some comparisons might be feasible

Suncor

- The AOD data for the Suncor facility visibly suffers from cloud contamination and needs further filtering. One can nevertheless still see a baseline fine-mode AOD at ~0.1.

Flight maneuvers table

Table A2. Flight plan for June 18, 2018.

Date	NRC flight #	ECCC flight #	Flight pattern	Alt (ft)	From Time	To Time
2018/06/18	33	19	Take off		14:54:07	
Syncrude Mildred lake						
2018/06/18	33	19	west	500	15:11:48	15:15:59
2018/06/18	33	19	south	500	15:16:02	15:18:46
2018/06/18	33	19	east	500	15:18:47	15:22:41
2018/06/18	33	19	north	500	15:22:43	15:25:23
2018/06/18	33	19	west	750	15:25:31	15:29:40
2018/06/18	33	19	south	750	15:29:48	15:32:26
2018/06/18	33	19	east	750	15:32:27	15:36:02
2018/06/18	33	19	north	750	15:36:22	15:38:59
2018/06/18	33	19	West	1000	15:39:05	15:43:09
2018/06/18	33	19	south	1000	15:43:12	15:45:50
2018/06/18	33	19	east	1000	15:45:51	15:49:40
2018/06/18	33	19	north	1000	15:49:42	15:52:19
2018/06/18	33	19	west	1250	15:52:31	15:56:32
2018/06/18	33	19	south	1250	15:56:37	15:59:12
2018/06/18	33	19	east	1250	15:59:14	16:03:04
2018/06/18	33	19	north	1250	16:03:07	16:05:42

2018/06/18	33	19	west	1500	16:05:55	16:10:03
2018/06/18	33	19	south	1500	16:10:04	16:12:43
2018/06/18	33	19	east	1500	16:12:44	16:16:15
2018/06/18	33	19	spiral up		16:16:16	16:17:15
2018/06/18	33	19	spiral down		16:17:16	16:19:43
2018/06/18	33	19	spiral up		16:19:44	16:21:01
2018/06/18	33	19	north	1500	16:21:02	16:23:06
2018/06/18	33	19	west	1750	16:23:16	16:27:24
2018/06/18	33	19	south	1750	16:27:25	16:30:02
2018/06/18	33	19	east	1750	16:30:04	16:33:56
2018/06/18	33	19	north	1750	16:34:00	16:36:36
2018/06/18	33	19	west	2000	16:36:48	16:40:52
2018/06/18	33	19	south	2000	16:40:56	16:43:35
2018/06/18	33	19	east	2000	16:43:36	16:47:27
2018/06/18	33	19	north	2000	16:47:29	16:50:05
2018/06/18	33	19	transit		16:50:06	16:54:39
2018/06/18	33	19	east	2250	16:54:40	16:58:51
2018/06/18	33	19	east	2500	17:01:45	17:05:42
2018/06/18	33	19	east	2750	17:08:57	17:10:22
2018/06/18	33	19	spiral up		17:10:23	17:13:13
2018/06/18	33	19	spiral down		17:13:14	17:20:34
2018/06/18	33	19	spiral up		17:20:35	17:34:32
Suncor MacKay River						
2018/06/18	33	19	north	500	17:42:21	17:43:16
2018/06/18	33	19	west	500	17:43:18	17:44:30
2018/06/18	33	19	south	500	17:44:31	17:45:19
2018/06/18	33	19	east	500	17:45:20	17:46:24
2018/06/18	33	19	north	750	17:46:25	17:47:10
2018/06/18	33	19	west	750	17:47:11	17:48:26
2018/06/18	33	19	south	750	17:48:27	17:49:18
2018/06/18	33	19	east	750	17:49:19	17:50:18
2018/06/18	33	19	north	1000	17:50:21	17:51:14
2018/06/18	33	19	west	1000	17:51:15	17:52:29
2018/06/18	33	19	south	1000	17:52:32	17:53:15
2018/06/18	33	19	east	1000	17:53:17	17:54:20
2018/06/18	33	19	north	1250	17:54:21	17:55:16
2018/06/18	33	19	west	1250	17:55:17	17:56:37
2018/06/18	33	19	south	1250	17:56:38	17:57:33
2018/06/18	33	19	east	1250	17:57:34	17:58:37
2018/06/18	33	19	north	1500	17:58:38	17:59:28

2018/06/18	33	19	west	1500	17:59:29	18:00:47
2018/06/18	33	19	south	1500	18:00:49	18:01:37
2018/06/18	33	19	east	1500	18:01:39	18:02:40
2018/06/18	33	19	north	2000	18:02:41	18:03:33
2018/06/18	33	19	west	2000	18:03:35	18:04:48
2018/06/18	33	19	south	2000	18:04:50	18:05:41
2018/06/18	33	19	east	2000	18:05:42	18:06:47
2018/06/18	33	19	north	2500	18:06:49	18:07:40
2018/06/18	33	19	west	2500	18:07:42	18:08:55
2018/06/18	33	19	south	2500	18:08:57	18:09:55
2018/06/18	33	19	east	2500	18:09:57	18:11:06
2018/06/18	33	19	north	3000	18:11:08	18:11:51
2018/06/18	33	19	west	3000	18:11:53	18:13:12
2018/06/18	33	19	south	3000	18:13:14	18:14:02
2018/06/18	33	19	east	3000	18:14:04	18:15:05
2018/06/18	33	19	north	3500	18:15:07	18:15:54
2018/06/18	33	19	west	3500	18:15:56	18:17:06
2018/06/18	33	19	south	3500	18:17:10	18:17:58
2018/06/18	33	19	east	3500	18:18:00	18:18:42
2018/06/18	33	19	spiral down		18:19:00	18:21:06
2018/06/18	33	19	spiral up		18:21:07	18:22:45
2018/06/18	33	19	Landing			18:41:49

Flight imagery

Figure A13. Photographic imagery of the Syncrude plume.

Comparisons with AERONET before/after flight

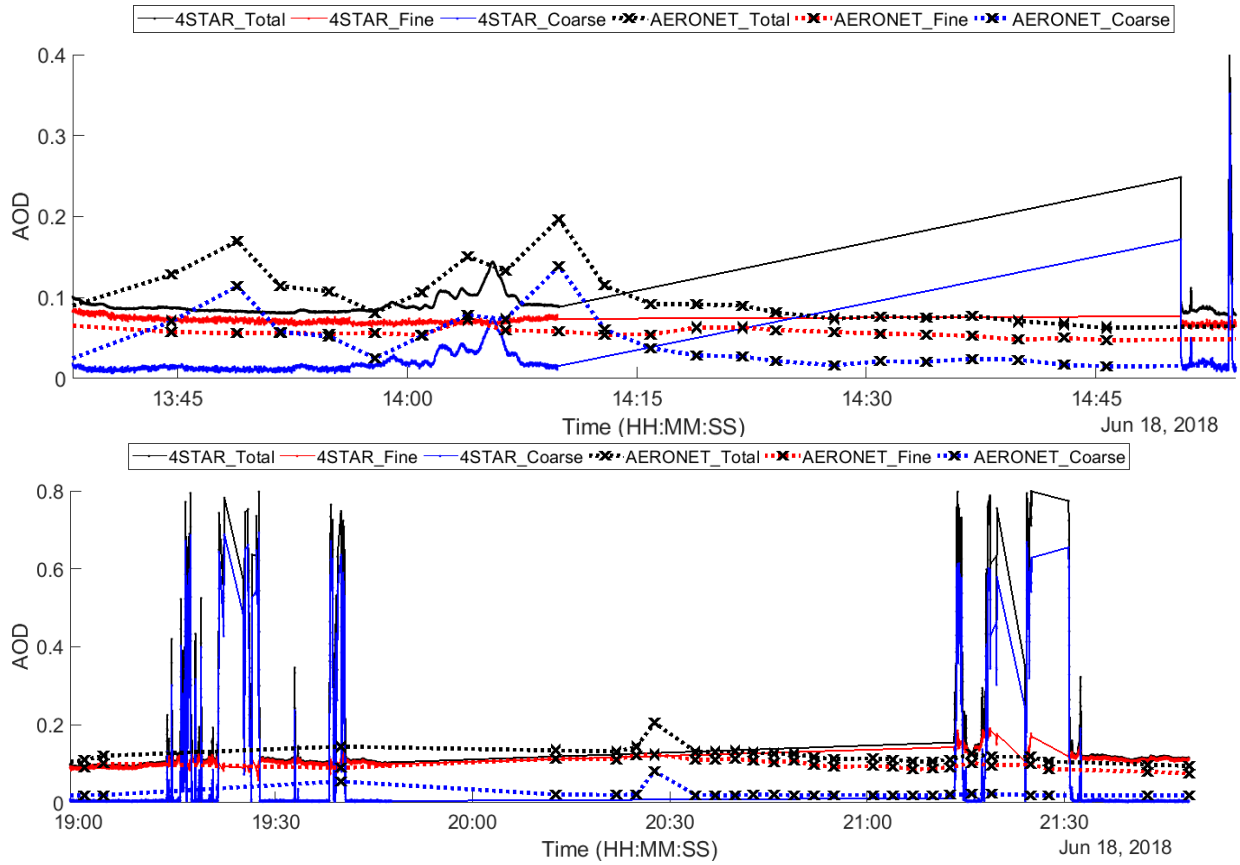

Figure A14. Comparisons with AERONET. Top: before the flight, bottom: after the flight. After the flight the data was acquired on the ground with uncleaned optics until ~19:45 and then with the cleaned optics starting at ~21:15. Default 4STAR cloud screening.

Flight track

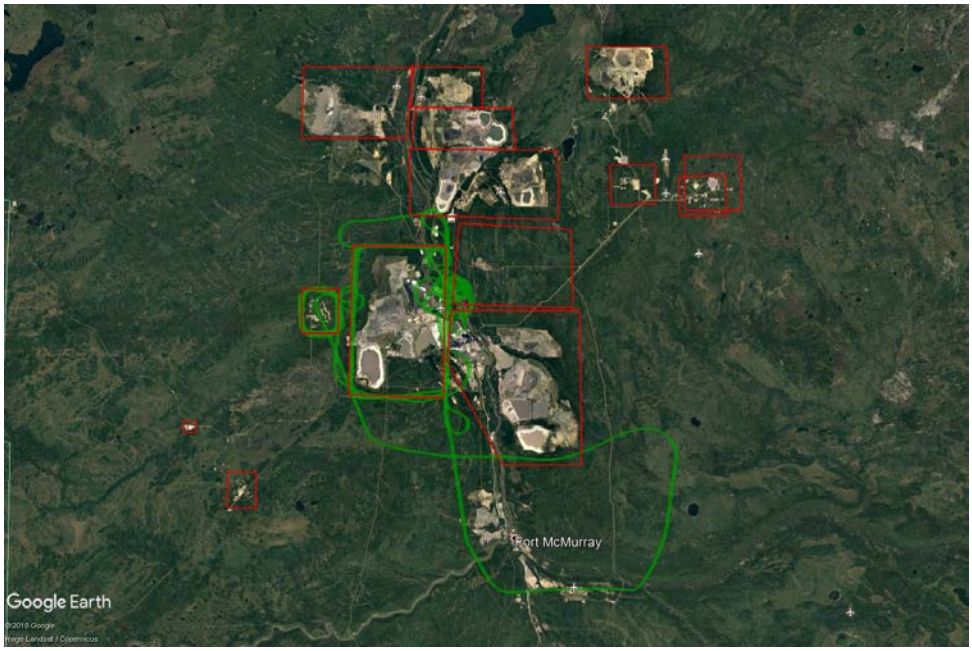

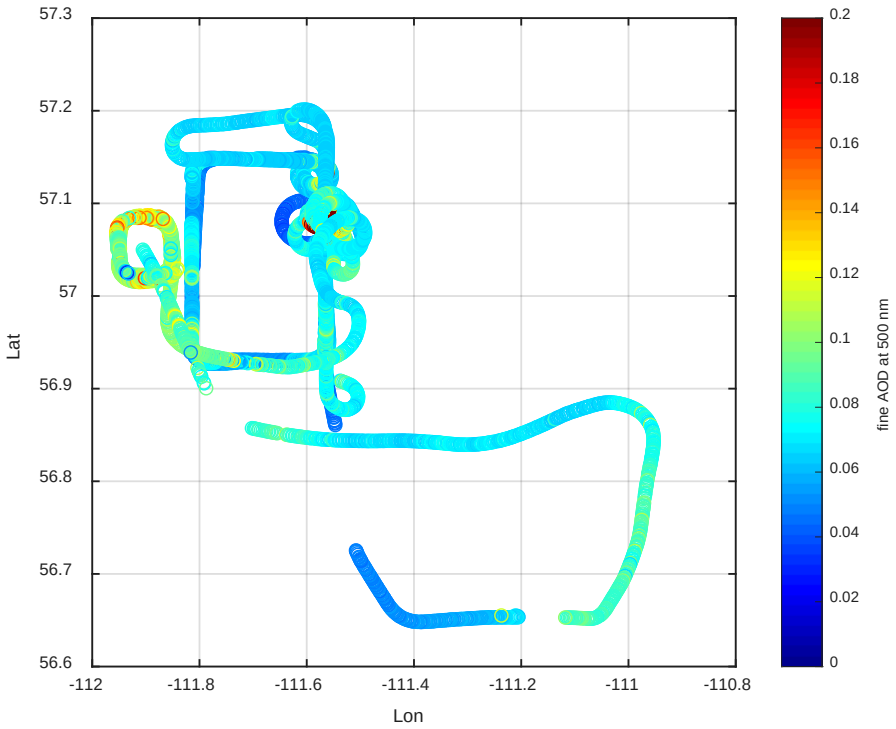

Figure A15. Description as in Figure A3 but for June 18, 2018. Default cloud screening applied.

AOD dynamics for each facility

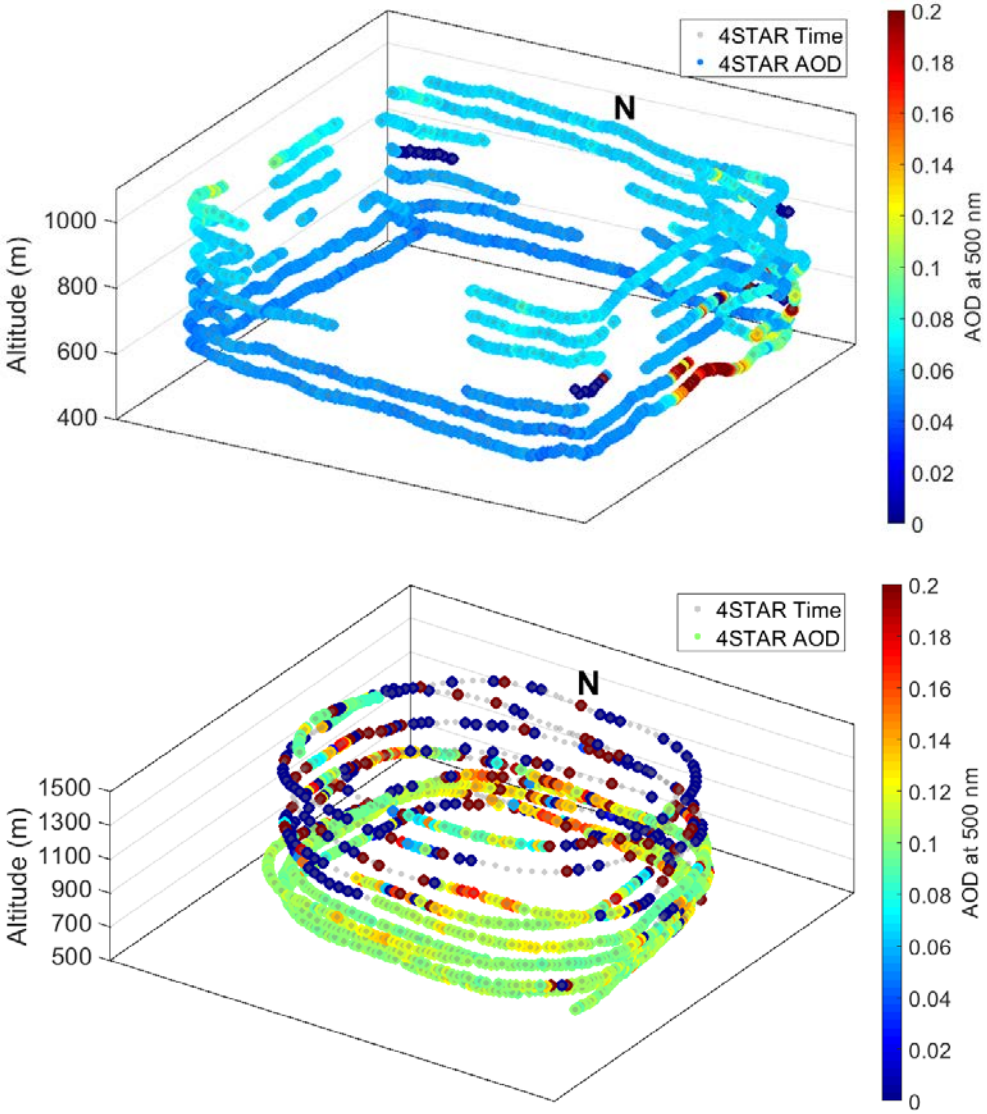

Figure A16. Fine mode AOD dynamics, default cloud screening. Top: Syncrude Mildred Lake, bottom: Suncor MacKay River.

SDA dynamics and intercomparisons

Syncrude

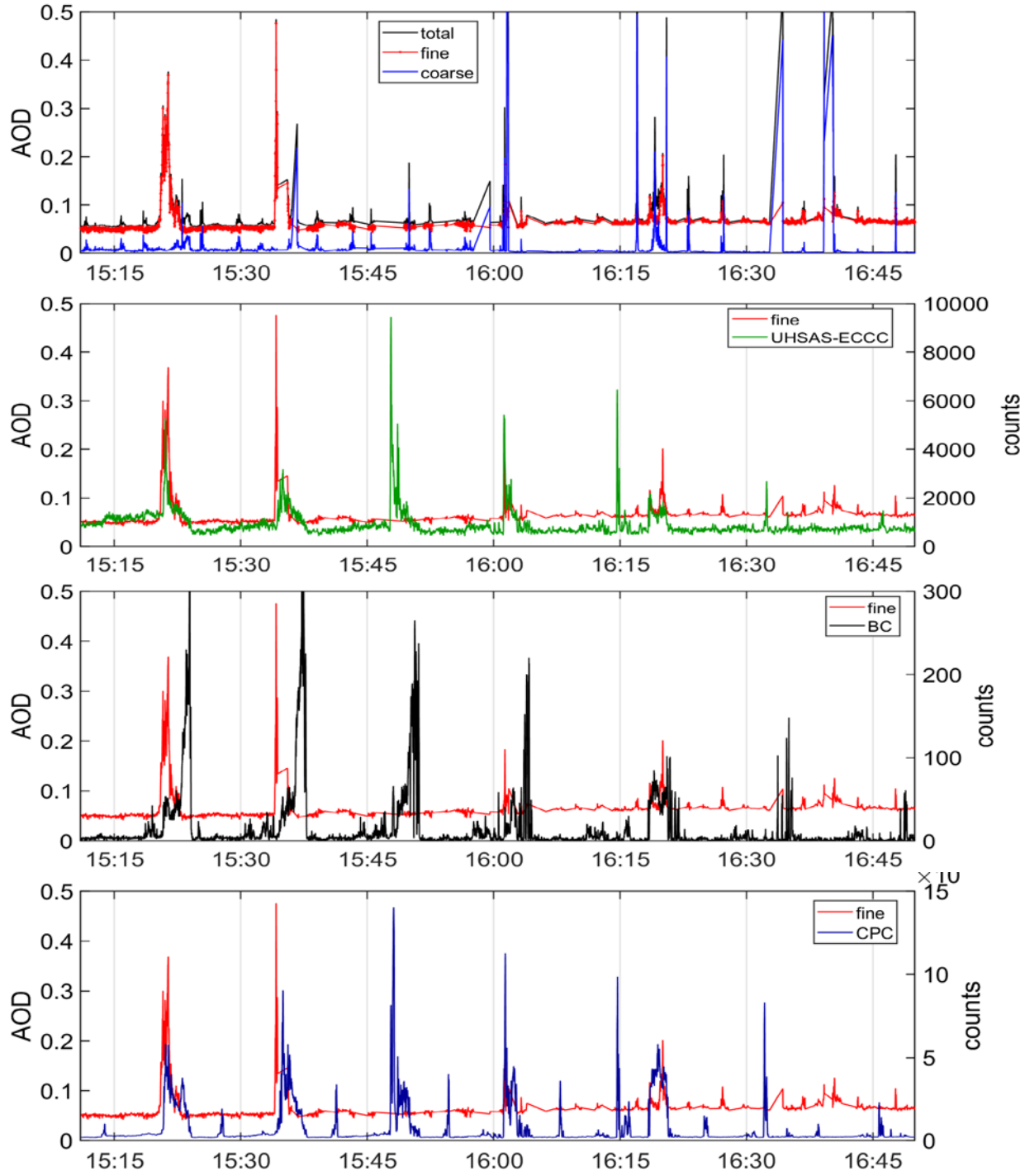

Figure A17. First three panes as in Figure A5, bottom pane: fine-mode AOD and CPC counts

Suncor

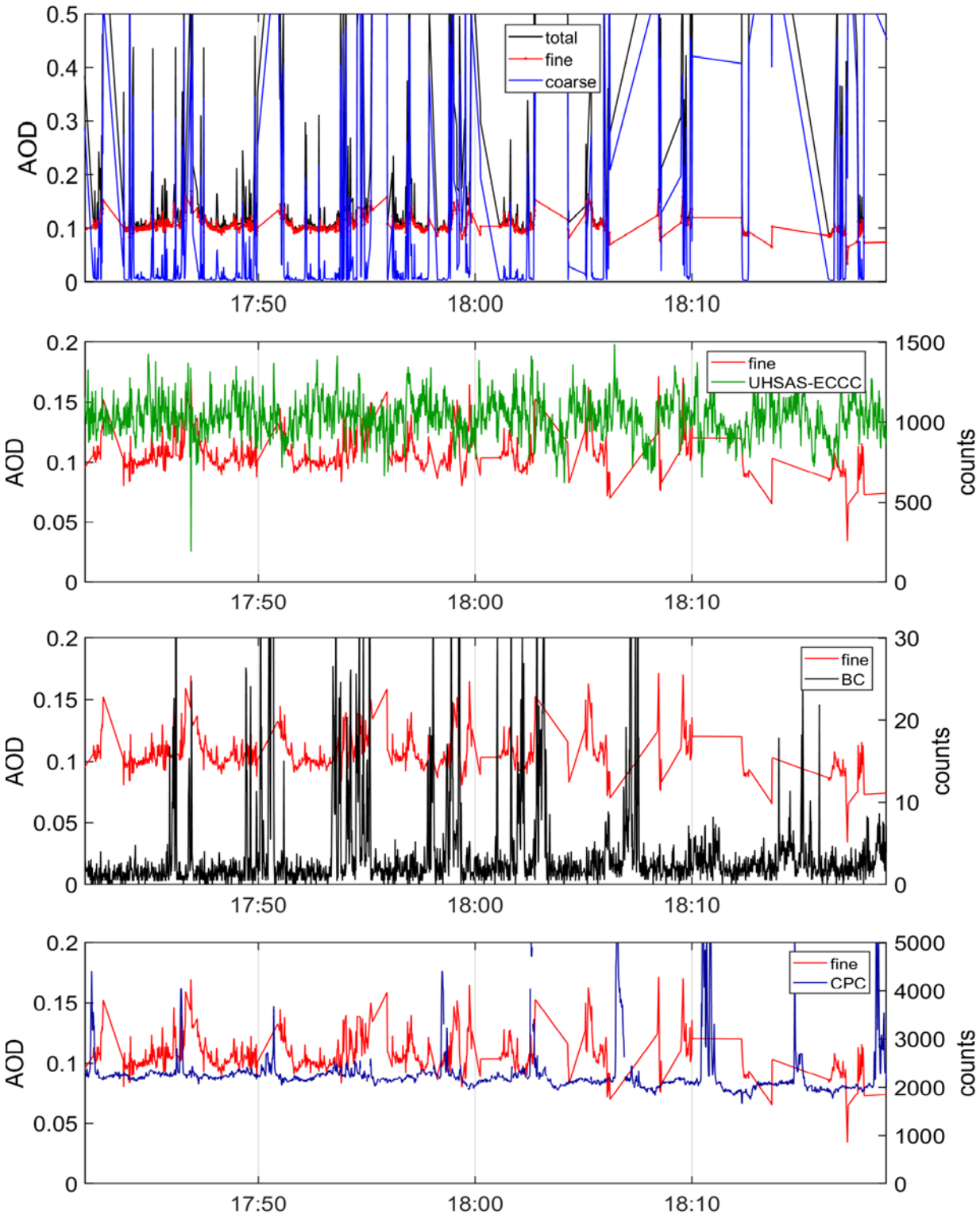

Figure A18. Description as in Figure A17 but for Suncor MacKay River. Note that the data is heavily influence by incomplete cloud screening.

Spiral data

Insifgnificant cloud free data

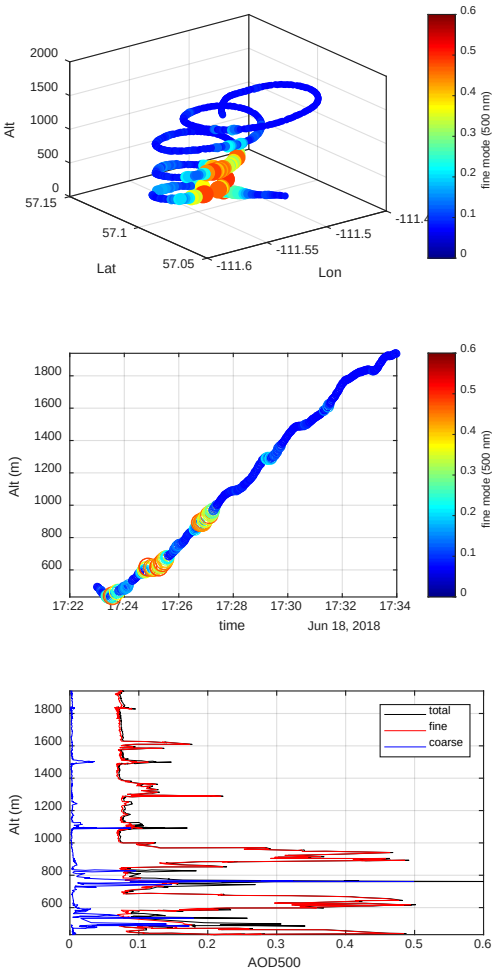

a. Spiral down b. Spiral up

Figure A19. Syncrude Mildred Lake box. Description as in Figure A9. Default cloud screening. For this case, the spiral down maneuver preceeded spiral up.

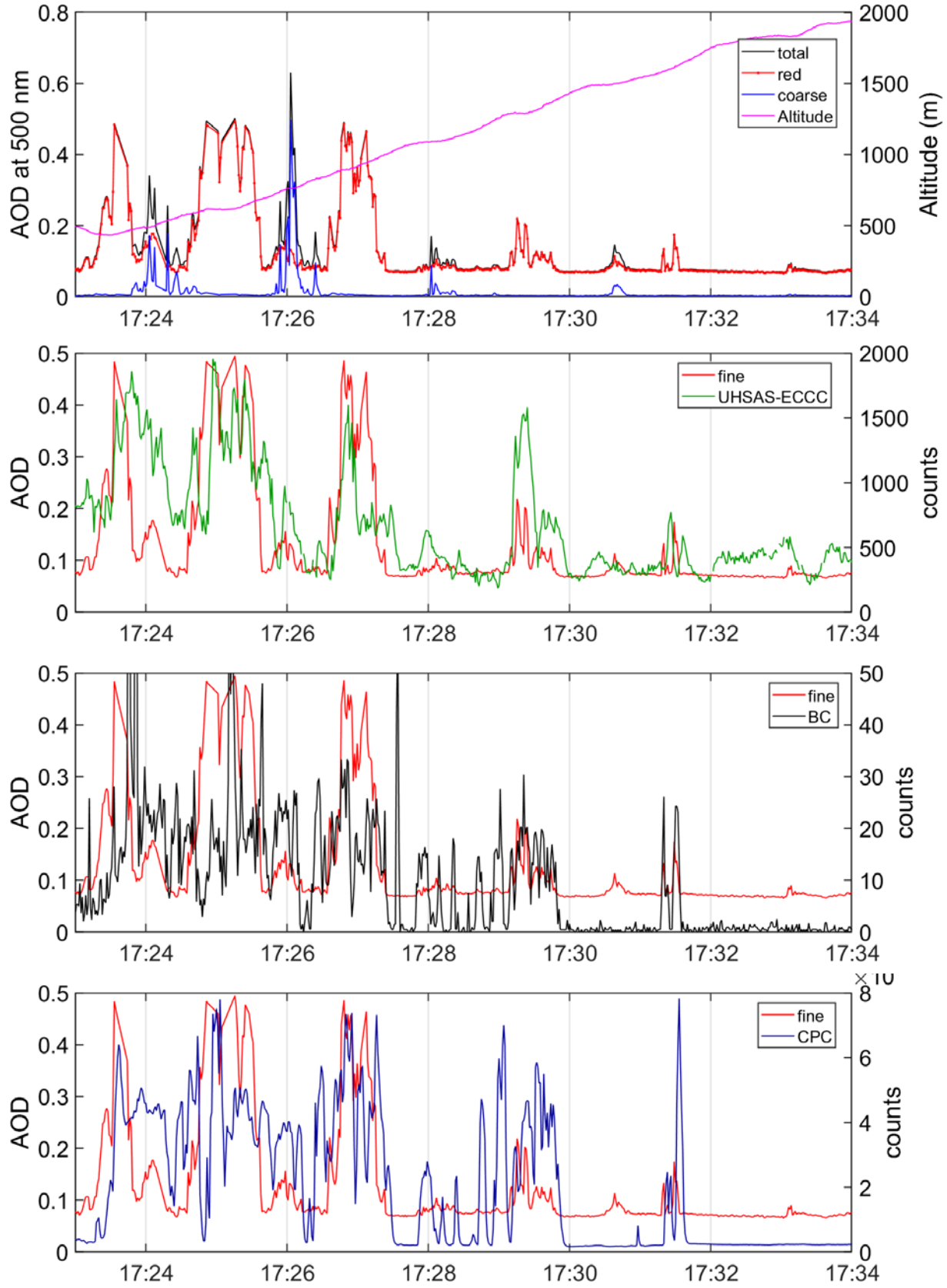

Figure A20. Time series during the spiral up maneuver. Description as in Figure A17

June 20, 2018 – Emissions over IKOS and Suncor Millennium

Observations

General

- No UHSAS-ECCC data
-

IKOS

- Slowly decreasing with height AODs from ~0.08 to to 0.06. No significant peaks in AOD.

Suncor Millennium

- A fine-mode plume could be detected at the southern end of the box with fine-mode peaking from ~0.07 to 0.10. The peaks appear to be offset from the in-situ peaks by 5-7 seconds.
- When finishing the Suncor Millennium box, the pilots reported fresh flares going up as high as 100 ft into the air. Consequently a screen was set up at the northern end of the box to potentially characterize the flares effect.

Flight maneuvers table

Table A3. Flight plan for June 20, 2018.

Date	NRC flight #	ECCC flight #	Flight pattern	Alt (ft)	From Time	To Time
2018/06/20	35	21	Take off		14:50:59	
Box 1 – Imperial Kearl Oil Sands (IKOS)						
2018/06/20	35	21	north	250	15:13:47	15:15:55
2018/06/20	35	21	west	250	15:15:56	15:17:51
2018/06/20	35	21	south	250	15:17:52	15:19:56
2018/06/20	35	21	east	250	15:19:57	15:21:51
2018/06/20	35	21	north	250	15:21:52	15:23:48
2018/06/20	35	21	west	500	15:23:49	15:25:48
2018/06/20	35	21	south	500	15:25:49	15:27:55
2018/06/20	35	21	east	500	15:27:56	15:29:51
2018/06/20	35	21	north	500	15:29:53	15:31:51
2018/06/20	35	21	west	750	15:31:52	15:33:52
2018/06/20	35	21	south	750	15:33:55	15:35:49
2018/06/20	35	21	east	750	15:35:51	15:37:41
2018/06/20	35	21	north	750	15:37:44	15:39:37
2018/06/20	35	21	west	1000	15:39:38	15:41:28
2018/06/20	35	21	south	1000	15:41:30	15:43:39
2018/06/20	35	21	east	1000	15:43:40	15:45:34

2018/06/20	35	21	north	1000	15:45:35	15:47:27
Box 2 – Suncor Millennium						
2018/06/20	35	21	north	250	15:58:30	16:02:05
2018/06/20	35	21	west	250	16:02:06	16:06:27
2018/06/20	35	21	south	500	16:06:28	16:08:37
2018/06/20	35	21	east	500	16:08:39	16:12:56
2018/06/20	35	21	north	500	16:12:57	16:16:06
2018/06/20	35	21	west	500	16:16:07	16:20:25
2018/06/20	35	21	south	750	16:20:26	16:22:35
2018/06/20	35	21	east	750	16:22:38	16:26:47
2018/06/20	35	21	north	750	16:26:48	16:29:55
2018/06/20	35	21	west	750	16:29:56	16:34:16
2018/06/20	35	21	south	1000	16:34:17	16:36:22
2018/06/20	35	21	east	1000	16:36:25	16:40:39
2018/06/20	35	21	north	1000	16:40:40	16:43:43
2018/06/20	35	21	west	1000	16:43:44	16:48:05
2018/06/20	35	21	south	1250	16:48:07	16:50:19
2018/06/20	35	21	east	1250	16:50:21	16:54:35
2018/06/20	35	21	north	1250	16:54:36	16:57:29
2018/06/20	35	21	west	1250	16:57:30	17:01:53
2018/06/20	35	21	south	1500	17:01:54	17:04:05
2018/06/20	35	21	east	1500	17:04:06	17:08:20
2018/06/20	35	21	north	1500	17:08:21	17:11:13
2018/06/20	35	21	west	1500	17:11:14	17:15:30
2018/06/20	35	21	transformation	1750	17:49:58	17:53:41
2018/06/20	35	21	transformation	1500	17:55:25	17:59:09
2018/06/20	35	21	transformation	1250	18:00:21	18:03:50
2018/06/20	35	21	transformation	1000	18:05:22	18:09:21
2018/06/20	35	21	transformation	750	18:10:32	18:13:51
2018/06/20	35	21	transformation	500	18:15:21	18:18:42
2018/06/20	35	21	Landing			18:37:50

Comparisons with AERONET before/after flight

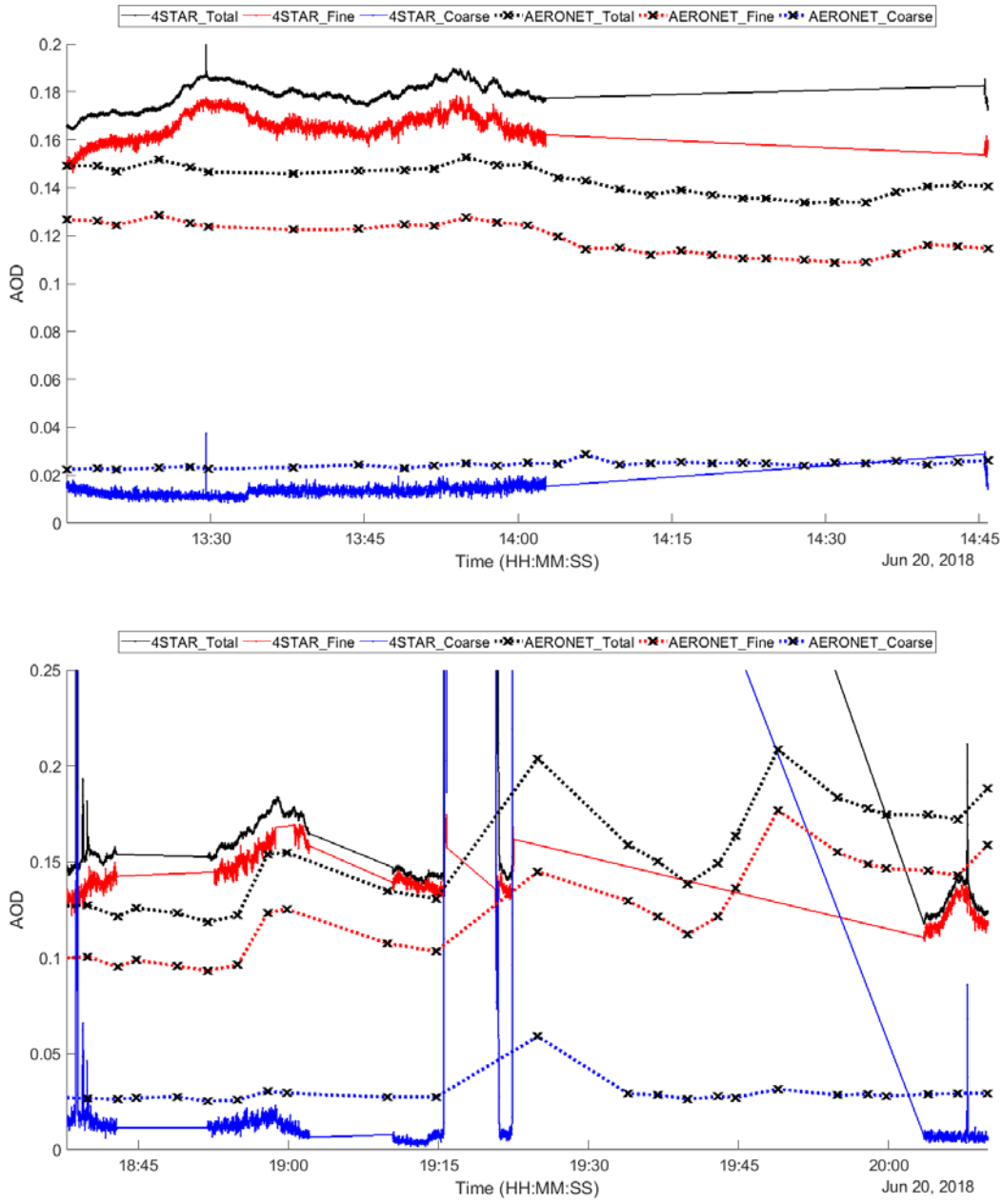

Figure A21. Comparisons with AERONET. Description as in Figure A2

Flight track

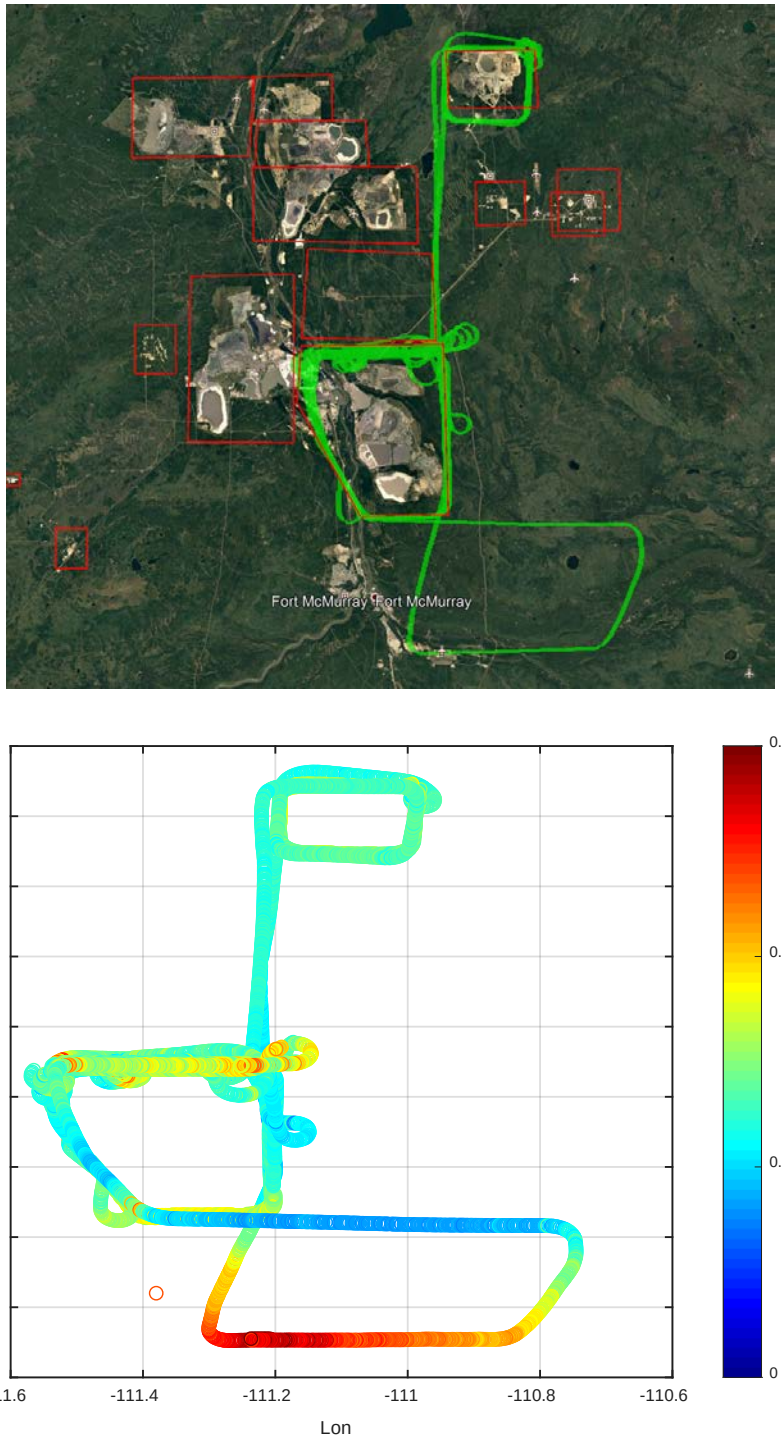

Figure A22. Flight path and fine-mode AOD dynamics. Description as in Figure A3

AOD dynamics for each facility

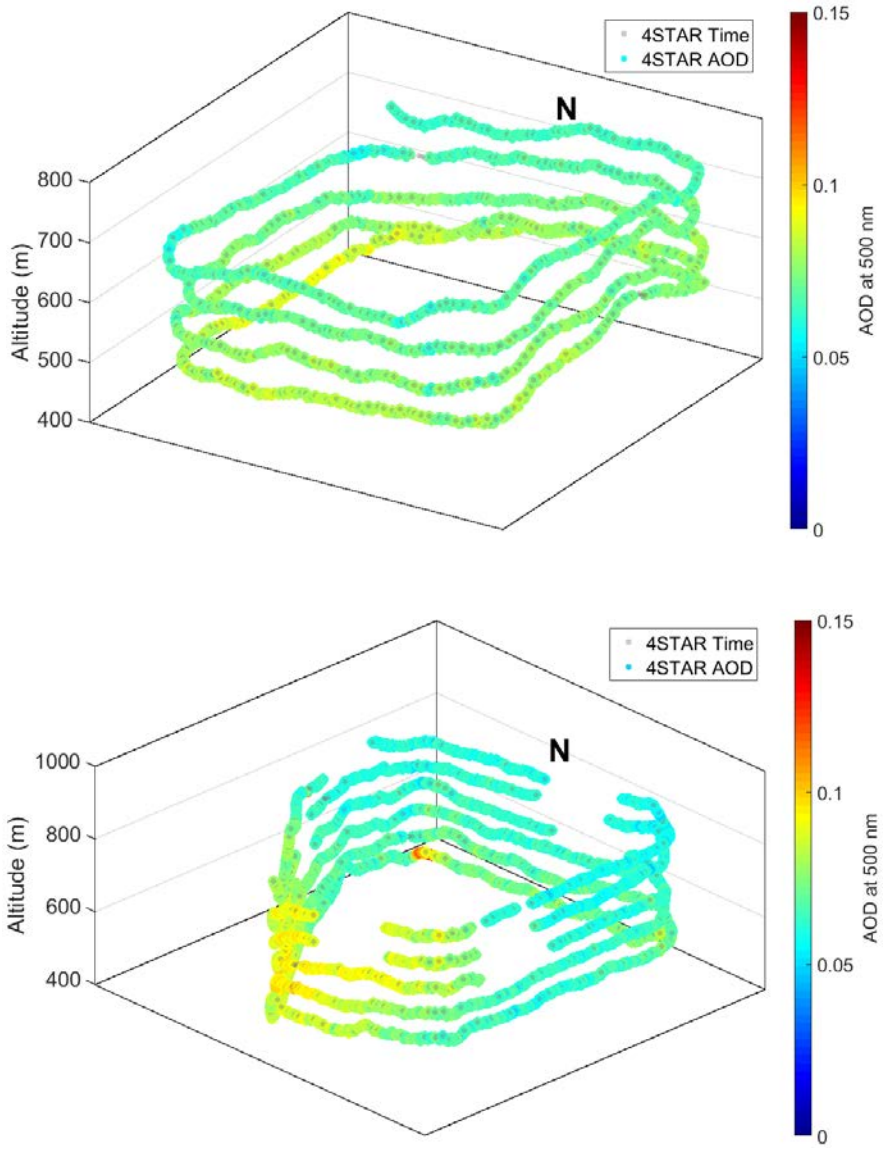

Figure A23. Fine mode AOD dynamics, default cloud screening. Top: IKOS, bottom: Suncor Mil.

AOD dynamics

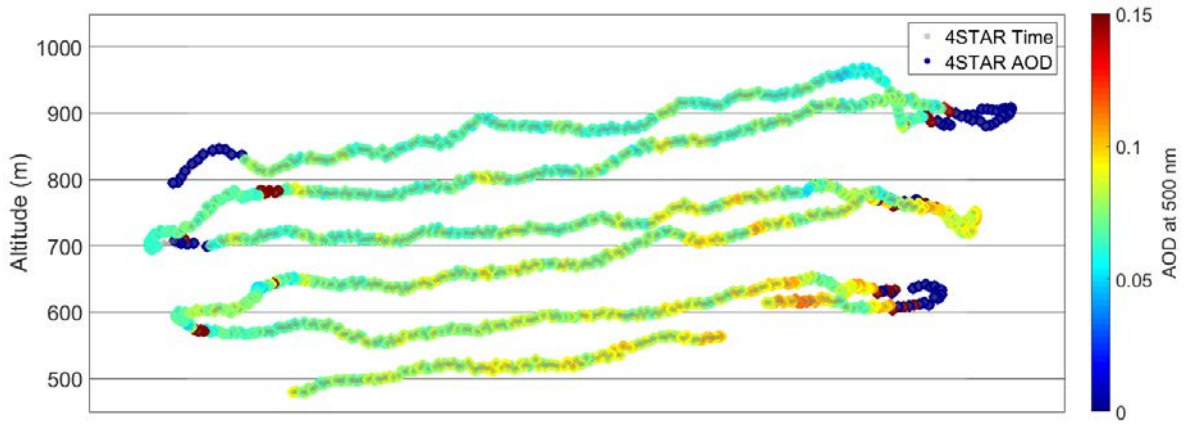

Figure A24. Fine mode AOD dynamis for one screen along the norther side of the Suncor Mil. Box

SDA dynamics and intercomparisons

Imperial Kearl Oil Sands (IKOS)

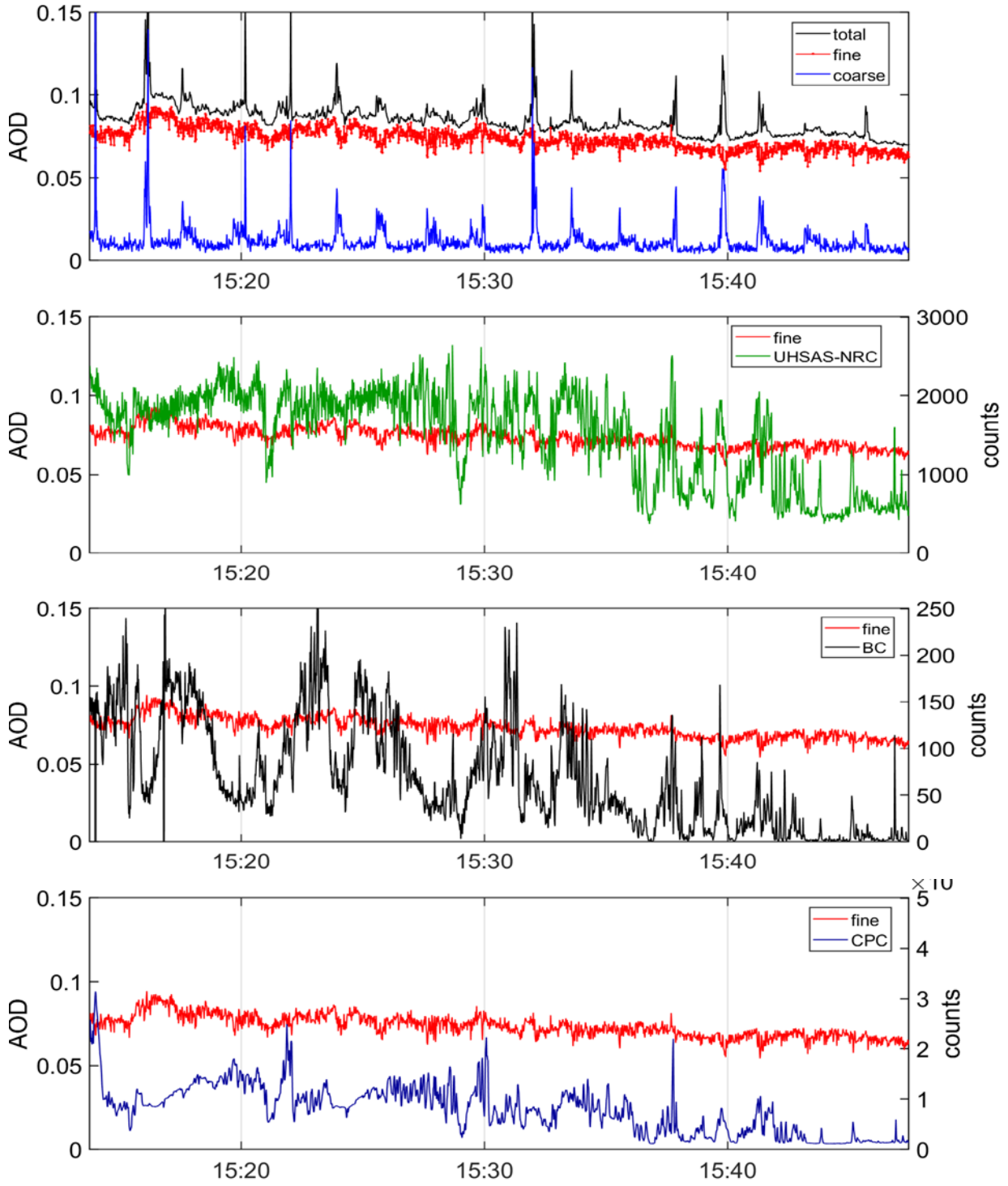

Figure A25. Time series for IKOS. Description as in Figure A17

Suncor Millenium

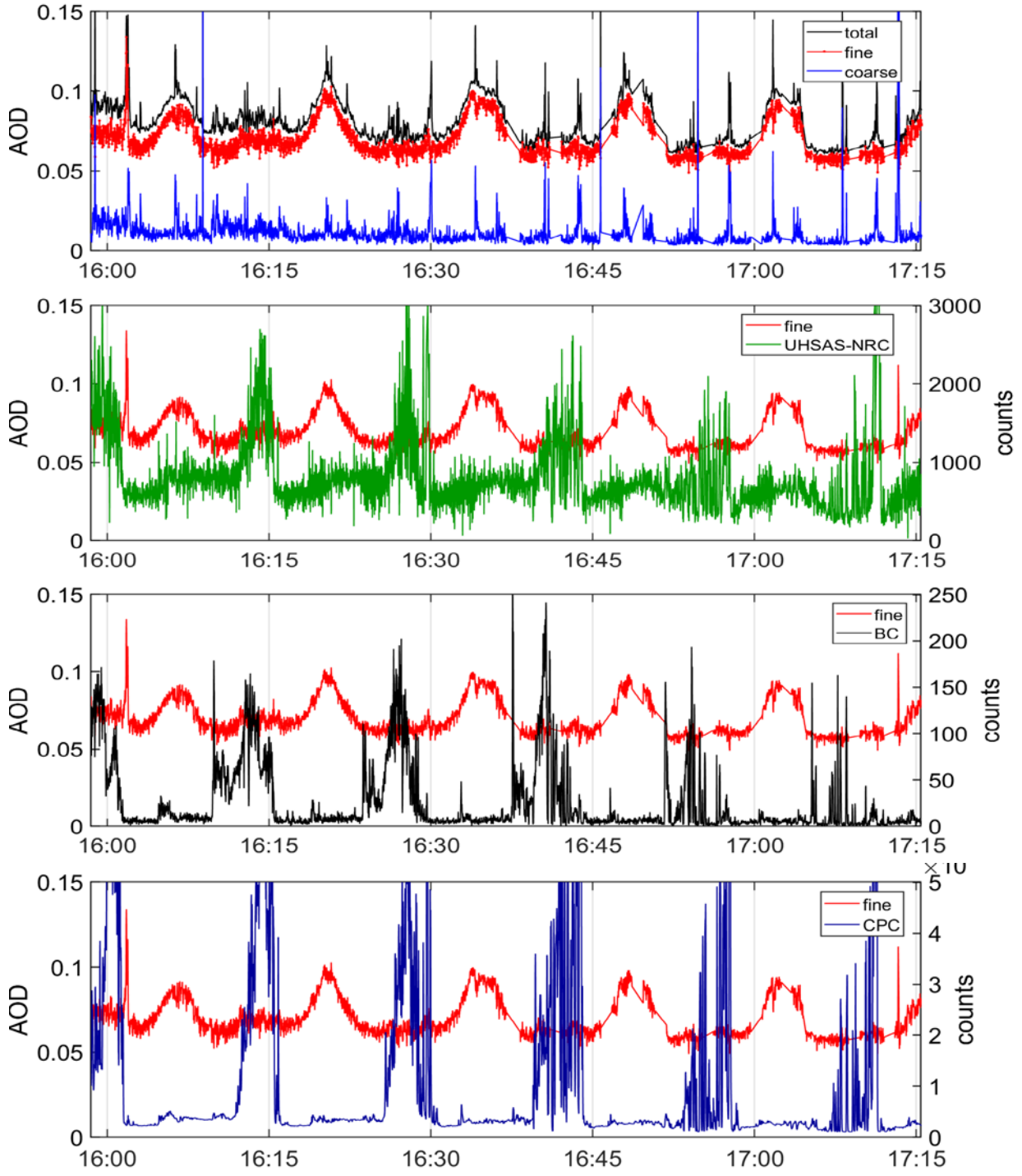

Figure A26. Time series for Suncor Millenium. Description as in Figure A17

Suncor Millenium (screen)

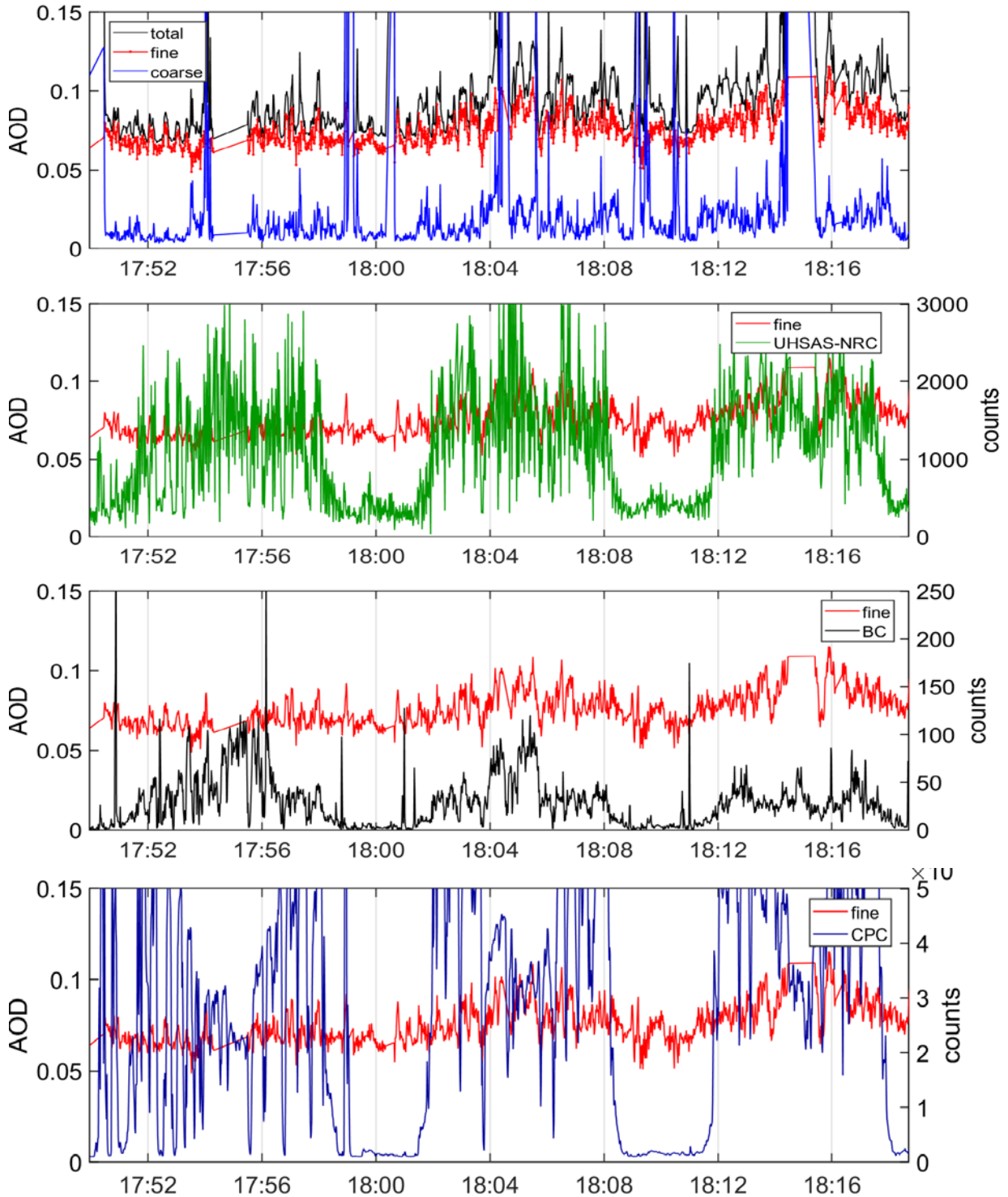

Figure A27. Time series for the screen set up at the northern end of the Suncor Millennium box. Description as in Figure A17

June 24, 2018 – Industrial plume transformation flight

Observations

- Three practically cloud-free transformation screens set up north east of the facilities
- Relatively low (~0.10-0.15), slow varying AOD values
- Correlations with in-situ probes are harder to notice, compared to other cases
- High AODs (~0.8) on landing most likely due to forest fires
- The positions of the screens are somewhat similar to those of July 5, might consider comparisons.

Flight maneuvers table

Table A4. Flight plan for June 24, 2018.

Date	NRC flight #	ECCC flight #	Flight pattern	Alt (ft)	From Time	To Time
2018/06/24	38	24	Take off		14:49:01	
Screen 1						
2018/06/24	38	24	transformation	500	14:58:35	15:14:14
2018/06/24	38	24	transformation	750	15:16:13	15:32:07
2018/06/24	38	24	transformation	1000	15:34:02	15:46:57
2018/06/24	38	24	transformation	1250	15:48:45	16:08:16
2018/06/24	38	24	spiral up		15:53:42	15:56:47
2018/06/24	38	24	spiral down		15:56:48	15:59:22
Screen 2						
2018/06/24	38	24	transformation	500	16:16:27	16:31:33
2018/06/24	38	24	transformation	750	16:33:42	16:47:39
2018/06/24	38	24	transformation	1000	16:49:36	17:03:35
2018/06/24	38	24	transformation	1250	17:05:37	17:23:22
2018/06/24	38	24	spiral up		17:12:34	17:14:43
2018/06/24	38	24	spiral down		17:14:44	17:16:02
Screen 3						
2018/06/24	38	24	transformation	500	17:28:01	17:45:27
2018/06/24	38	24	transformation	750	17:47:14	18:06:19
2018/06/24	38	24	transformation	1000	18:08:17	18:26:55
2018/06/24	38	24	transformation	1250	18:28:38	18:50:22
2018/06/24	38	24	spiral up		18:37:09	18:39:12
2018/06/24	38	24	spiral down		18:39:13	18:41:26
2018/06/24	38	24	Landing			19:15:16

Comparisons with AERONET before/after flight

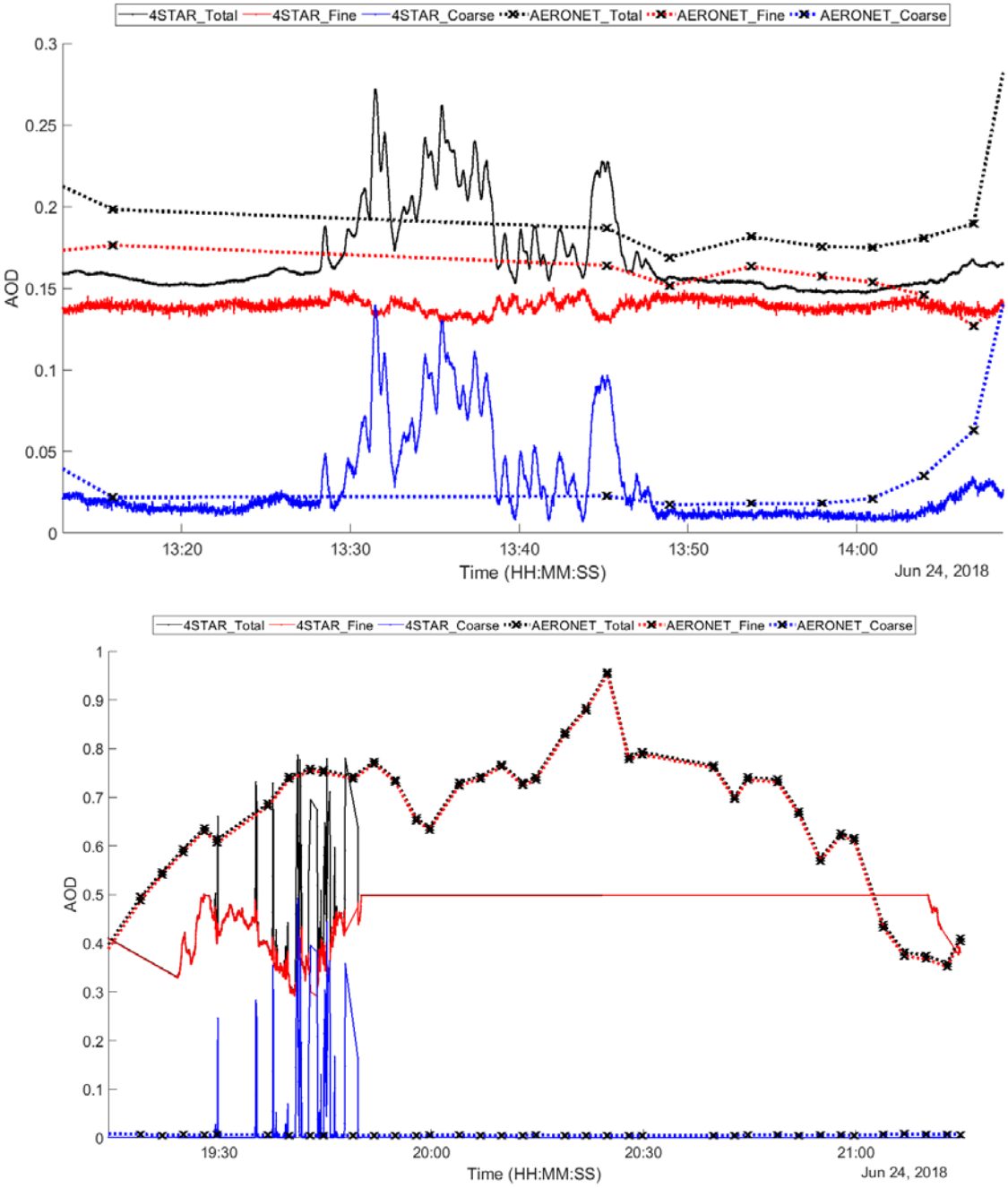

Figure A28. Comparisons with AERONET. Description as in Figure A2

Flight track

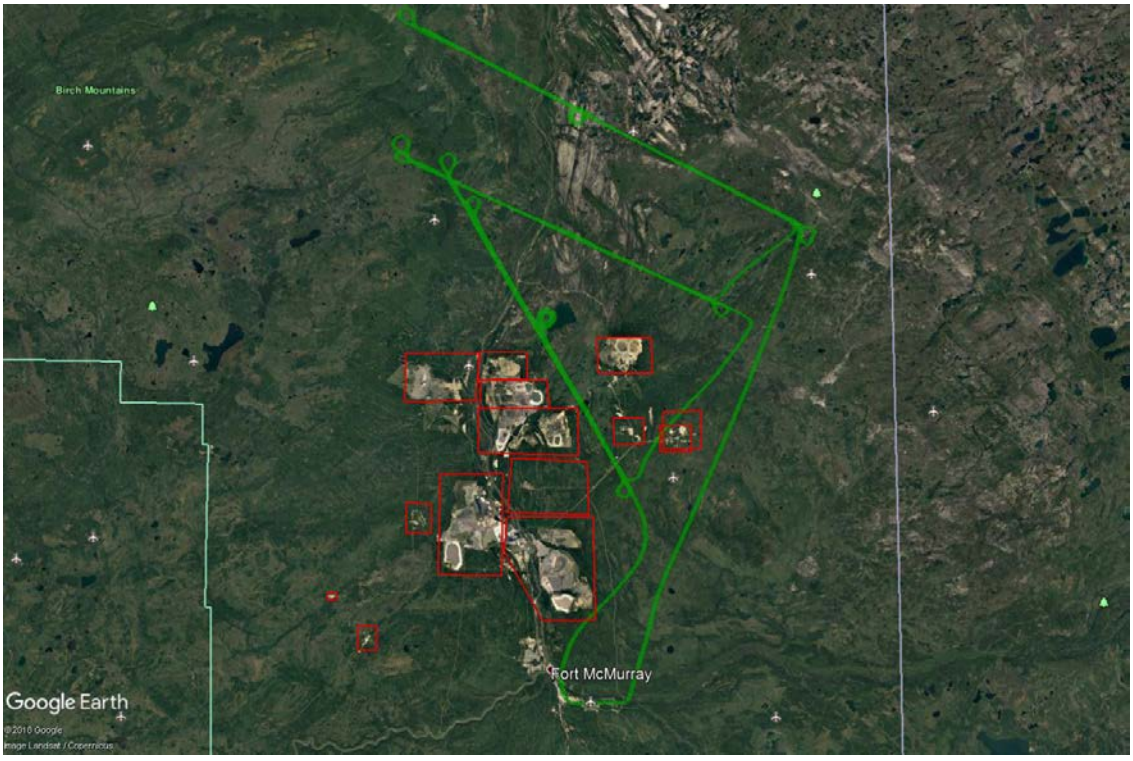

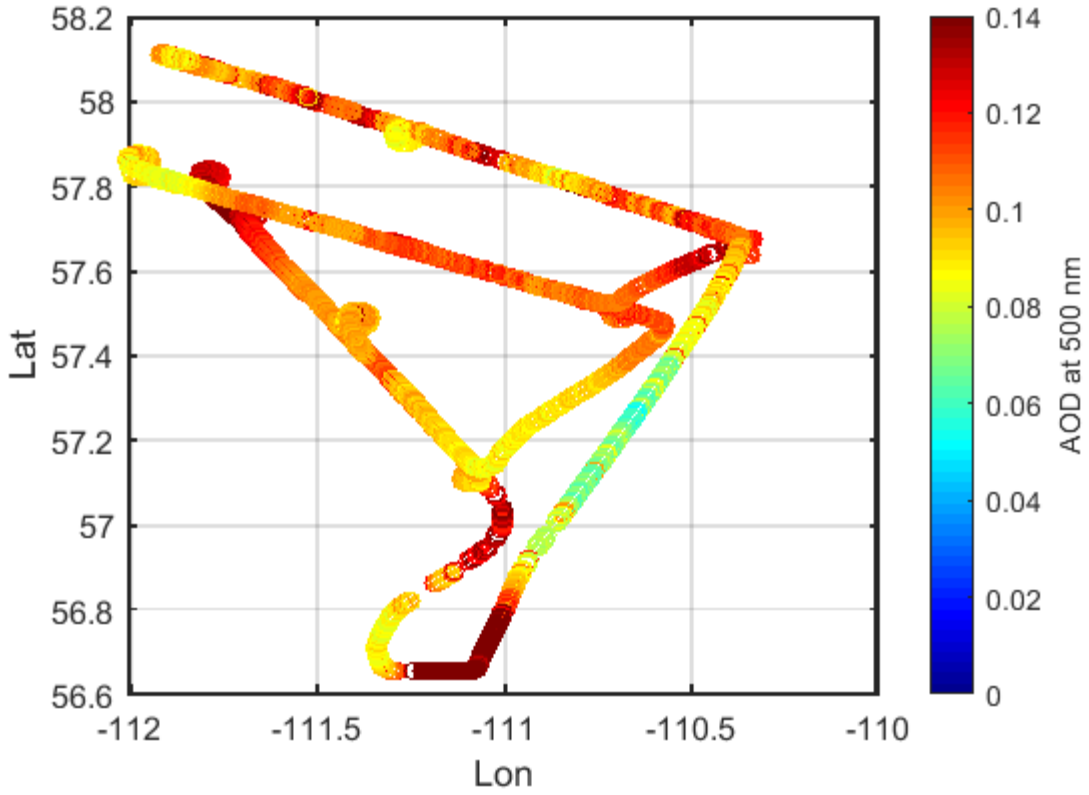

Figure A29. Flight path and fine-mode AOD dynamics (all points). Description as in Figure A3

AOD dynamics for each screen

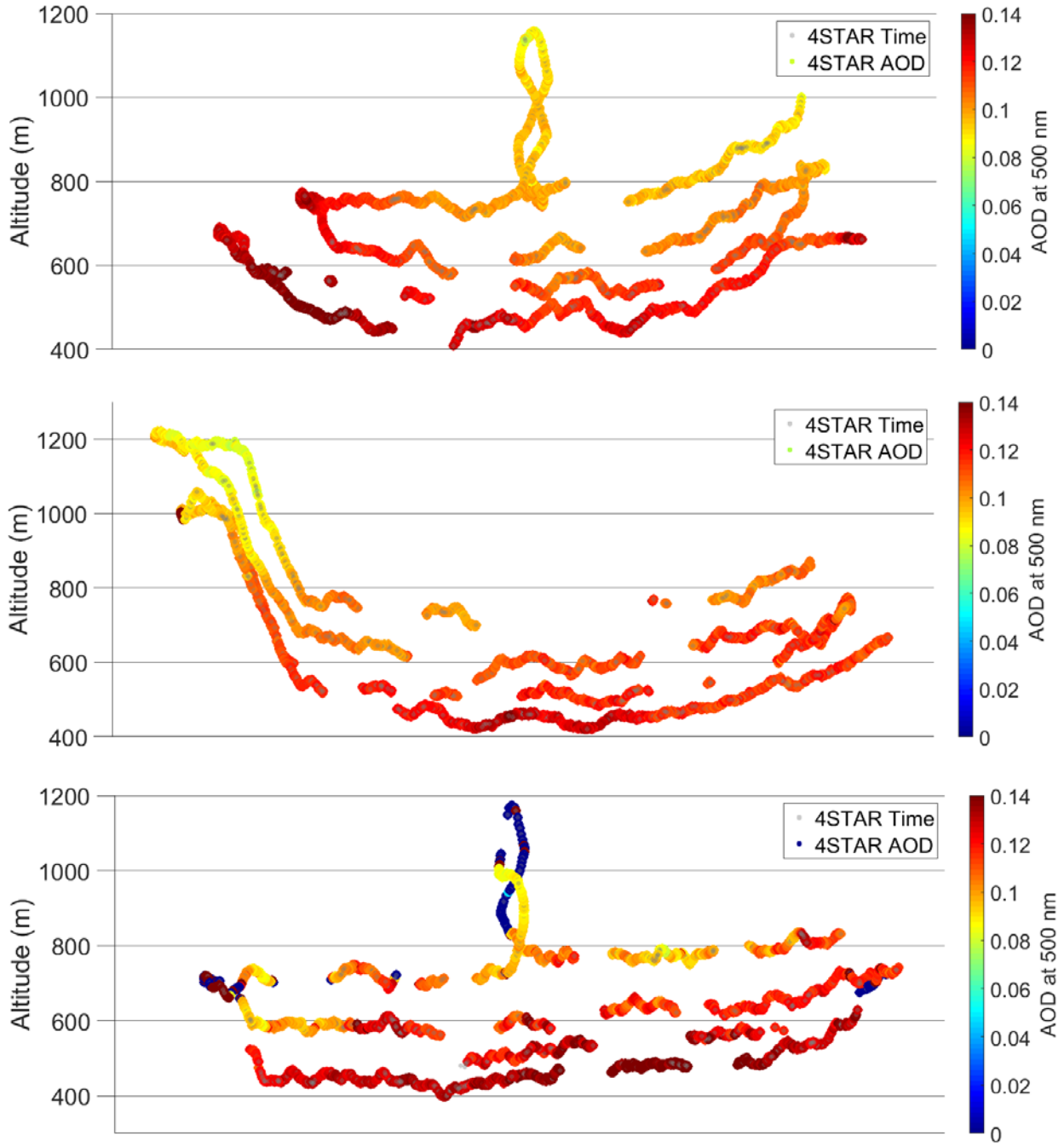

Figure A30. AOD in-flight dynamis for transformation screens 1 to 3 (top to bottom). The X-axis is parallel to the flight track.

SDA dynamics and intercomparisons

Screen 1

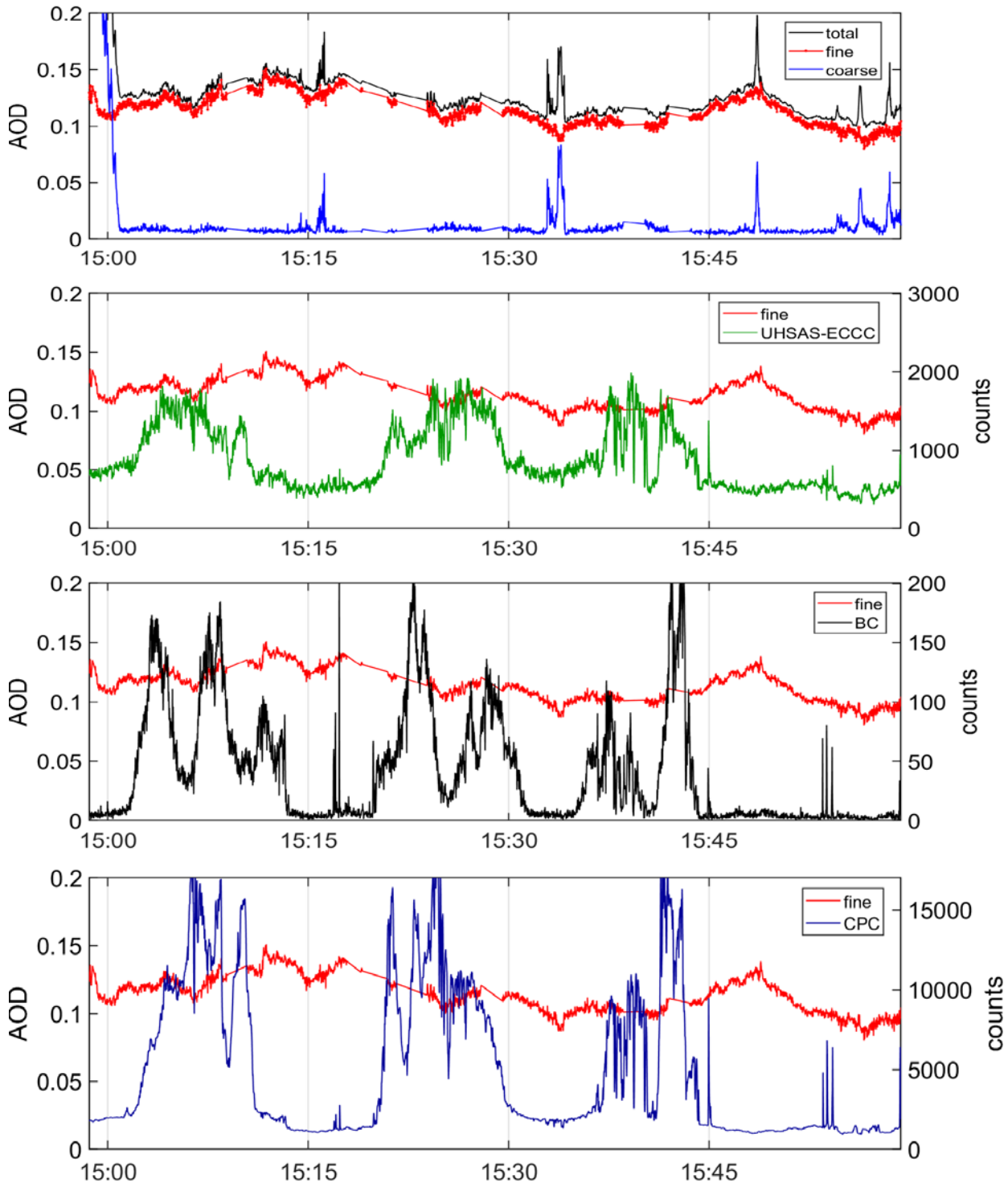

Figure A31. Time series for screen 1 on June 24, 2018. Description as in Figure A17

Screen 2

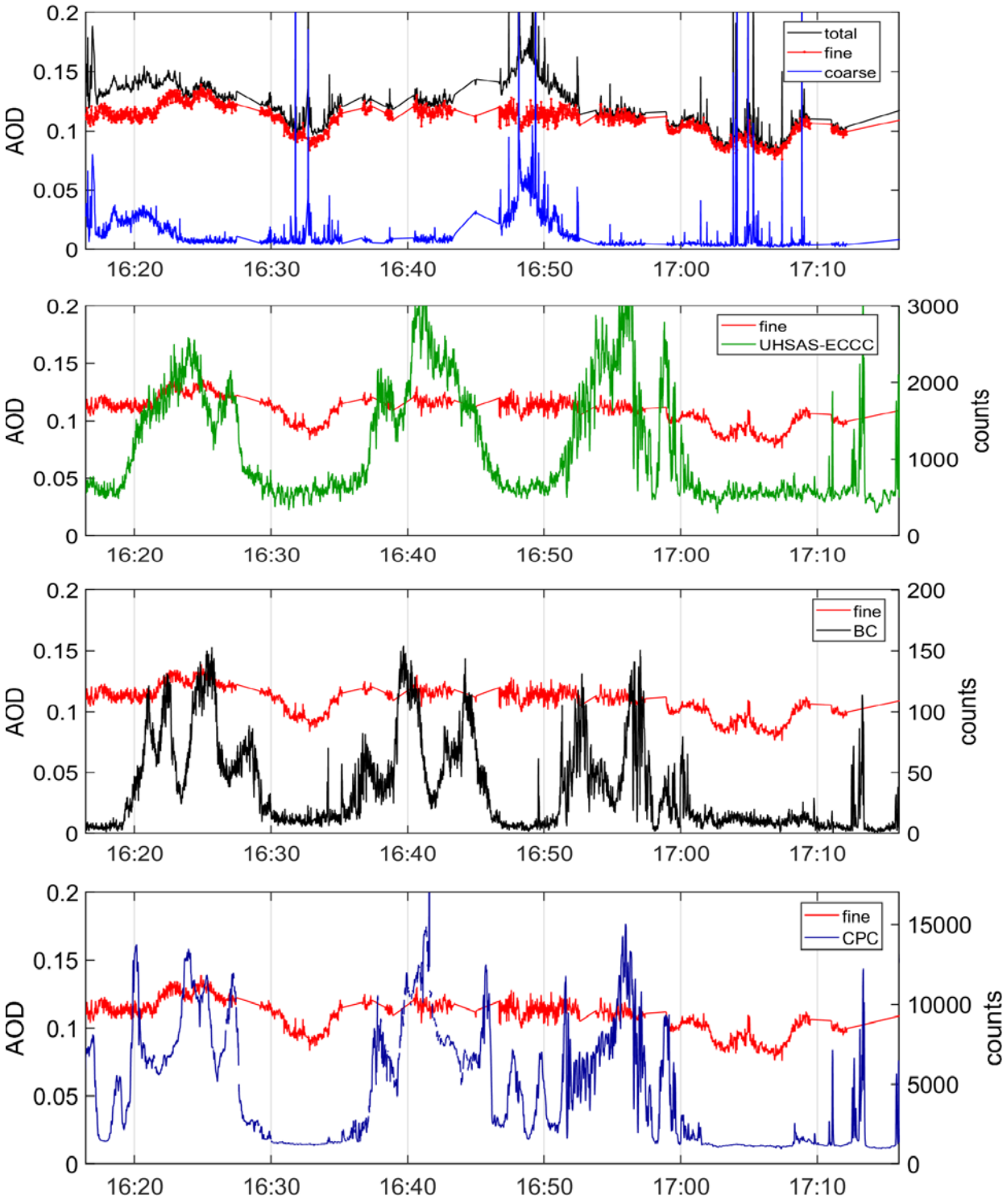

Figure A32. Time series for screen 2 on June 24, 2018. Description as in Figure A17

Screen 3

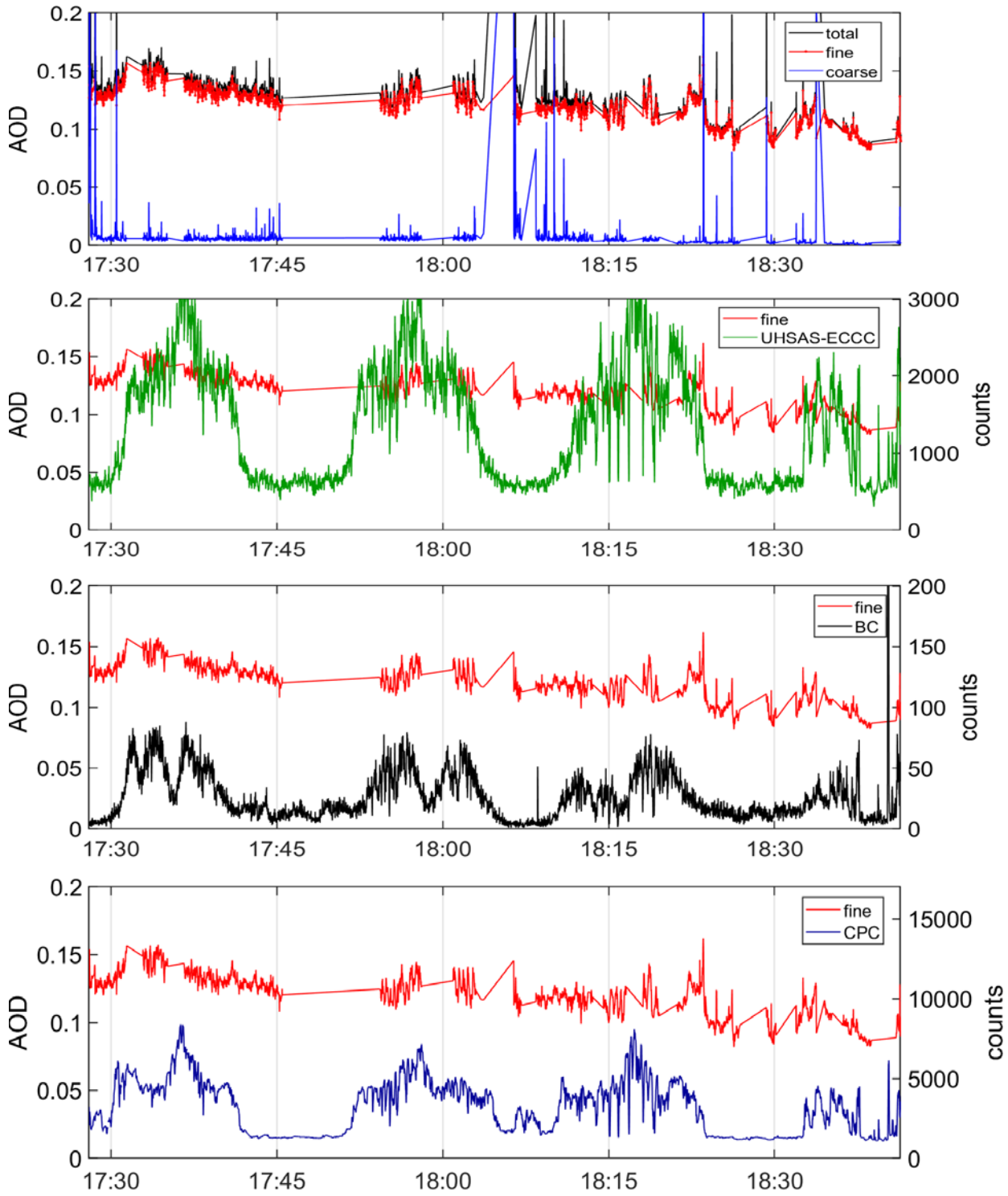

Figure A33. Time series for screen 3 on June 24, 2018. Description as in Figure A17

Spiral data

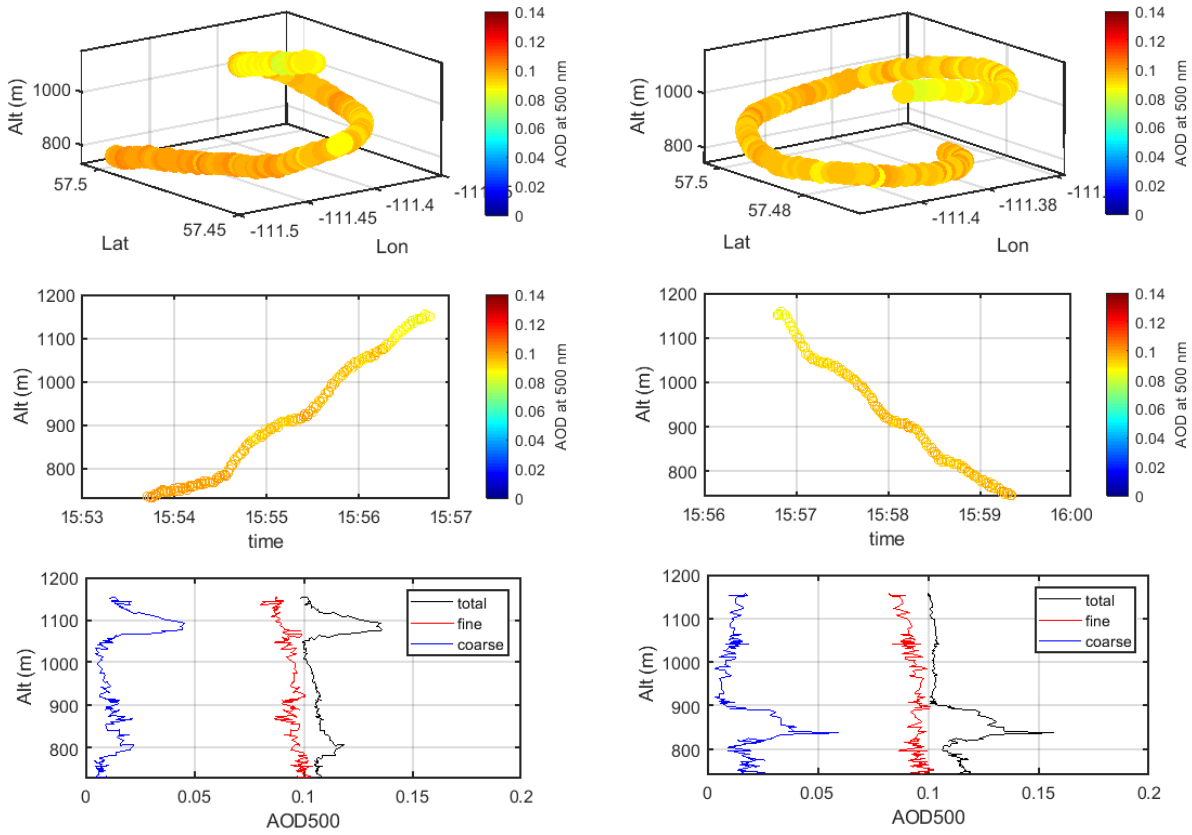

Figure A34. *S*pirals during screen 1. Description as in Figure A9

No 4STAR spiral data is available for screen 2.

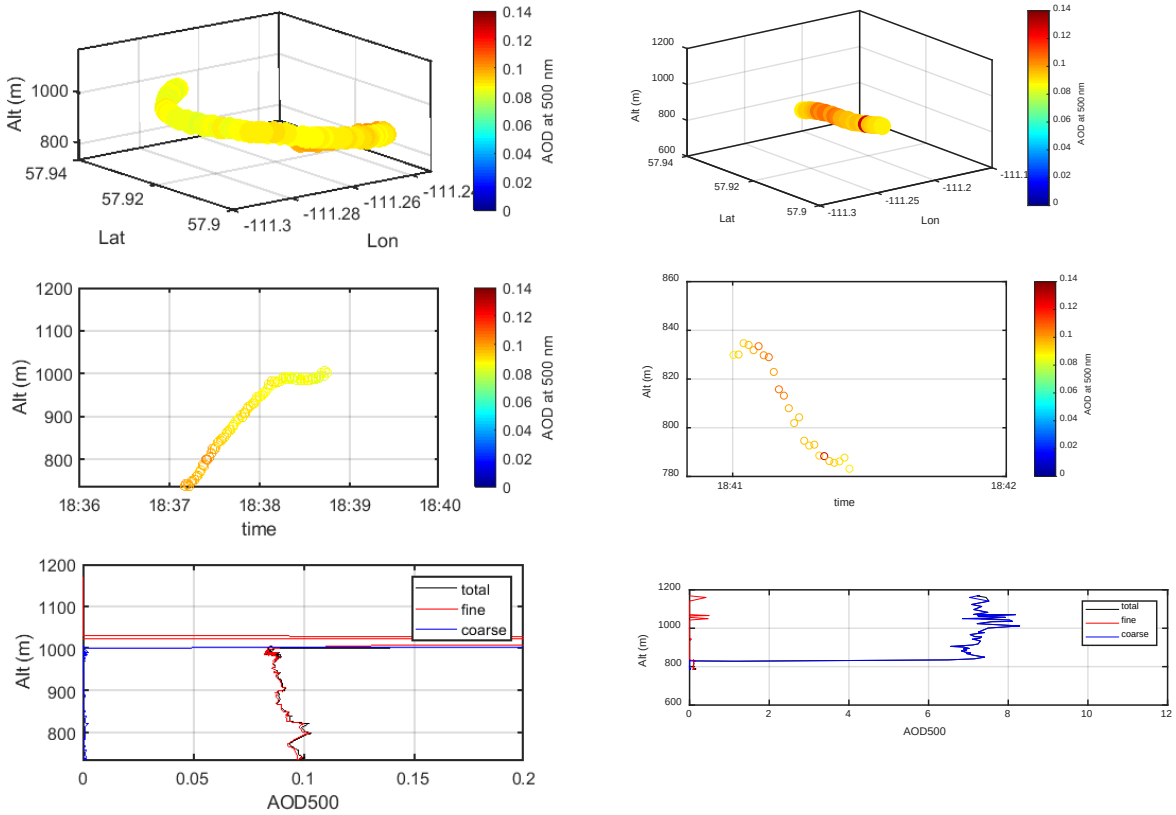

Figure A35. *S*pirals during screen 3. Note that the descending spiral is contaminated by clouds. Description as in Figure A9.

June 25, 2018 – Forest fires transformation flight

Observations

- The forest fires plume can be readily identified in the first 4 screens. The fine-mode AOD is below 0.5 for screen 1 but reaches as high as 1 for all other screens. The measurements during screen 5 are heavily contaminated by clouds.
- Screen 5 is most likely influenced by a mixture of forest fires plume and industrial pollution. The atmosphere was well-mixed by then and the boundary layer height was quite high.
- No cloud screening was applied for this date, because it would filter out some of what seems to be reasonable aerosol data
- In general, there is a level of correlation between fine-mode AOD and UHSAS, BC and CPC peaks.
- Profile data: good data for screens 1-3, no data for screen 4, cloud contaminated data for screen 5. During most spirals the aircraft stayed for an extra minute at the highest point

Flight maneuvers table

Table A5. Flight plan for June 25, 2018.

Date	NRC flight #	ECCC flight #	Flight maneuver	Alt (ft)	From Time	To Time
2018/06/25	39	25	Take off		14:45:23	
Screen 1						
2018/06/25	39	25	transformation	500	15:01:44	15:11:10
2018/06/25	39	25	transformation	750	15:13:05	15:22:58
2018/06/25	39	25	transformation	1000	15:24:23	15:34:25
2018/06/25	39	25	transformation	1250	15:36:02	16:02:02
2018/06/25	39	25	spiral up		15:43:09	15:52:31
2018/06/25	39	25	spiral down		15:52:32	15:58:06
2018/06/25	39	25	transformation	1750	16:04:21	16:15:03
Screen 2						
2018/06/25	39	25	transformation	500	16:19:40	16:29:27
2018/06/25	39	25	transformation	750	16:31:14	16:41:07
2018/06/25	39	25	transformation	1000	16:43:08	16:52:35
2018/06/25	39	25	transformation	1250	16:54:34	17:16:38
2018/06/25	39	25	spiral up		16:58:28	17:04:06
2018/06/25	39	25	spiral down		17:04:07	17:09:49
Screen 3						
2018/06/25	39	25	transformation	500	17:22:42	17:33:06
2018/06/25	39	25	transformation	750	17:34:45	17:45:57
2018/06/25	39	25	transformation	1000	17:48:00	17:59:12

2018/06/25	39	25	transformation	1250	18:01:16	18:23:49
2018/06/25	39	25	spiral up		18:05:04	18:11:57
2018/06/25	39	25	spiral down		18:11:58	18:15:44
Screen 4						
2018/06/25	39	25	transformation	500	18:28:59	18:39:46
2018/06/25	39	25	transformation	750	18:43:05	18:55:01
2018/06/25	39	25	transformation	1000	18:57:11	19:09:39
2018/06/25	39	25	Landing			19:16:30
2018/06/25	40	26	Take off		20:17:36	
Screen 5 – Flight 2						
2018/06/25	40	26	transformation	500	20:42:42	21:02:05
2018/06/25	40	26	transformation	750	21:04:28	21:20:10
2018/06/25	40	26	transformation	1000	21:20:50	21:57:32
2018/06/25	40	26	spiral up		21:27:53	21:42:35
2018/06/25	40	26	spiral down		21:42:36	21:48:59
2018/06/25	40	26	transformation	1750	21:58:27	22:15:29
2018/06/25	40	26	transformation	2000	22:18:02	22:33:25
2018/06/25	40	26	transformation	2500	22:35:39	22:50:36
2018/06/25	39	25	Landing			23:18:40

Flight imagery

Figure A36. Photographic imagery from the flight.

Comparisons with AERONET before/after flight

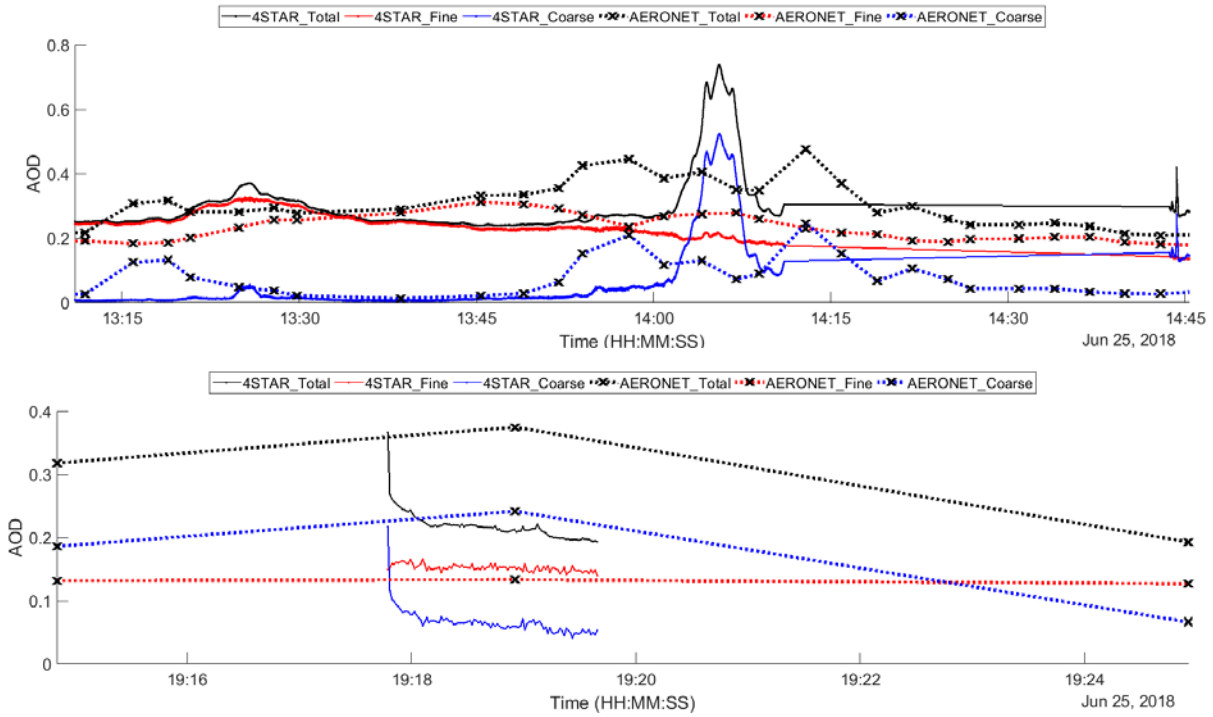

Comparisons with AERONET, NRC flight 39. Top: before the flight, bottom: after the flight

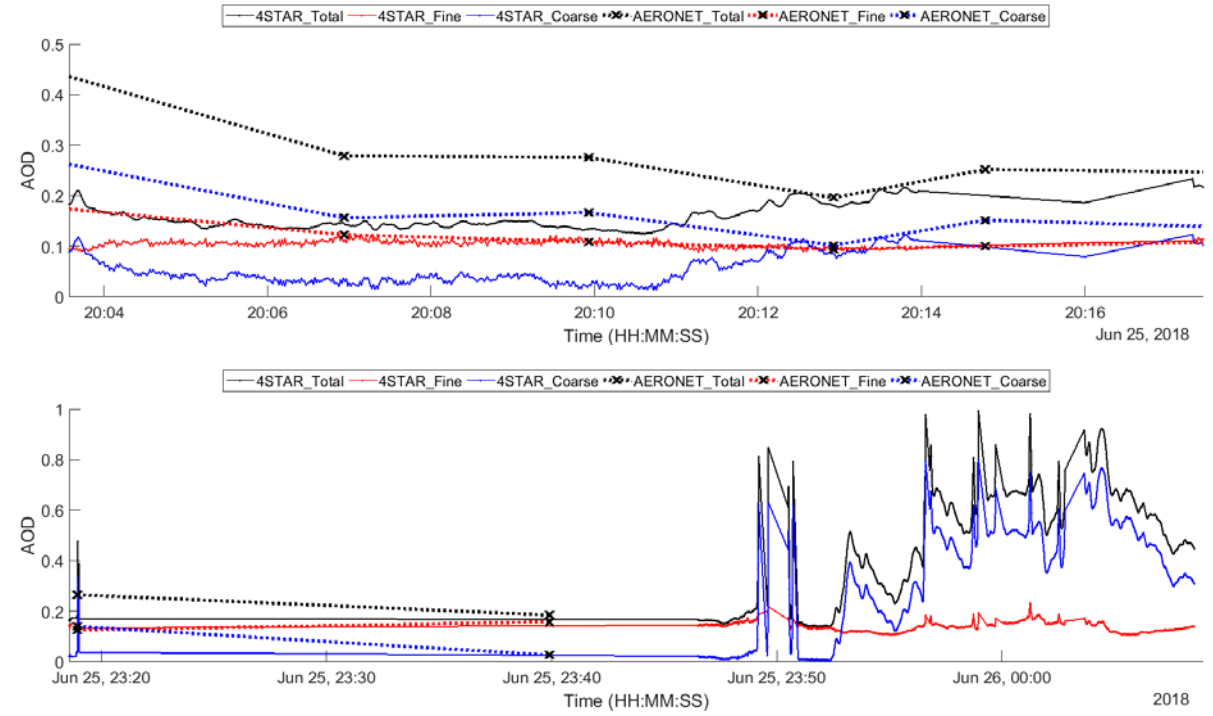

Figure A37. Comparisons with AERONET. Description as in Figure A2

Flight track

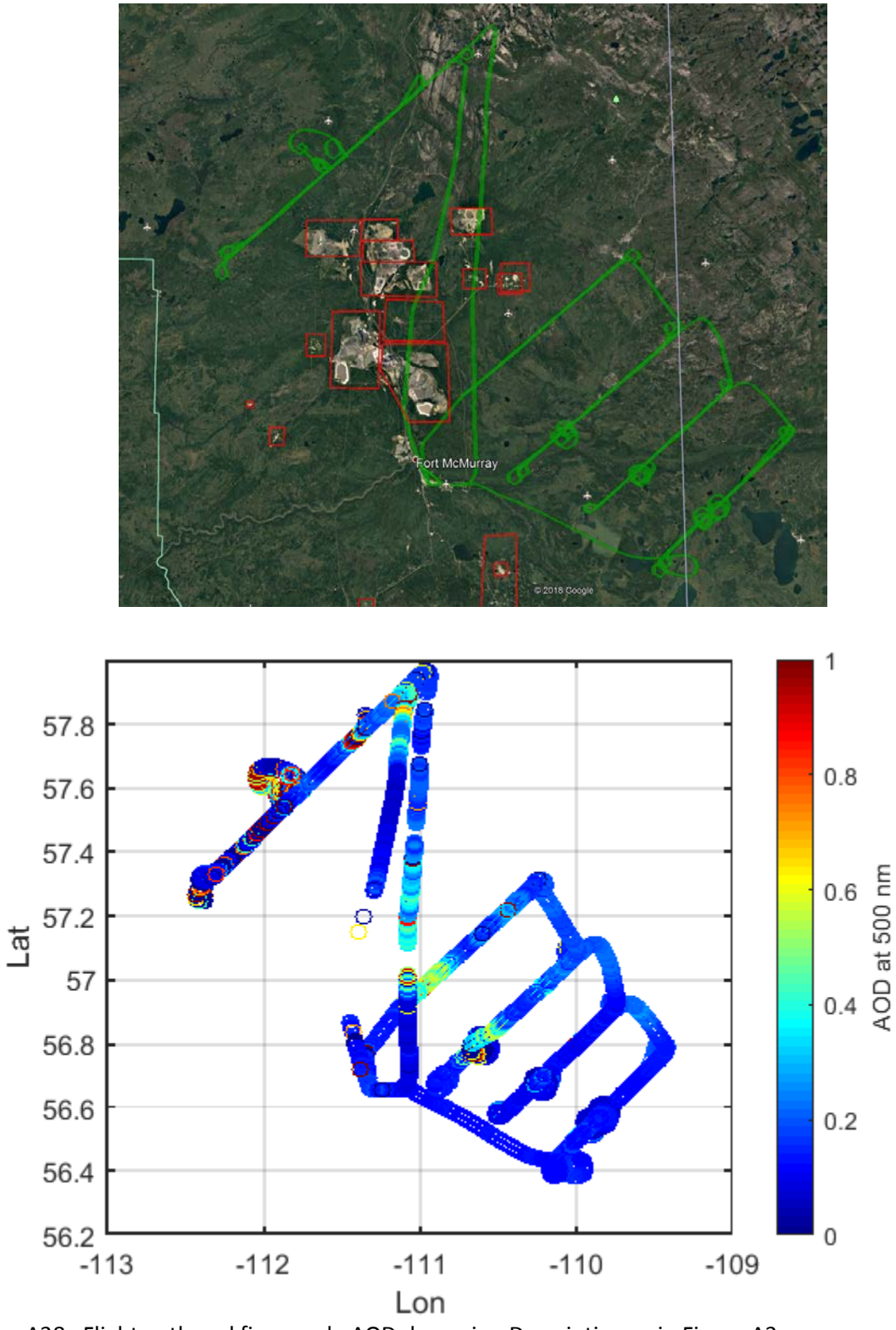

Figure A38. Flight path and fine-mode AOD dynamics. Description as in Figure A3

AOD dynamics for each screen

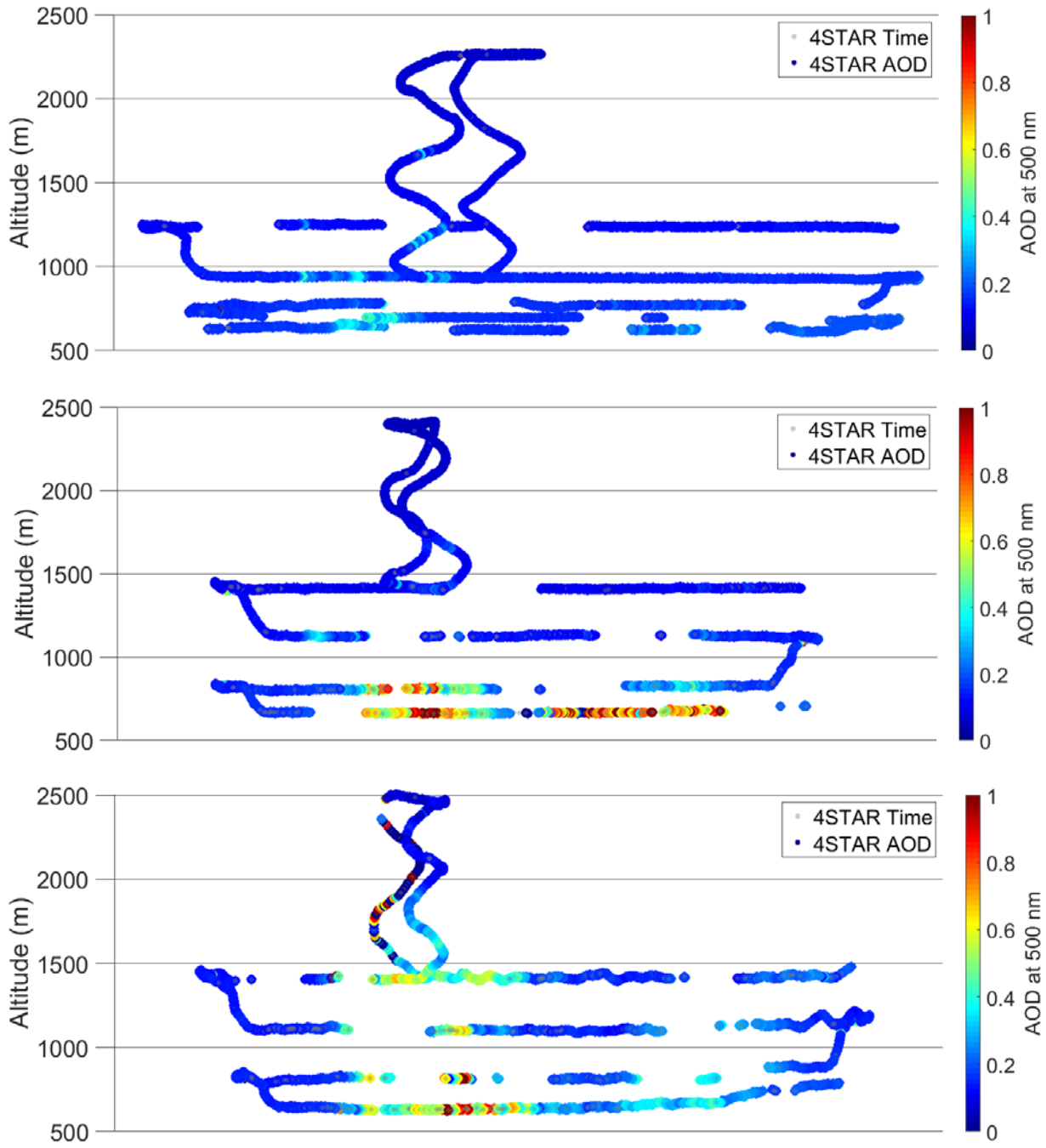

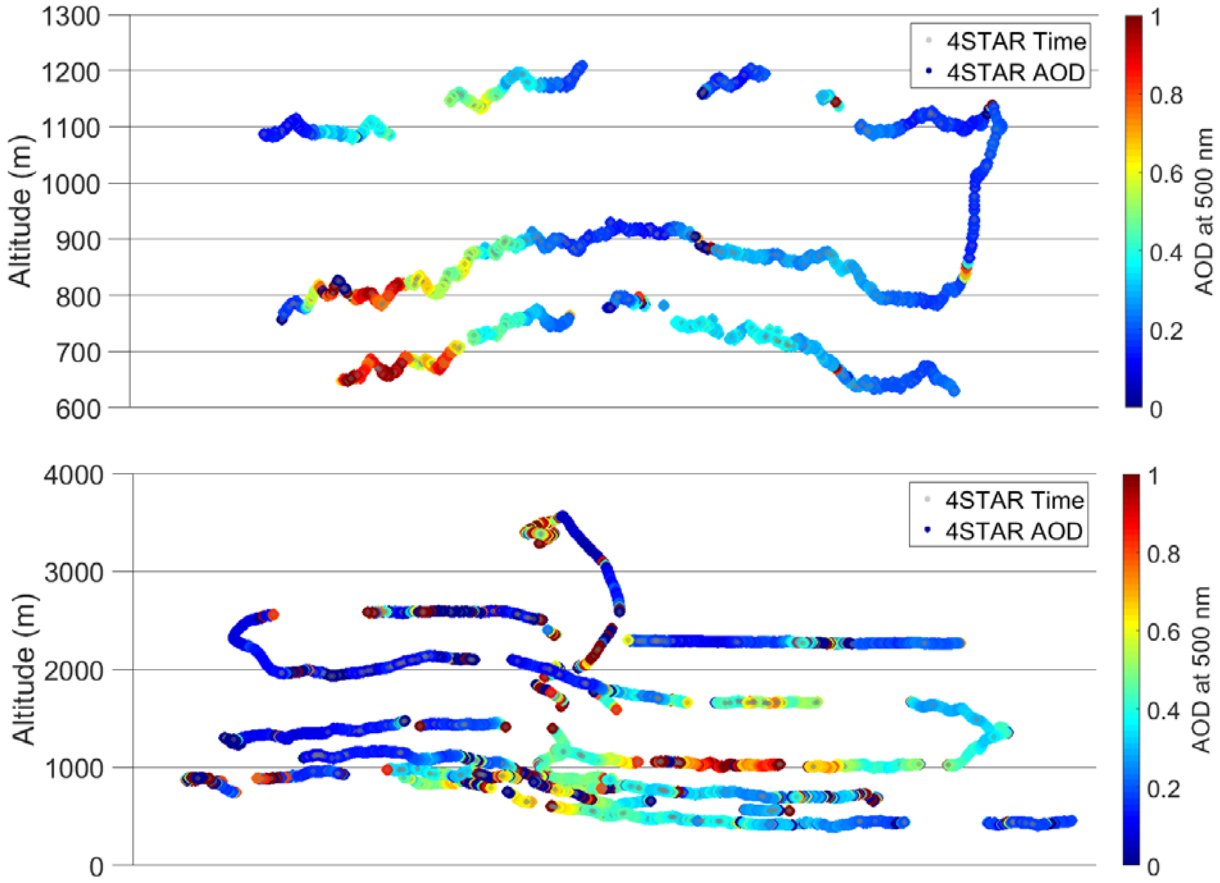

Figure A39. AOD fine-mode in-flight dynamics for transformation screens 1 to 5 (top to bottom). The X-axis is parallel to the flight track.

SDA dynamics and intercomparisons

Screen 1

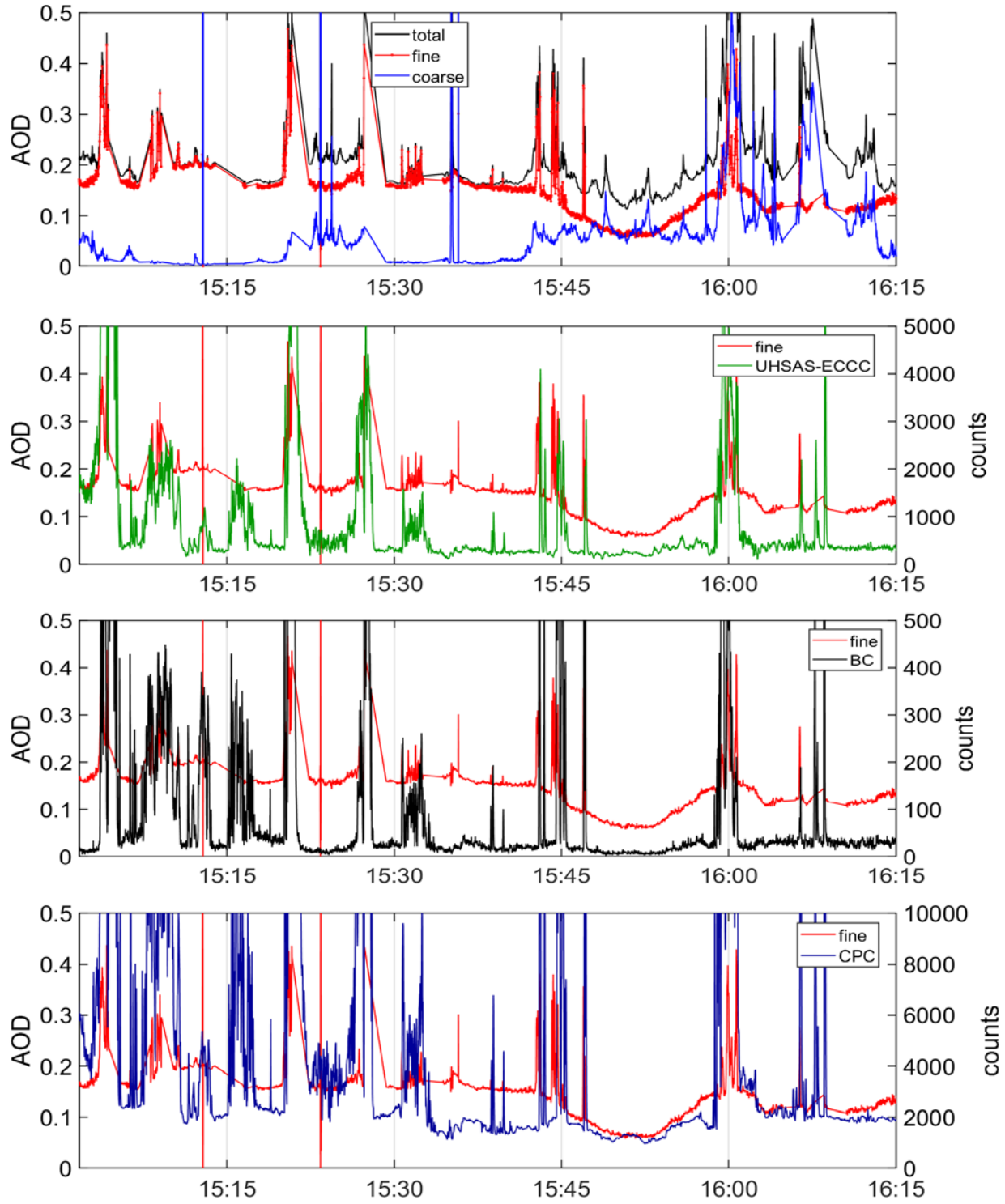

Figure A40. Time series for screen 1 on June 25, 2018. Description as in Figure A17

Screen 2

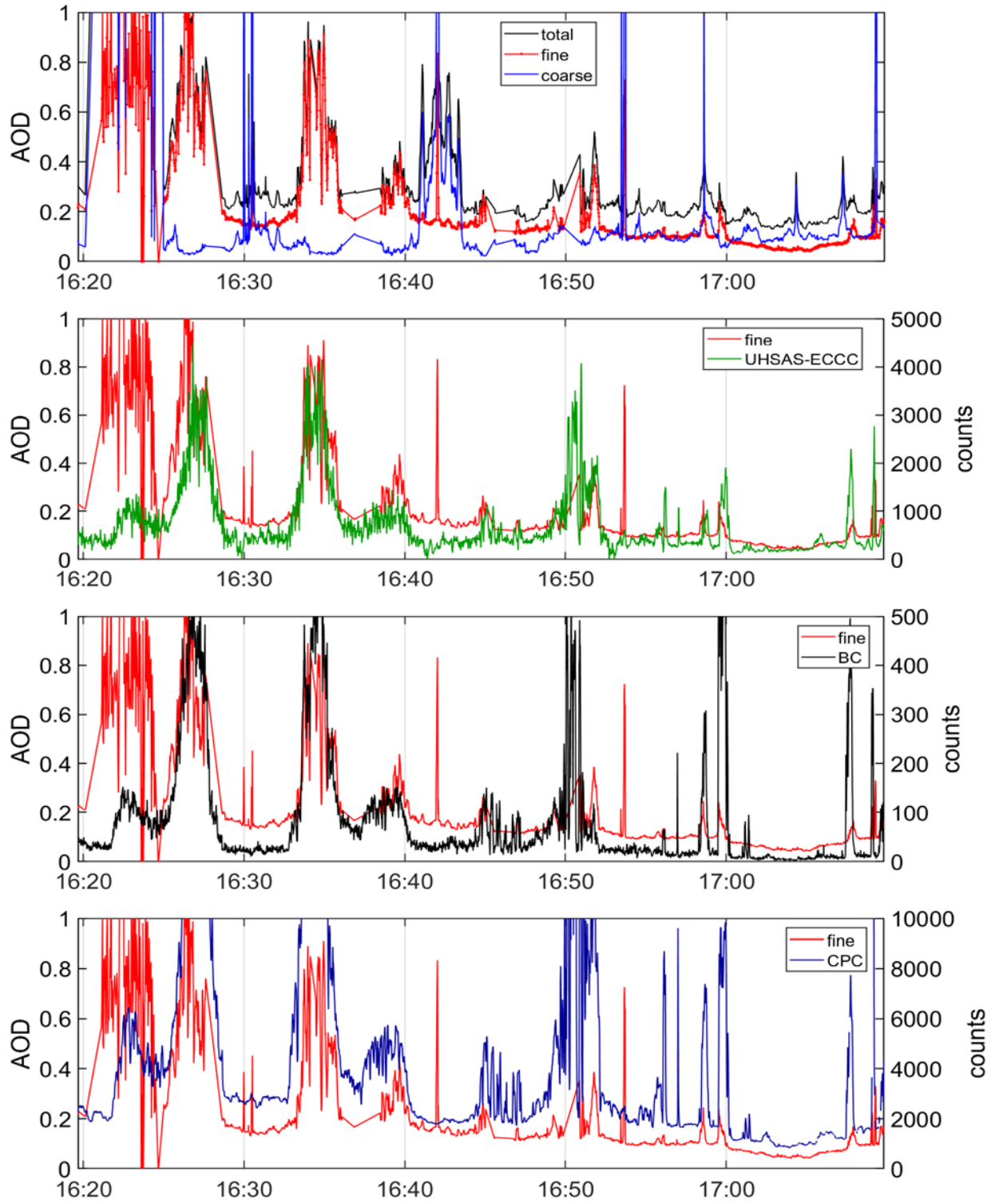

Figure A41. Time series for screen 2 on June 25, 2018. Description as in Figure A17

Screen 3

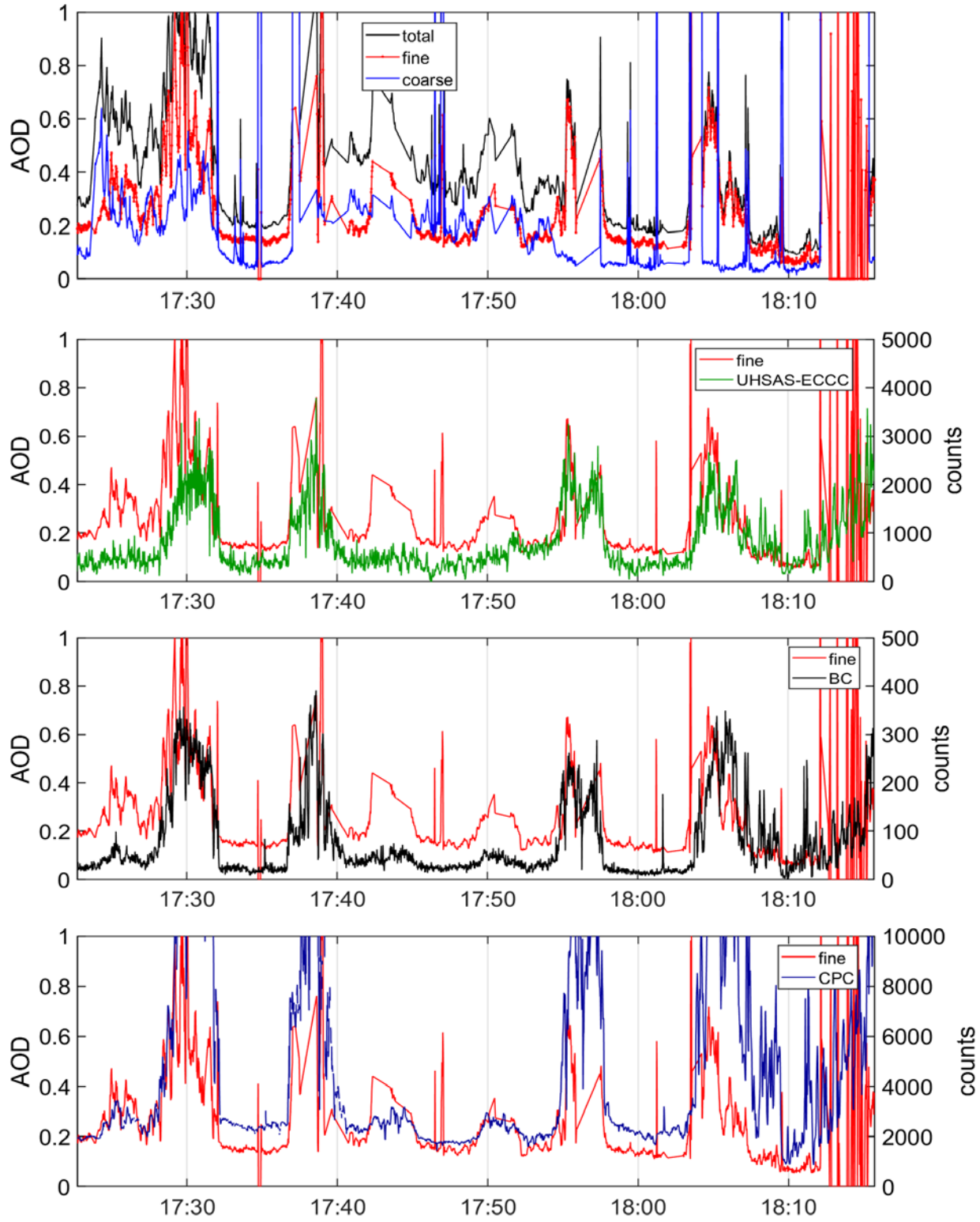

Figure A42. Time series for screen 3 on June 25, 2018. Description as in Figure A17

Screen 4

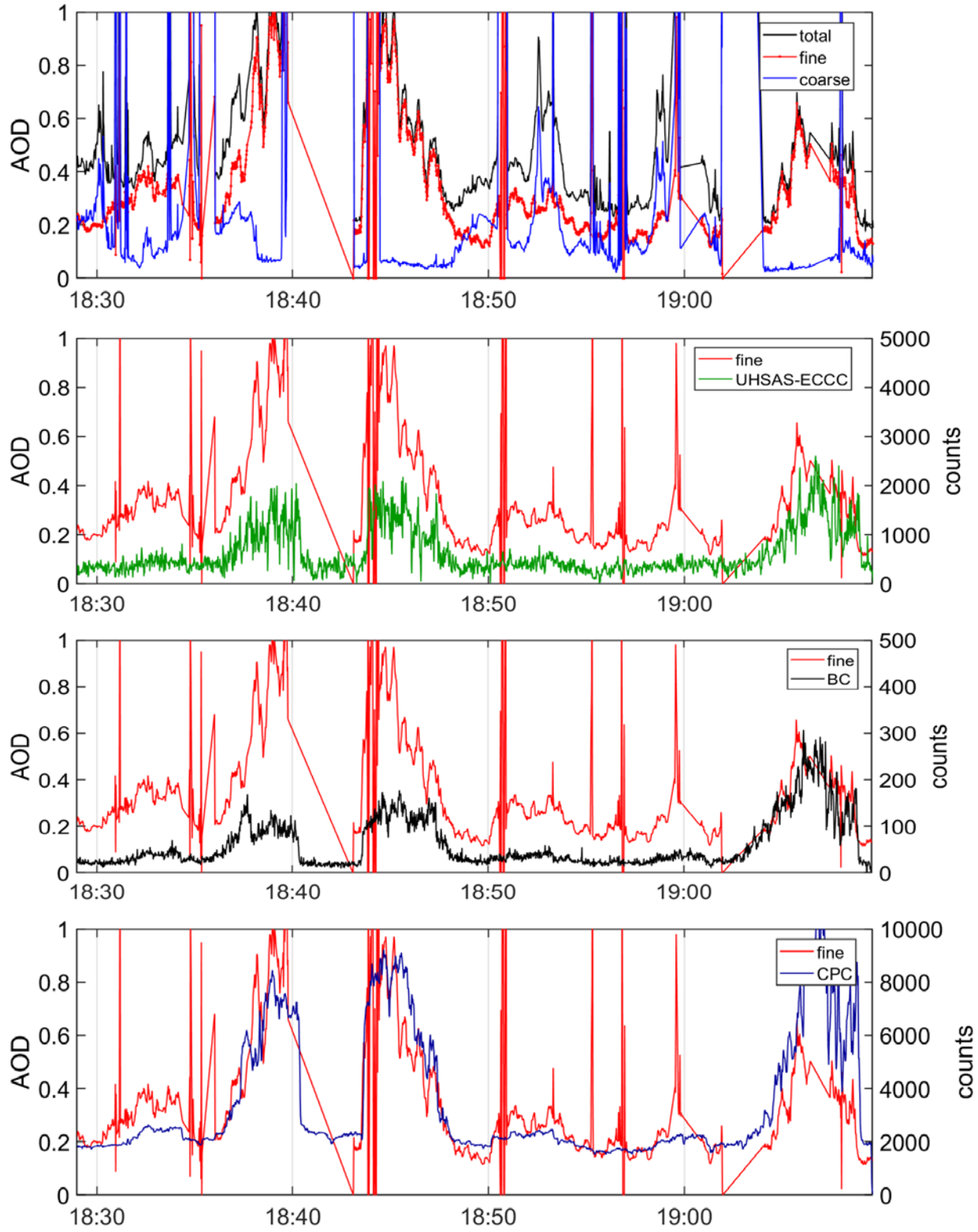

Figure A43. Time series for screen 4 on June 25, 2018. Description as in Figure A17

Screen 5

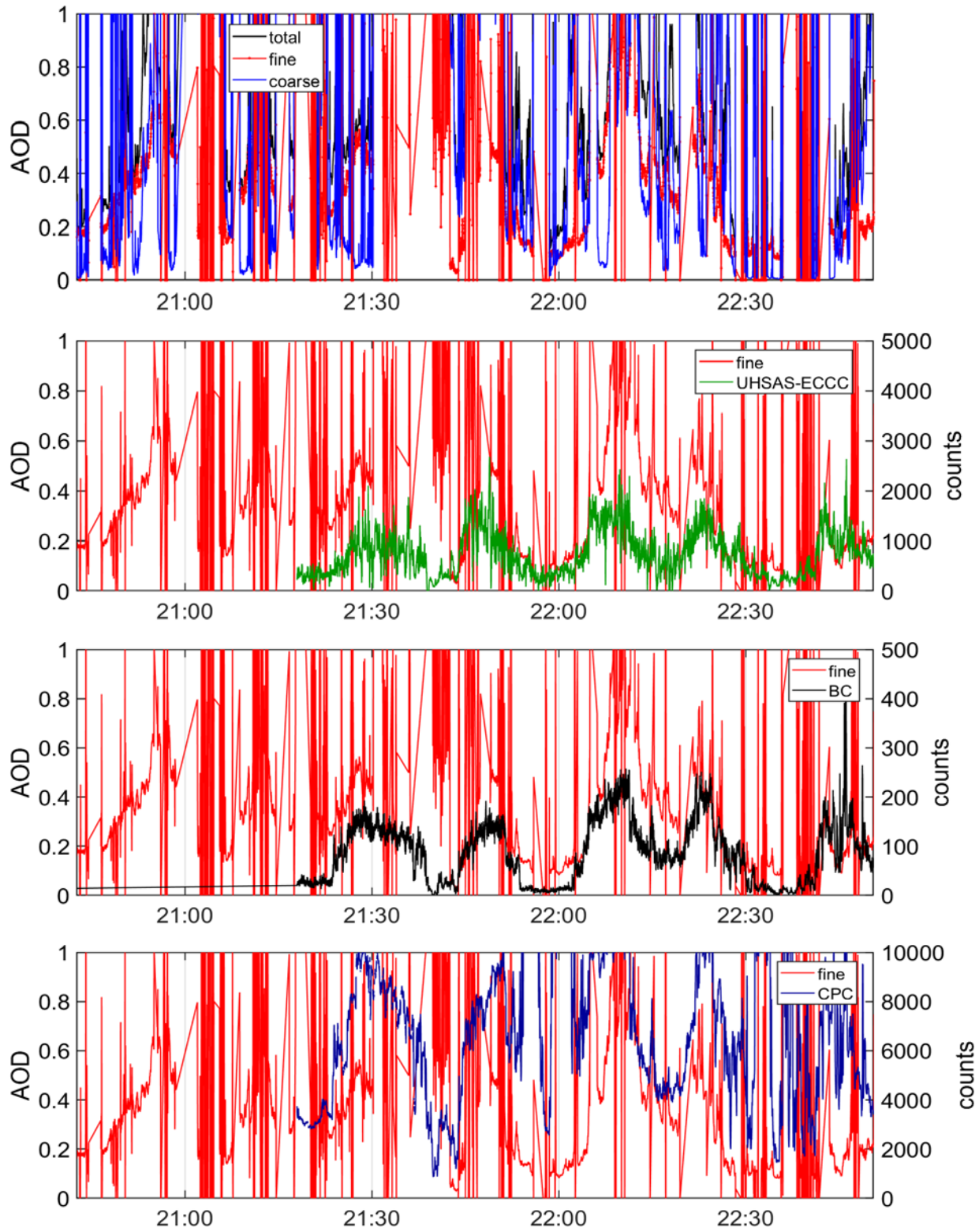

Figure A44. Time series for screen 5 on June 25, 2018. Description as in Figure A17

Spiral data

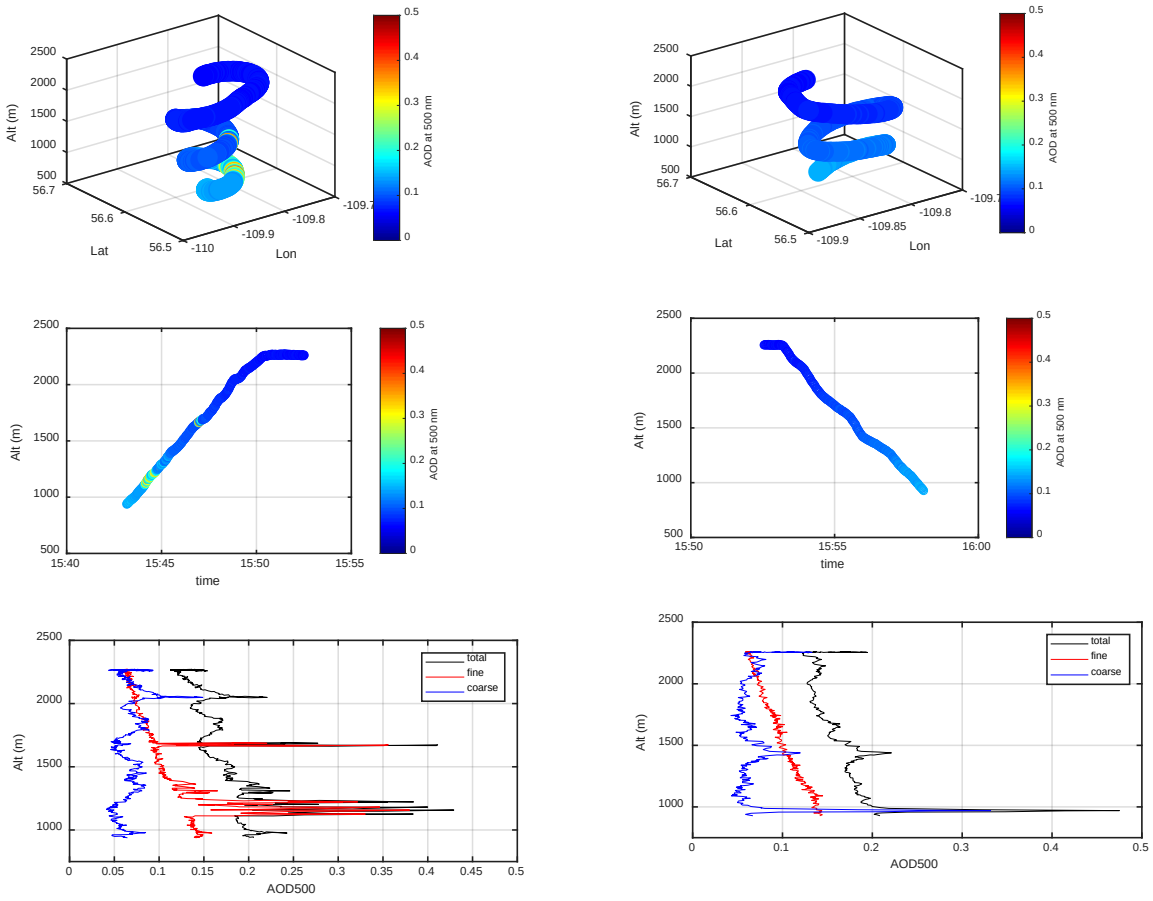

a. Spiral up b. Spiral down

Figure A45. *S*pirals during screen 1. Description as in Figure A9

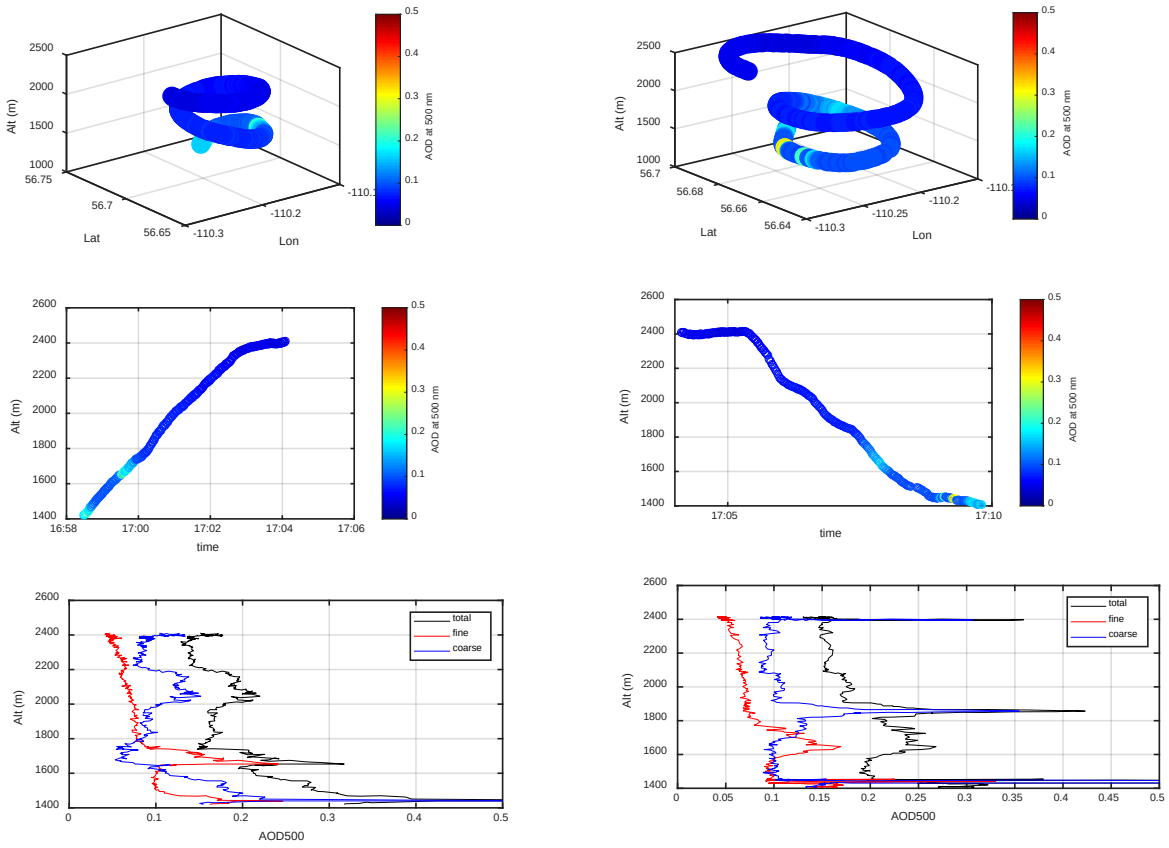

a. Spiral up b. Spiral down

Figure A46. *S*pirals during screen 2. Description as in Figure A9

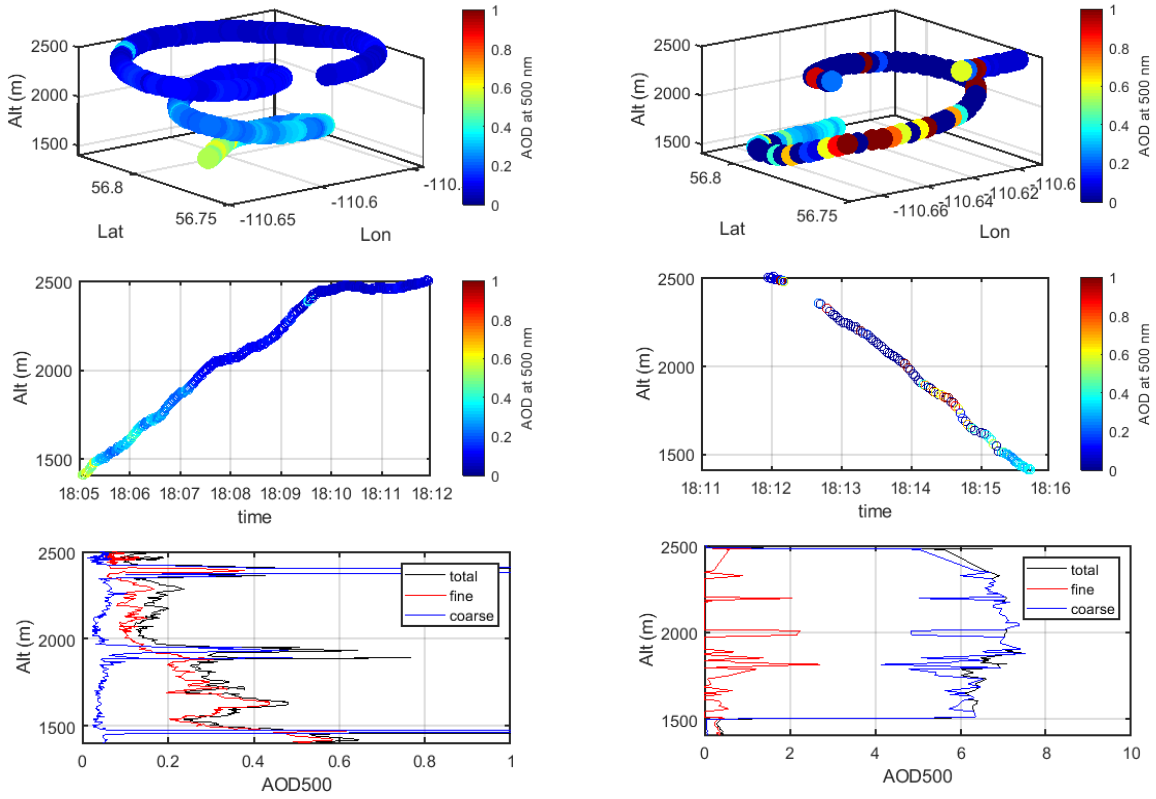

a. Spiral up b. Spiral down

Figure A47. *S*pirals during screen 3. Description as in Figure A9. Note that the descending spiral is heavily influenced by clouds

No 4STAR AOD data available for screen 4 spiral.

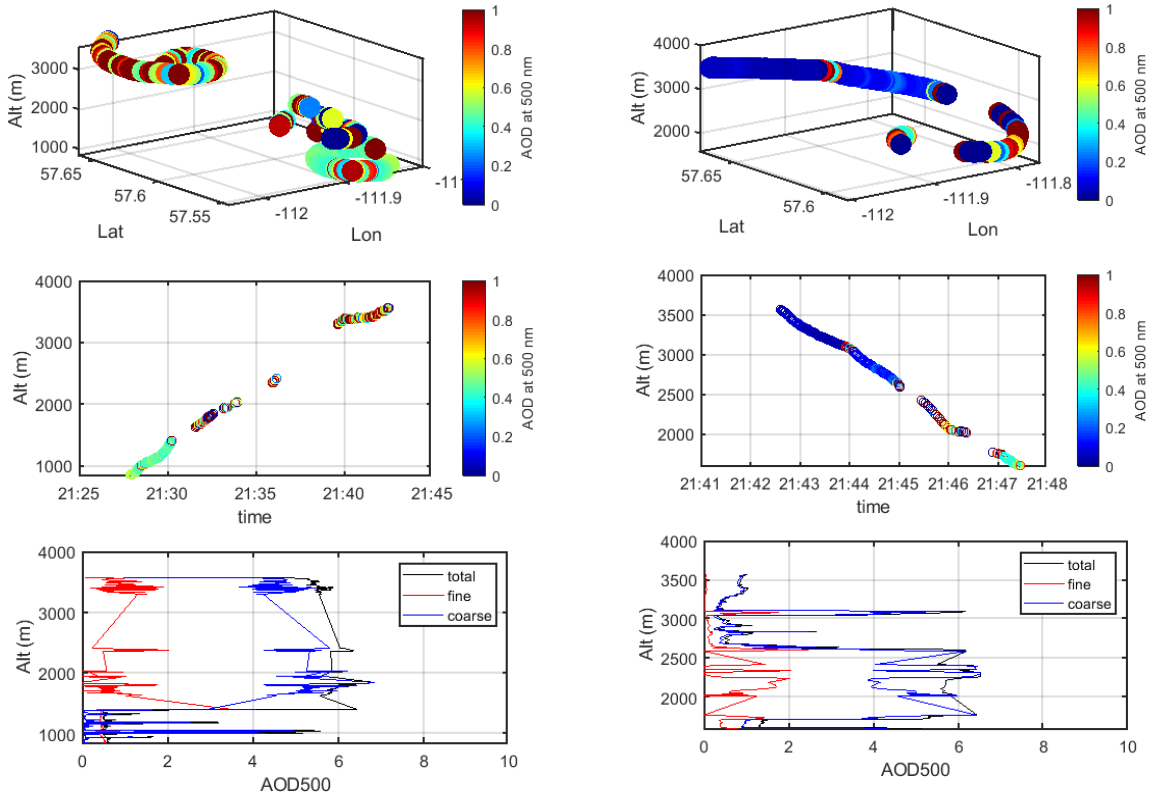

a. Spiral up b. Spiral down

Figure A48. *S*pirals during screen 5. Description as in Figure A9. Note that both spirals are heavily influenced by clouds

July 5, 2018 – Industrial plume transformation flight

Observations

- Low (~0.05), slow-varying AODs throughout the flight, mostly cloud free
- It appears that the average AOD slowly grows from screen to screen (~0.04 for screen 1, ~0.05 for screen 2, and ~0.05-0.06 for screen 3). One has to keep in mind, however, that the difference in AOD of 0.01 is commensurate with the 4STAR measurement error and might be potentially affected by the deposition on the optics
- Compared to other flights, no clear correlation with in-situ peaks as the AODs are varying on a small scale
- Profile data is indicative of the vertically well mixed boundary layer: no sharp AOD peaks
- The positions of the screens are somewhat similar to those of June 24, might consider comparisons.

Flight maneuvers table

Table A6. Flight plan for July 5, 2018.

Date	NRC flight #	ECCC flight #	Flight maneuver	Alt (ft)	From Time	To Time
2018/07/05	46	31	Take off		14:43:08	
Screen 1						
2018/07/05	46	31	transformation	500	15:12:16	15:29:05
2018/07/05	46	31	transformation	1000	15:30:43	15:47:22
2018/07/05	46	31	transformation	750	15:48:58	15:46:57
2018/07/05	46	31	spiral up		15:58:15	16:00:44
2018/07/05	46	31	spiral down		16:00:45	16:02:20
Screen 2						
2018/07/05	46	31	transformation	500	16:14:51	16:34:33
2018/07/05	46	31	transformation	750	16:36:13	17:01:36
2018/07/05	46	31	spiral up		16:43:35	16:47:36
2018/07/05	46	31	spiral down		16:47:37	16:50:25
2018/07/05	46	31	transformation	1000	17:02:54	17:22:11
Screen 3						
2018/07/05	46	31	transformation	500	17:26:39	17:46:48
2018/07/05	46	31	transformation	750	17:48:27	18:18:31
2018/07/05	46	31	spiral up		17:56:46	18:01:39
2018/07/05	46	31	spiral down		18:01:40	18:06:43
2018/07/05	46	31	transformation	1000	18:20:26	18:40:45
2018/07/05	46	31	transformation	1500	18:42:35	19:18:07
2018/07/05	46	31	spiral up		18:50:12	18:55:08

2018/07/05	46	31	spiral down		18:55:09	18:59:47
2018/07/05	46	31	Landing			19:43:22

Comparisons with AERONET before/after flight

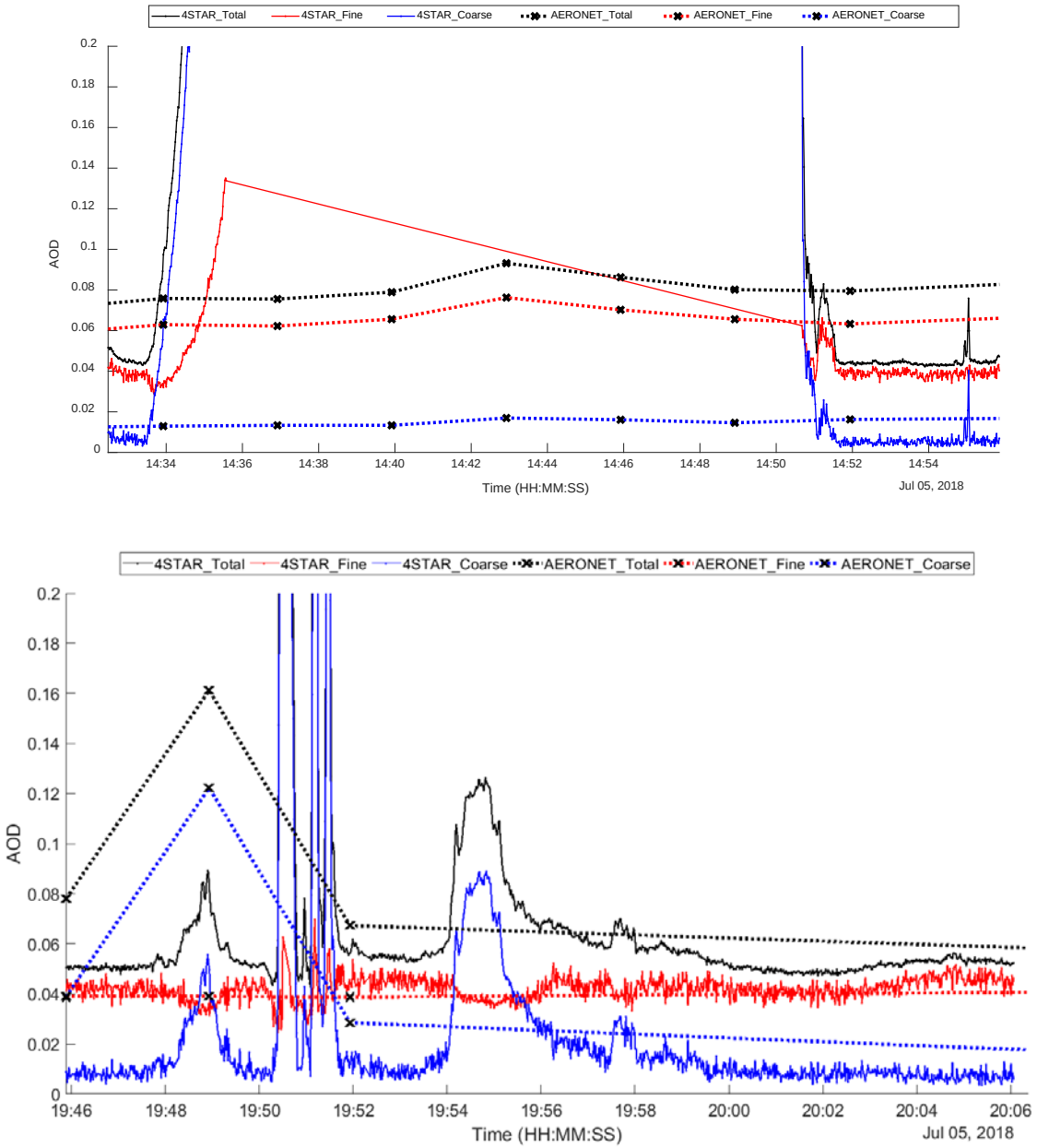

Figure A49. Comparisons with AERONET. Description as in Figure A2

Flight track

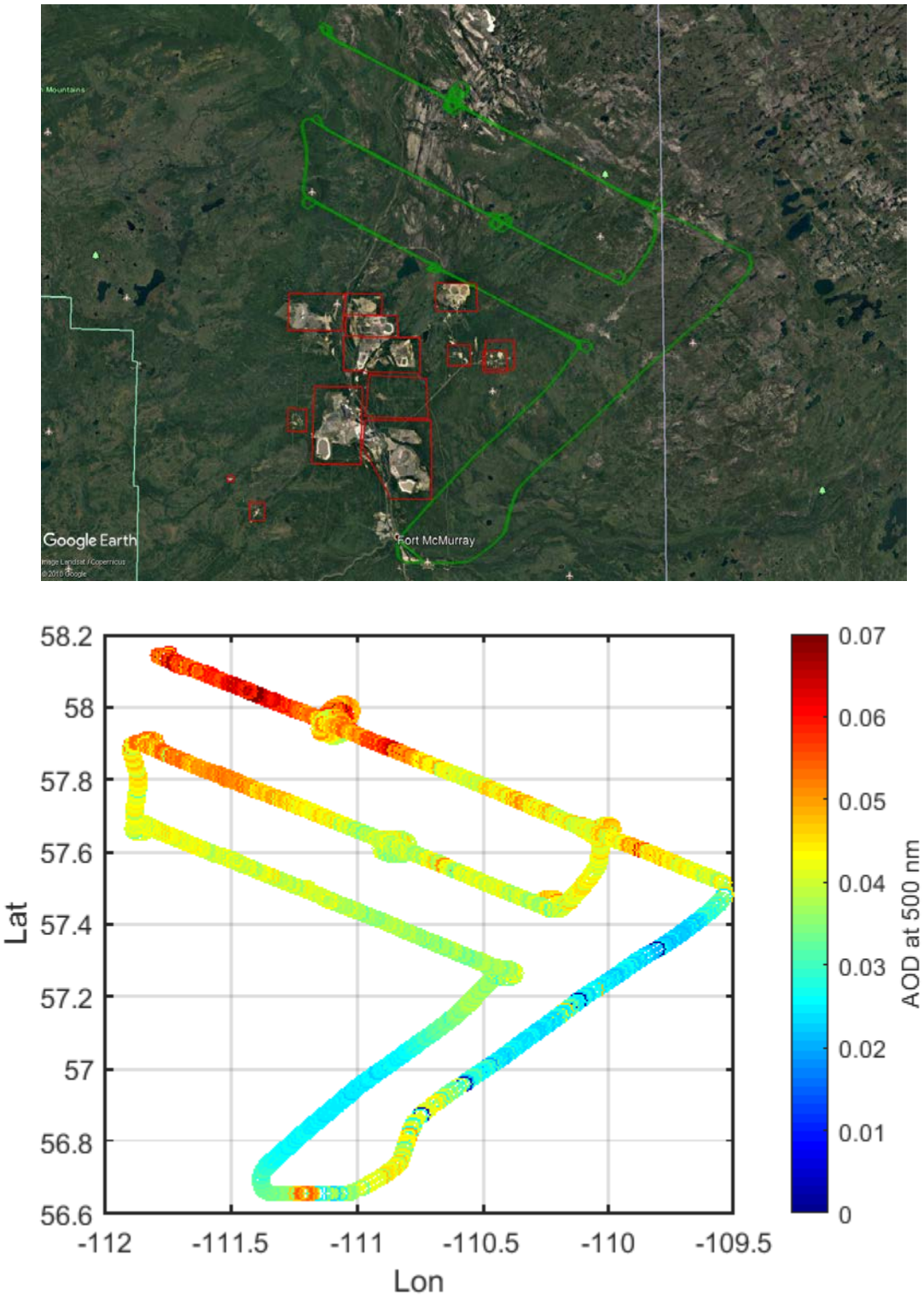

Figure A50. Flight path and fine-mode AOD dynamics. Description as in Figure A3

AOD dynamics for each screen

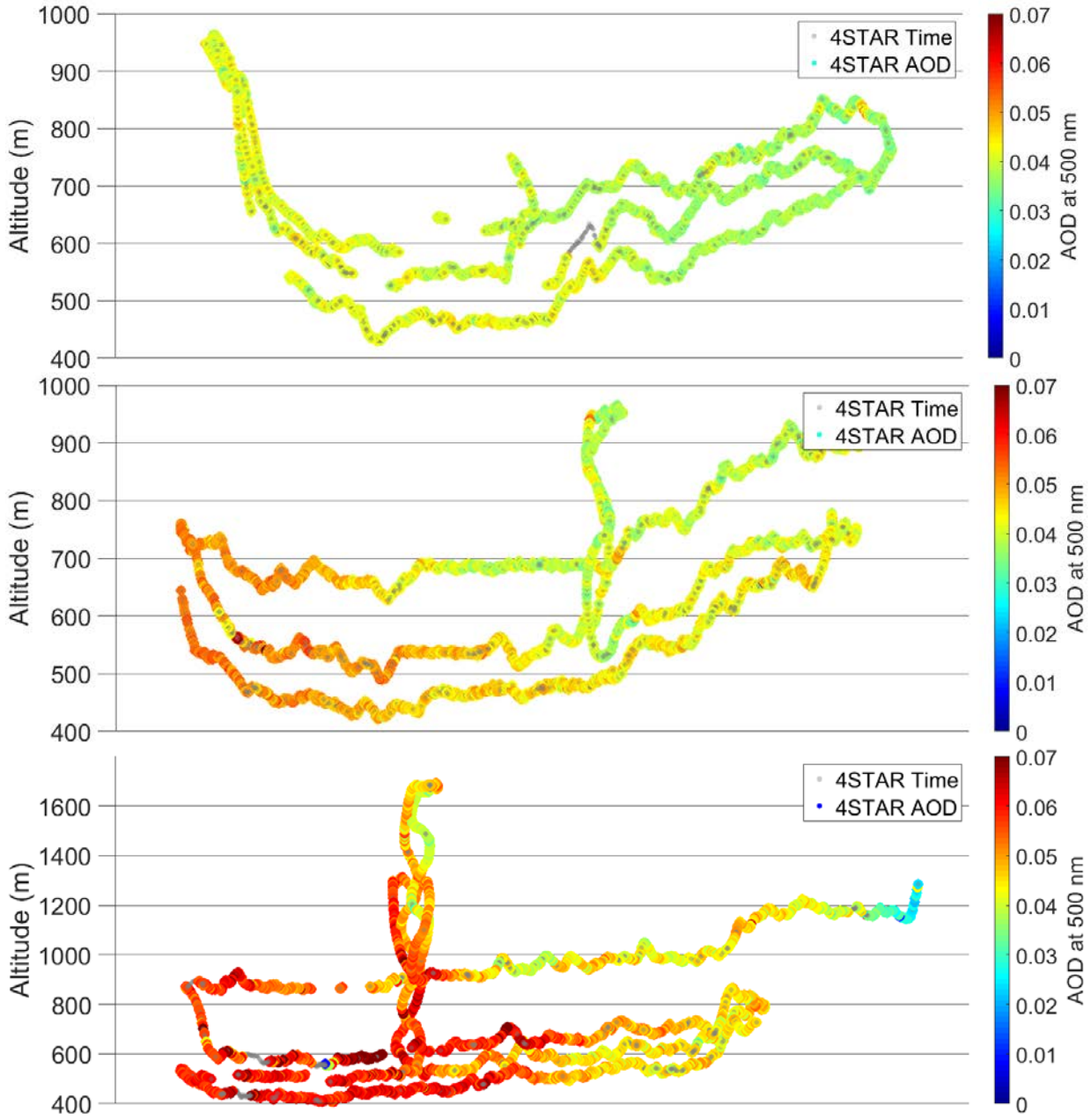

Figure A51. Fine mode AOD dynamis for transformation screens 1 to 3 (top to bottom). The X-axis is parallel to the flight track.

SDA dynamics and intercomparisons

Screen 1

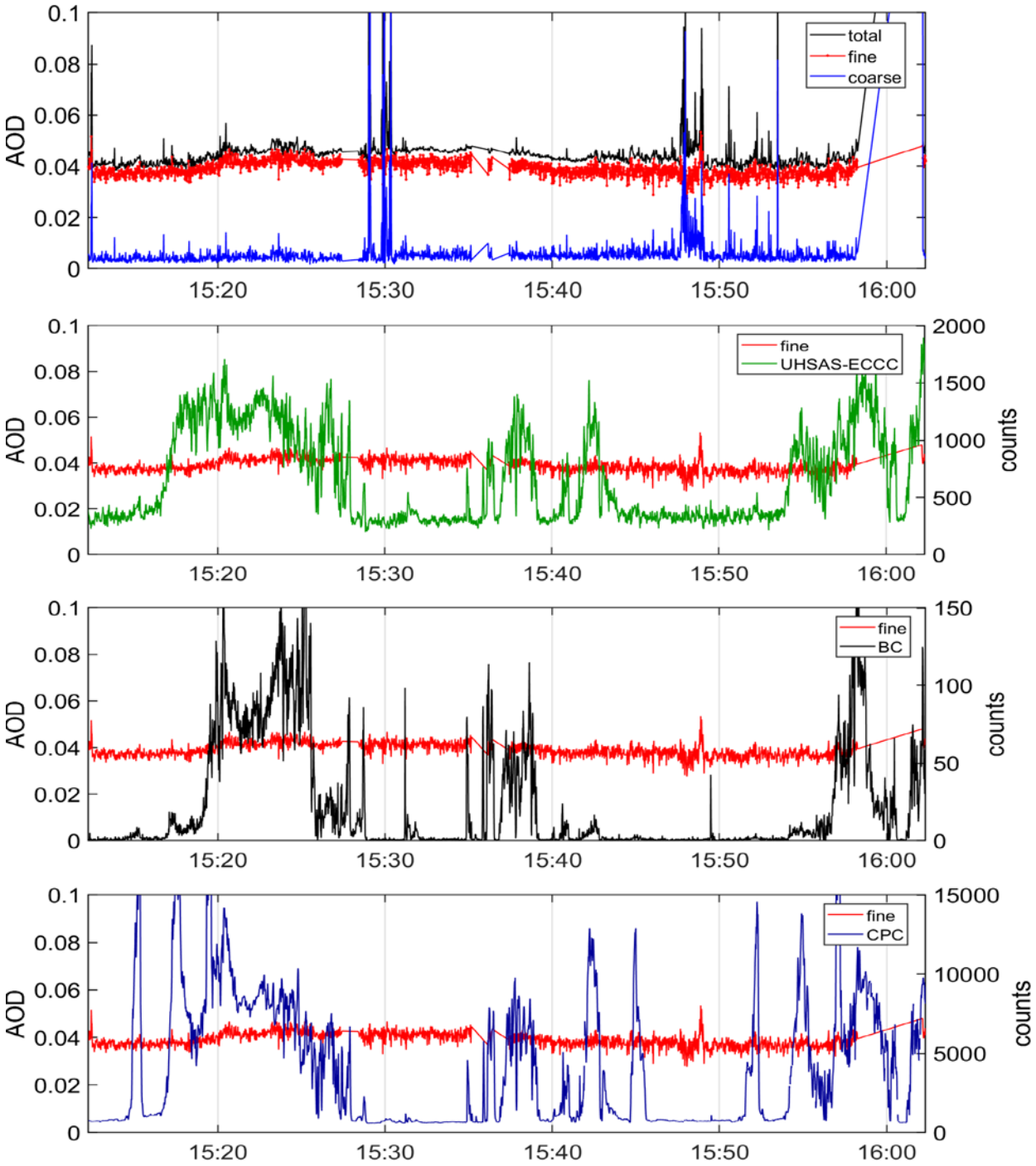

Figure A52. Time series for screen 1 on July 5, 2018. Description as in Figure A17

Screen 2

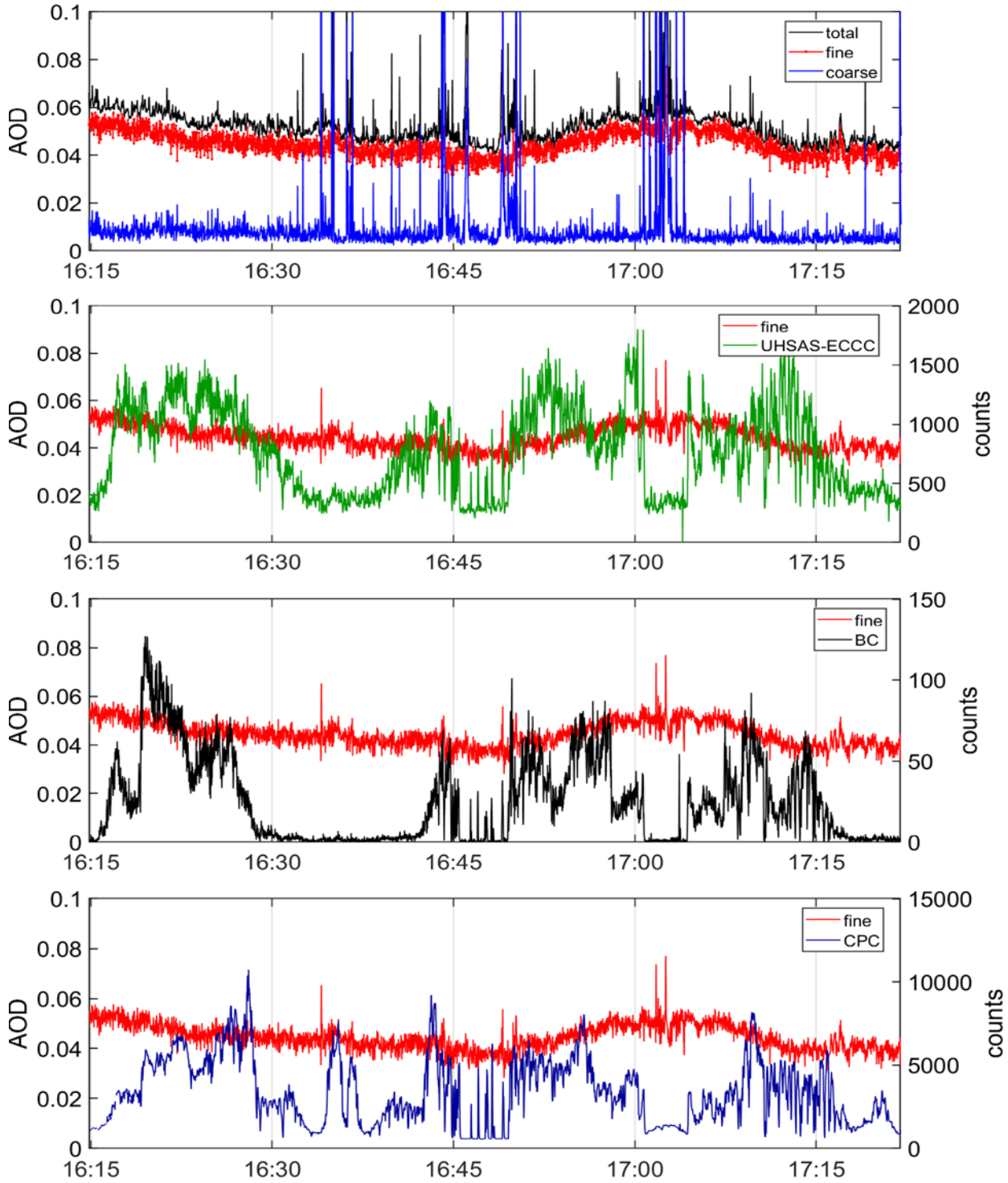

Figure A53. Time series for screen 2 on July 5, 2018. Description as in Figure A17

Screen 3

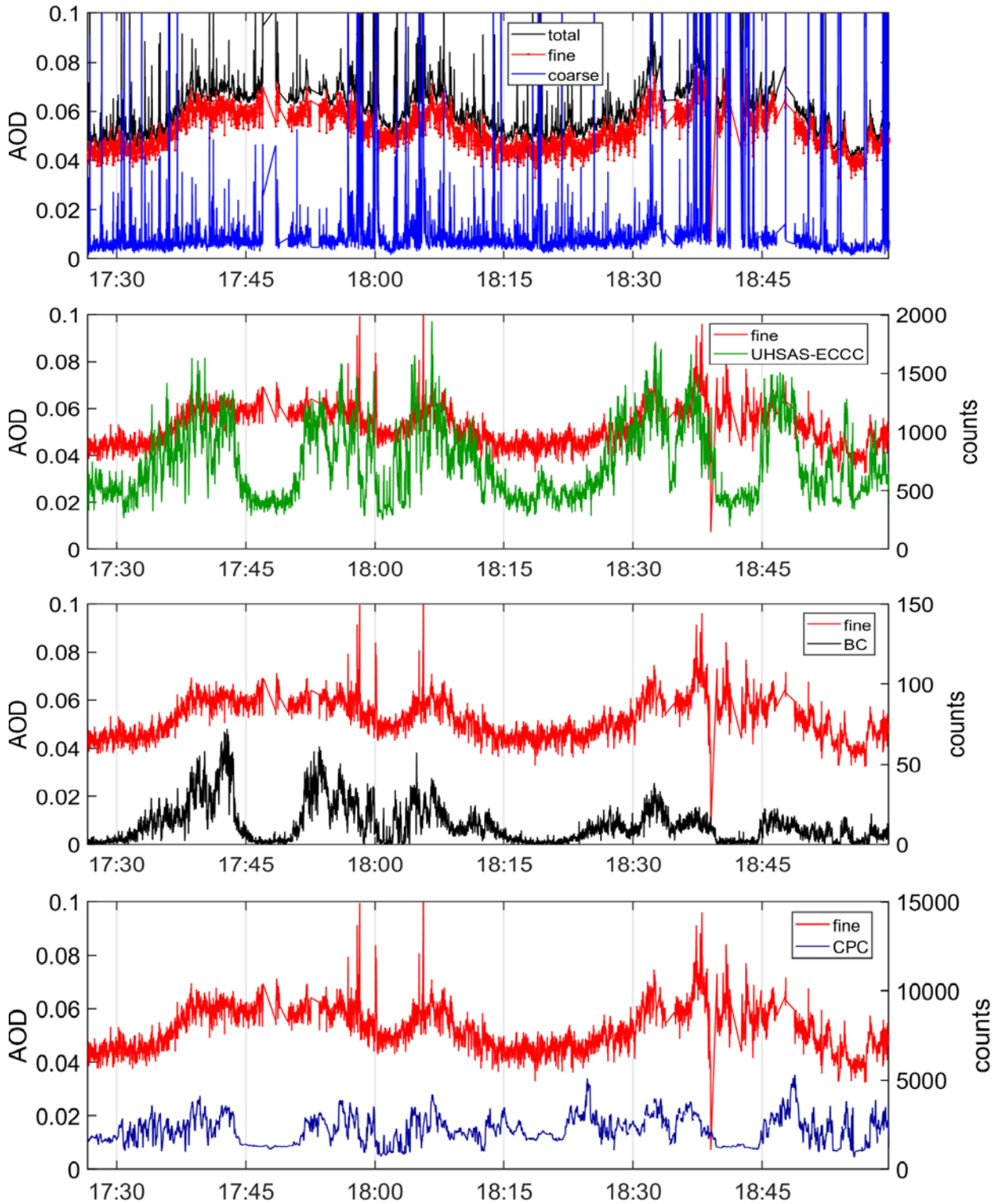

Figure A54. Time series for screen 3 on July 5, 2018. Description as in Figure A17

Spiral data

Insifgnificant cloud free data during screen 1.

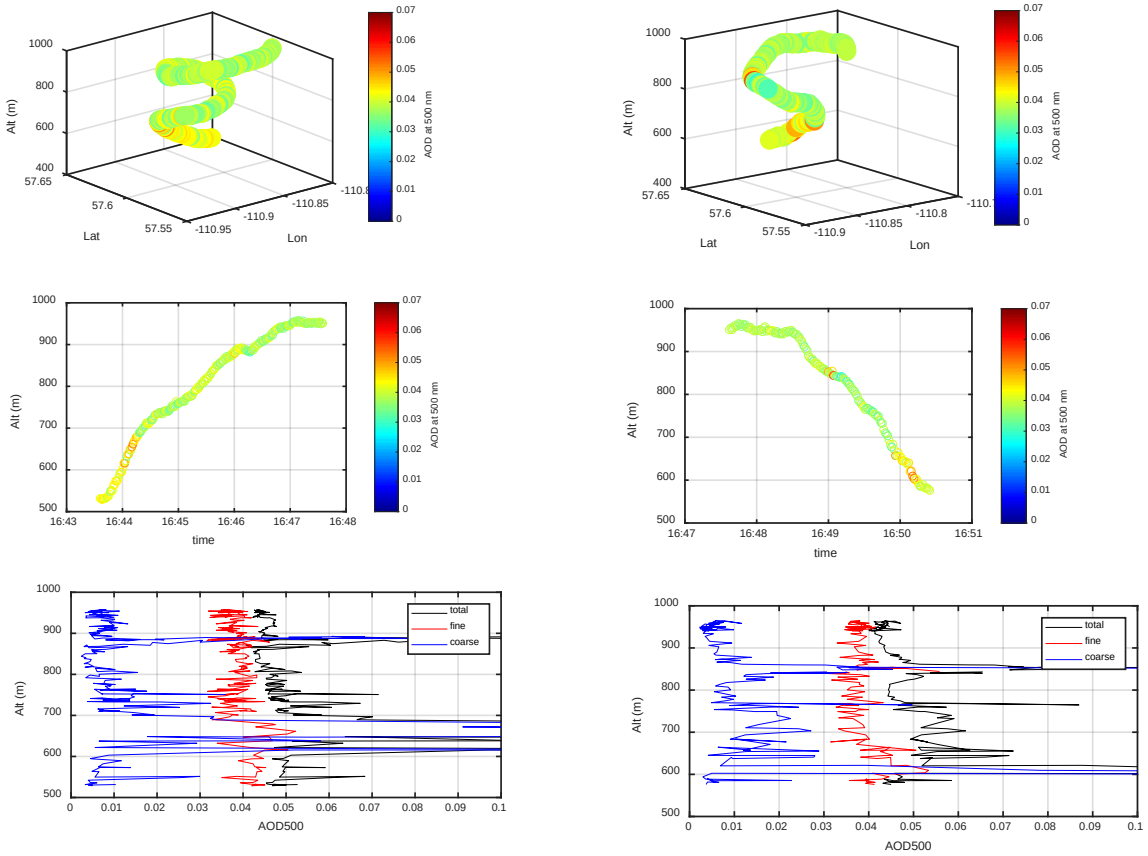

a. Spiral up b. Spiral down

Figure A55. *S*pirals during screen 2. Description as in Figure A9

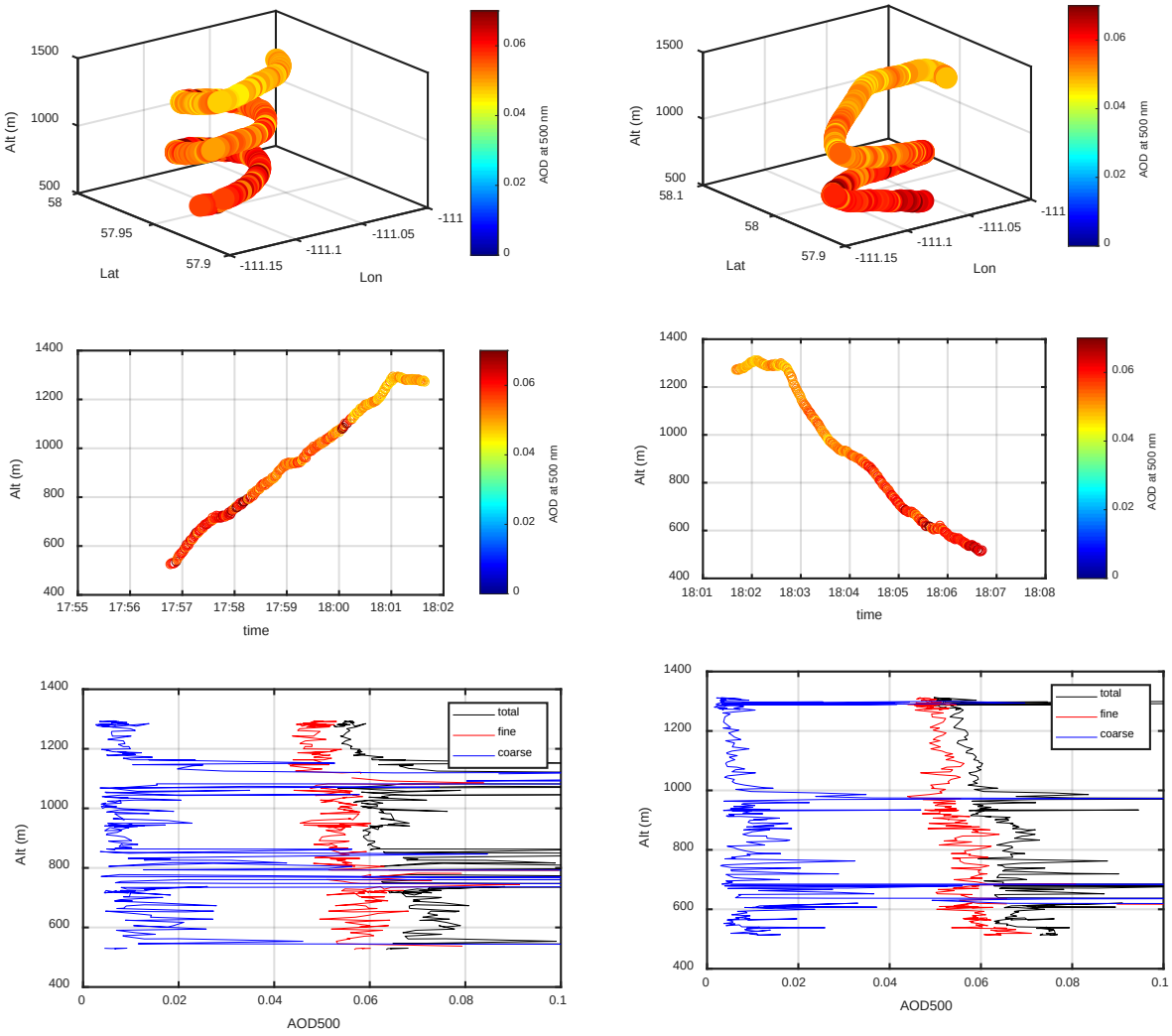

a. Spiral up b. Spiral down

Figure A56. *S*pirals during screen 3 (set 1). Description as in Figure A9

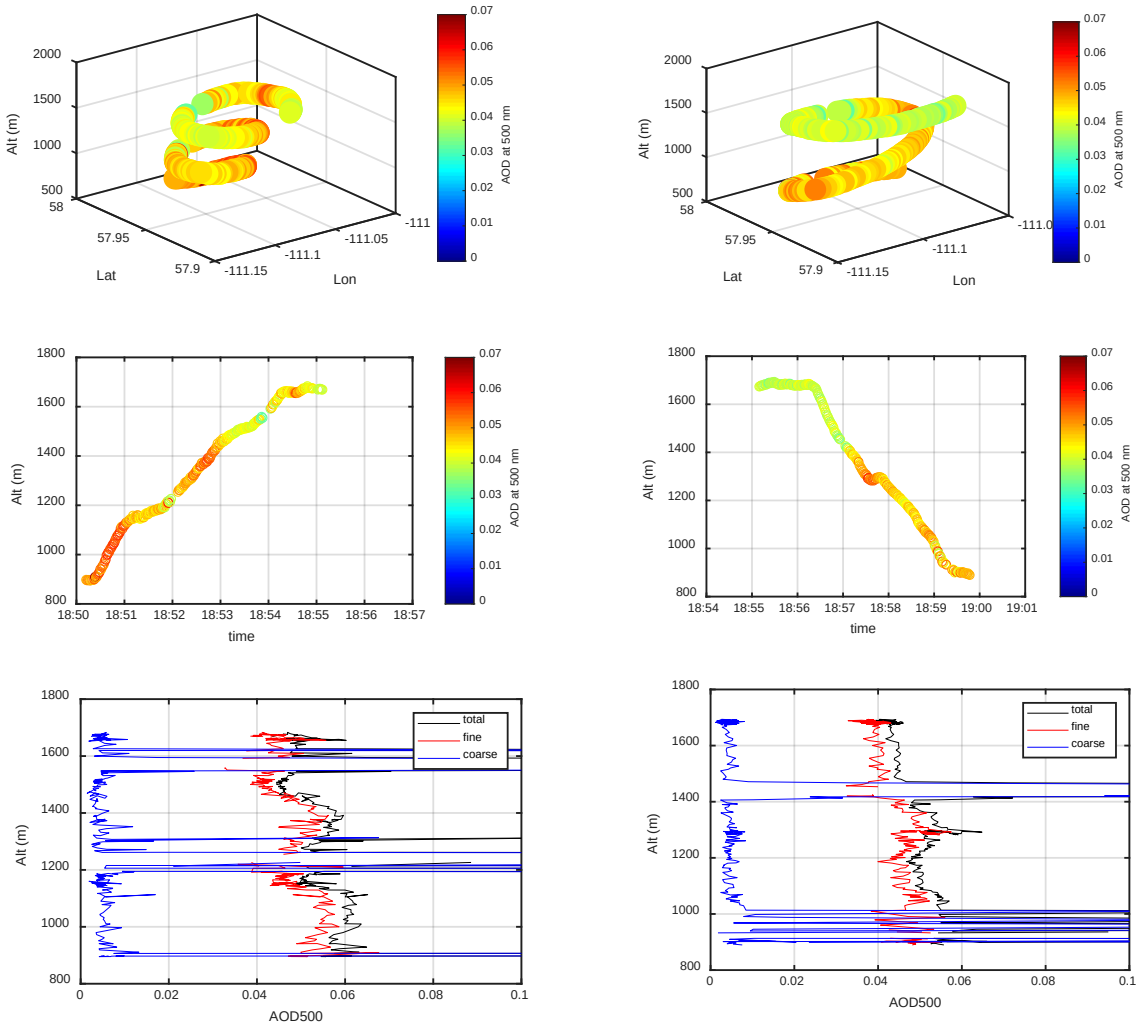

a. Spiral up b. Spiral down

Figure A57. *S*pirals during screen 3 (set 1). Description as in Figure A9

Appendix B – CIMEL sky scan description

The following are the descriptions of the almucantar (ALMU) and parallel plane (PP) measurements taken from the Cimel, 2015.

ALMU (Standard, BRDF) / ALMUP (Polarised): The almucantar technique consists in measuring the sky radiance in aerosol channels, keeping a constant zenithal angle equal to the zenith solar angle with varying azimuthal angle.
In the ALMU scenario, azimuthal angles vary from 0° to +180° for an almucantar right and 0° to -180° for an almucantar left using:

- SUN gain on the sun
- AUREOLE gain between -6° and +6°
- AUREOLE and SKY gain for 6° and SKY gain between 6° and 150°

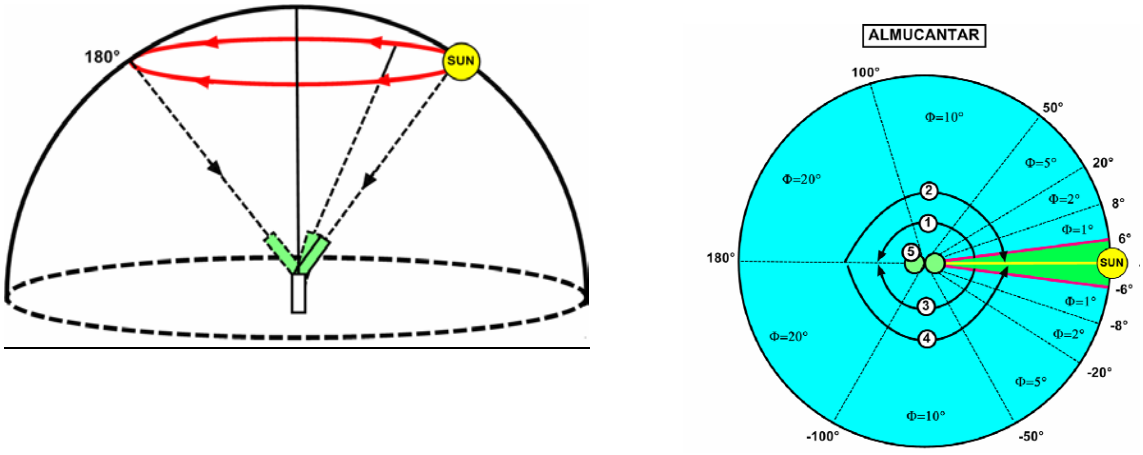

Figure B1. Almucantar measurement technique. From Cimel, 2015.

PP (Standard, BRDF) / PPP (Polarised): The **P**rincipal **P**lan technique also consists in measuring the sky radiance in the aerosol channels. The azimuthal angle is maintained in the solar plane with varying the zenithal angle .
In the PP scenario, zenithal angles vary from -6° to +150° using:

- SUN gain on the sun
- AUREOLE gain between -6° and +6°
- AUREOLE and SKY gain for 6° and SKY gain between 6° and 150°

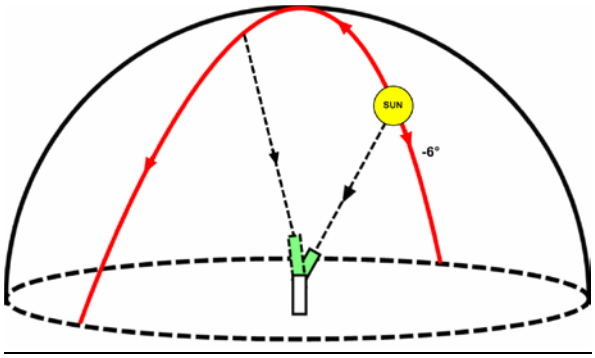

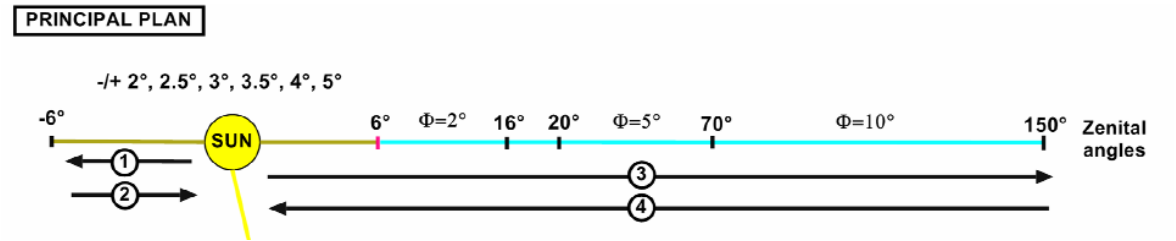

Figure B2. Principal plane measurement technique. From Cimel, 2015.